THE IMMUNOIMMOBILIZATION OF LIVING BACTERIA ON SOLID SURFACES AND ITS APPLICATIONS

by

Muhammedin Deliorman

A dissertation submitted in partial fulfillment
of the requirements for the degree

of

Doctor of Philosophy

in

Physics

MONTANA STATE UNIVERSITY
Bozeman, Montana

November 2012

APPROVAL

of a dissertation submitted by

Muhammedin Deliorman

This dissertation has been read by each member of the dissertation committee and has been found to be satisfactory regarding content, English usage, format, citation, bibliographic style, and consistency and is ready for submission to The Graduate School.

Dr. Recep Avci

Approved for the Department of Physics

Dr. Richard J. Smith

Approved for The Graduate School

Dr. Ronald W. Larsen

STATEMENT OF PERMISSION TO USE

In presenting this dissertation in partial fulfillment of the requirements for a doctoral degree at Montana State University, I agree that the Library shall make it available to borrowers under rules of the Library. I further agree that copying of this dissertation is allowable only for scholarly purposes, consistent with "fair use" as prescribed in the U.S. Copyright Law. Requests for extensive copying or reproduction of this dissertation should be referred to ProQuest Information and Learning, 300 North Zeeb Road, Ann Arbor, Michigan 48106, to whom I have granted "the exclusive right to reproduce and distribute my dissertation in and from microform along with the non-exclusive right to reproduce and distribute my abstract in any format in whole or in part."

Muhammedin Deliorman

November 2012

To my pearl of the stars, Inci Deliorman:

"Whatever you can do or dream you can, begin it.
*Boldness has genius, power and magic in it."**

*Source unknown; sometimes attributed to Johann Wolfgang von Goethe.

ACKNOWLEDGEMENTS

First and foremost, I am deeply grateful to my advisor, Dr. Recep Avci, for introducing me to the world of scientific research and for giving me the exceptional opportunity to do research in his lab. I owe him much in terms of scientific knowledge and methods: he taught me how to tackle a scientific problem and motivated me to gain insight into different fields of research, ranging from surface science to biological physics. His patience and support as a mentor and friend will always be remembered.

I want to express my gratitude to Dr. Zhiyong "Jahson" Suo for his friendship, for his exceptional mentorship in conjugate biochemistry, and for his help with designing experiments and analyzing data. I would like to thank Dr. Xinghong Yang for providing me with the antibodies and genetically modified bacteria from his stocks. This work would not have been possible without their help and guidance. I also would like to thank Dr. Iwona Beech and Dr. Jan Sunner for their insightful advice.

I thank Laura Kellerman for her help with the AFM imaging of bacteria, and Linda Loetterle for her help with making agar plates and preparing broth media and PBS buffer. I also thank Nancy Equall for her support and for being a good listener to me. I value their friendship very much.

I thank and acknowledge greatly Mrs. Lois Avci for her time and patience to edit this thesis carefully and for her meticulous attention to detail that helped to fine-tune it.

I thank all the new and past members of ICAL for their friendship: Dr. Mark Wolfenden, Bo Glaspey, Melody Bechberger, Kilean Lucas, and Bret Davis. It has been a great pleasure and fun working with them in ICAL.

Finally, I thank my wife, Sibel Kahraman Deliorman, my sister, Hatice Celik, and my parents, Aysegul and Veli Deliorman, for their constant support, unwavering encouragement, and everlasting love, which gave me the strength to complete this adventure.

TABLE OF CONTENTS

TABLE OF CONTENTS − CONTINUED

LIST OF TABLES

Table Page

LIST OF FIGURES

LIST OF FIGURES – CONTINUED

Figure Page

LIST OF FIGURES – CONTINUED

Figure Page

LIST OF FIGURES – CONTINUED

Figure Page

LIST OF FIGURES – CONTINUED

Figure Page

LIST OF FIGURES – CONTINUED

Figure Page

LIST OF FIGURES – CONTINUED

Figure Page

LIST OF FIGURES – CONTINUED

Figure Page

LIST OF FIGURES – CONTINUED

Figure Page

LIST OF FIGURES – CONTINUED

Figure Page

LIST OF FIGURES – CONTINUED

Figure Page

ABSTRACT

This thesis focuses on immobilizing living bacteria on material surfaces in their physiological environment without jeopardizing cell viability or replication. The ability to immobilize an individual bacterium opens up new research frontiers, as it not only enables us to conduct fundamental research on an individual living bacterium but also creates new opportunities for biosensor applications. A number of pathogenic organisms from *Salmonella enterica* and *Escherichia coli* strains are used to develop bacterial immobilization, herein referred to as immunoimmobilization. Our findings suggest that the most efficient, specific and reliable immunoimmobilization hinges on the use of affinity-purified antibodies raised against bacterial surface antigens such as fimbriae, lipopolysaccharides, and flagella. This approach produces a full monolayer of densely packed living bacteria (limited only by steric hindrance) on an antibody-activated area on a flat surface. Immunoimmobilization does not influence the viability or cell replication of the bacteria. To the best of our knowledge, to this day this is the highest packing density of immobilized bacteria reported in the literature. For successful immobilization, a monolayer of antibodies with full freedom of motion must be covalently linked to a flat surface (typically a silicon wafer). This has been achieved through a carefully optimized series of chemical reactions. More importantly, it was essential to monitor the activated surface using surface-sensitive analytical techniques to verify each step of the linker chemistry.

A *new* technique was developed for quantifying the initial rate of cell capture in terms of the number of bacteria immobilized per unit time per unit area per cell concentration in the physiological environment of the bacteria. This rate turned out to be $(7.2 \pm 0.3) \times 10^{-6}$ cells/(min·(100 μm)^2)/(cells/mL) for *S.* Typhimurium, and $(1.1 \pm 0.1) \times 10^{-6}$ cells/(min·(100 μm)^2)/(cells/mL) for *E. coli*, both expressing fimbriae. The lowest detection limit was ~3×10^4 cells/mL in 30 minutes of incubation.

For the first time, immunoimmobilization studies were conducted in a number of Navy fuels, including biofuels. It was discovered that antibodies subjected to the fuel environment preserve their structure, functionality and stability. The immuno-immobilization process works as efficiently in fuels as in aqueous environments.

.

1. INTRODUCTION

Motivation

General Background

The presence of bacteria, viruses, and other harmful microorganisms in water, food, and the environment is a significant threat to human and animal health [1]. Accurate, and if possible rapid, identification of such infectious agents at an early stage is vital to locating the origin of an infection and implementing appropriate treatment. Unlike standard culture methods [2], which are time consuming and less sensitive, molecular methods such as polymerase chain reaction (PCR), 16S ribosomal RNA gene (16S rDNA) sequence analysis, and DNA microarrays [3], given a reasonable turnaround time, offer an accurate and sensitive analysis of DNA sequences of nearly every possible origin. For example, if every step goes as planned, the time needed for a typical bacterial identification and characterization using the 16S rDNA sequencing method is about 7 hours, of which 20 minutes is spent on DNA extraction, 2 hours or less on PCR amplification, 4 hours or less on nucleotide sequencing and 30 minutes on amplicon (PCR end product) analysis [4]. As an additional advantage, these methods also offer the identification of species that are slow-growing and difficult to culture, such as mycobacteria [5]. In general, however, molecular methods suffer from severe limitations. Some methods, such as 16S rDNA sequence analysis, are focused on DNA that is shared within a given genus or even by different genera of bacteria; thus, the differentiation of bacterial species using these methods is difficult or even impossible. For example, *Escherichia coli* and *Shigella flexner* have identical 16S rDNA sequencing and cannot be

differentiated using the 16S rDNA sequence analysis method [4]. Other methods, such as DNA microarrays, are inconclusive on the viability of microorganisms; these methods may overestimate the number of viable organisms present in the tested environment. Although it remains to be determined whether cells in the non-culturable state retain their pathogenicity, in many situations it may be beneficial to get information on their viability [6]. Thus, the development of a versatile platform that is an alternative means of detecting and identifying species of microorganisms would be extremely useful in clinical settings. This can now be done with fair speed and efficiently using the antibody-based detection method described in this thesis.

The second motivation for this work is that the immobilization of a living bacterium offers the possibility of conducting new lines of research that focus on an individual bacterium rather than a group of bacteria. The monitoring of a living bacterium in response to an external stimulus is lacking in the literature, and our approach is a first step toward filling this gap in the field. For example, the nanoelastic properties of a living *Caulobacter* during its division cycle are of fundamental importance, and we were approached by a Stanford group [7] about mapping out the nanoelastic properties of a living *Caulobacter*. This was carried out (*see* Figure 1.1) by us, and the results are waiting to be published. The methods presented in this thesis have already been applied to some of the fundamental and practical questions posed by us: for example, whether a living bacterium would be killed by being punctured multiple times with a sharp tip in its physiological environment [8], and whether specific bacterial species can be sorted out of a mixed culture within a relatively short period of time (< 1 hour) [9]. These aspects of

our work will not be presented in this thesis; they are already in the literature. Here we present only new results that are yet to be published.

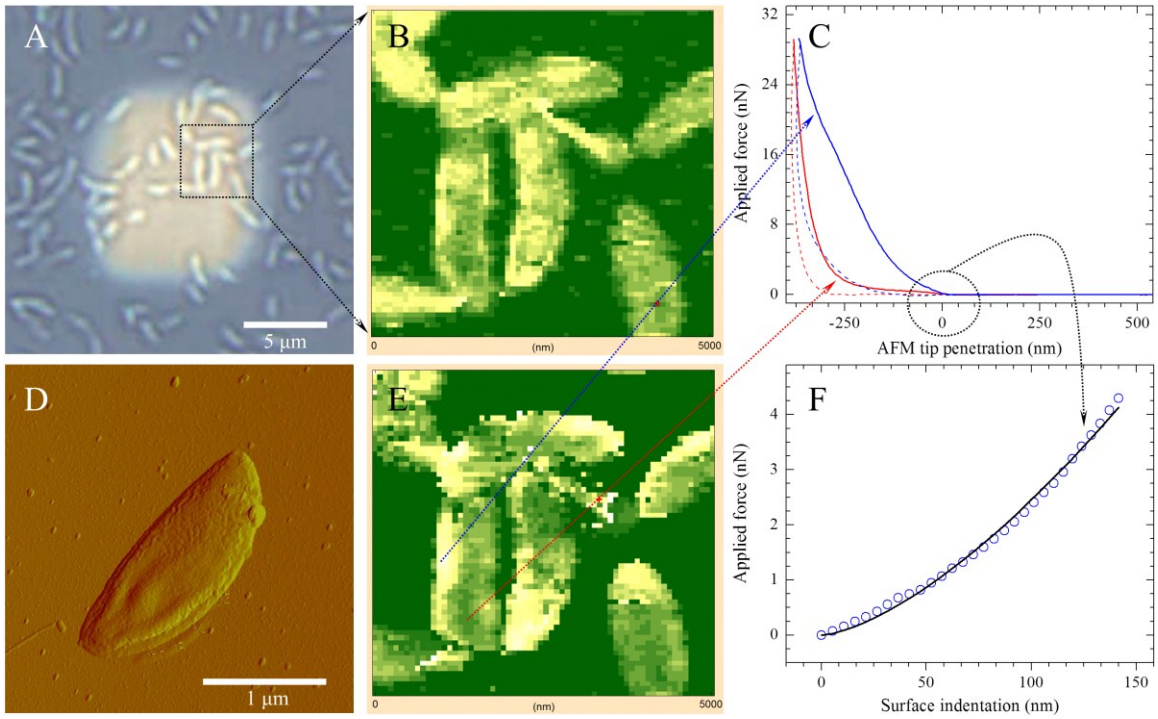

Figure 1.1. Quantitative mapping of nanoelasticity of living *Caulobacter crescentus* (*C. crescentus*) cells in their physiological environment. An atomic force microscope image of a bacterium is shown in Panel D. The optical image in Panel A shows immobilized *C. crescentus* cells on silicon substrate. Cells located within the black dashed square were used for nanoelasticity measurements using a sharp AFM tip. The bright pixels in the force image in Panel B correspond to the locations of *C. crescentus* cells confined within the dashed square in Panel A. The applied force vs. surface indentation curve (Panel F) was obtained from a force vs. AFM tip penetration profile (Panel C). A MATLAB (MathWorks, USA) code was developed in our lab to analyze a force curve by fitting an indentation curve to a theoretical model such as the Hertzian Model [10] (black solid line in Panel F), from which a local modulus of elasticity is extracted. As shown in Panel E, the local modulus of elasticity varied between ~25 kPa and ~200 kPa, depending on the location on the bacterial surface. Panel E suggests that the elasticity shows large variations over the surface, which is a most unexpected result.

Current Antibody-Based Detection Methods: Strengths and Limitations

Currently, a large variety of antibody-based methods are available in clinical laboratories. They are useful tools for rapid qualitative and quantitative analysis of bacterial presence in liquid and/or solid samples of clinical relevance. Examples of such methods include agglutination tests, immunofluorescence (IF) microscopy and enzyme-linked immunosorbent assay (ELISA) [11]. Compared with other methods, agglutination is simple, specific, and extremely rapid (~15 minutes), but it suffers from limited sensitivity, as large amounts of antigen are required for visible agglutination [12]. Some other methods, such as IF and ELISA, have displayed high degrees of sensitivity and specificity but are comprised of a number of steps [1, 13], including the labeling of reporter antibodies with fluorescent molecules or enzymes for the detection, identification and quantification of bacteria. As a consequence, these methods often require lengthy analysis times, which may be problematic in instances where the rapid and accurate detection and identification of bacteria are desired [1]. Furthermore, once the presence of bacteria is confirmed, the usefulness of these methods stops there.

In the course of this work, we proposed a new label-free, antibody-based method (herein referred to as the immunoimmobilization method) for efficiently detecting and identifying target bacteria, particularly of wild types, in an aqueous environment [14]. The fundamental concept of the method is the careful preparation of bioactive surfaces that facilitate the capturing of targeted bacteria using antibody-antigen interactions. Thus, in our work we first developed tether molecules that link the carefully selected antibodies to flat, solid surfaces with high density and preserved activity towards the bacterial

antigens against which they were raised. We showed that these surfaces, if properly prepared, are very effective at immobilizing and retaining a monolayer of bacterial cells. In the same work, we also demonstrated that, starting with just a few immuno-immobilized live bacteria, we can culture and grow them to fill the available space on a bioactive surface (self-enrichment). Next, we extended our work to determine the correlations between antibody-antigen pairs and immunoimmobilization efficiency. For this purpose we tested a variety of antibodies targeting different surface antigens of live *Salmonella enterica* (*S. enterica*) and *Escherichia coli* (*E. coli*). We demonstrated that the majority of bacterial antigens are not effective in the immobilization process, with the exception of surface antigens such as fimbriae (or pili), lipopolysaccharides (LPS), and flagella, which provided highly sensitive, rapid, and reliable immunoimmobilization of bacteria with high-throughput efficiency [9, 15]. Furthermore, in our more recent work we showed that specific antibody-antigen interactions can be used simultaneously in a single test to detect and identify multiple bacterial strains mixed in a culture within an hour [9]. These results were possible because we first immunoimmobilized bacterial cells on predefined areas of a highly polished substrate (silicon wafer) and subsequently imaged them *in situ*, without staining, using an optical microscope. This way, we achieved imaging sensitivity, in that within a $200 \times 200\ \mu m^2$ field of view we can track a single immobilized living or dead bacterium. Thus, unlike the multiple-step processes used in other antibody-based methods [2, 13], the immunoimmobilization method is a two-step process (incubate and image) that requires no extensive training or expert judgment of the operator for data interpretation.

The immunoimmobilization method described in this thesis not only exceeds the sensitivity, specificity, practicality and high-throughput applicability of the existing antibody-based methods, but also offers additional advantages that will be invaluable in clinical settings. It is readily applicable to sorting a mixed culture into predefined patterns [9] on a substrate surface within an hour, each spot containing a pure culture, thus eliminating the need for the standard purification methods. It is also readily applicable to concentrating bacteria in predefined patterns on a substrate surface, either through captures from the planktonic state or through the multiplication of the bacteria already captured on the substrate. This eliminates the need for the standard culture methods and offers a clean platform for testing the efficacies of antimicrobial drugs on living bacteria from a diseased or contaminated specimen. The method also captures viable but non-culturable bacteria, making it possible conclusively to determine their viability by observing their division. Finally, it offers a reliable approach for fundamental microbiological research on the behavior of bacteria as they respond to environmental changes: it provides opportunities for subjecting an individual living bacterium to *in situ* external manipulation and observing it following manipulation that none of the existing antibody-based methods can provide. For example, in our previous study [8] we demonstrated that the manipulation of single cells in their physiological environment by means of sharp AFM tips does not hinder their physiological activities. In the same study we also proved that multiple puncturings of the cell wall of a bacterium does not kill the bacterium. These results are promising for the future, since this approach opens up the possibility of introducing biological materials such as DNA, proteins, viruses or

nanoparticles into the cytoplasm of a bacterium and observing the bacterial responses to these intrusions.

To conclude, our recent publications on the immunoimmobilization method using model bacteria not only offer the first glimpses of light in the field of rapid bacterial detection and identification, but also point to the fact that more work needs to be conducted for this method to lead to the immunosensor applications discussed above. In that sense, the work presented in this thesis is the first empirical study that (a) provides direct quantitative assessment of immunosensor capture efficiency and (b) demonstrates the potential for immunosensors in field applications using model bacteria.

Dissertation Overview

Our aim in this work is three-fold: First, we want to functionalize and characterize silicon substrates using aminosilane and tether molecules for the preparation of bioactive surfaces with long stability and durability in aqueous environments for antibody immobilization. Second, we want to determine the capture efficiency (number of captured cells per unit area per unit time) and the detection limit (minimum detectable cell concentration) of the proposed immunosensor. Third, we want to test its potential as a tool for detecting microbial contamination in field use, more specifically in Navy fuels. For this purpose, (1) the immunosensor will have a binding layer coated with carefully selected antibodies specific to the corresponding antigens of targeted bacteria, (2) the immunosensor will capture targeted bacteria on predefined areas of the substrate surface through antibody-antigen interactions, and (3) optical microscopy will be used to investigate the amount of bacteria bound to the antibodies on the surface. In all

experiments, mainly wild-type pathogenic strains of *E. coli* and genetically modified *S. enterica* will be used as model bacteria.

The first step in the study presented in this thesis is the preparation of a reproducible antibody-binding layer. Chapter 2 explains in detail the surface chemistry used to activate silicon substrates for antibody immobilization. It includes X-ray photoelectron spectroscopy (XPS) results both prior to and after each chemical modification of the substrate. In addition, it demonstrates the necessity of material surface characterization to developing an effective chemically active surface for bacterial immunoimmobilization and reveals the detection efficiency for bacterial cells. Chapter 3 introduces a new method for determining the capture efficiency of an immunosensor by exposing pure cultures of *S. enterica* and *E. coli* strains to antibody-modified surfaces. Here, the cell capture rate is defined as the number of cells attached per $100 \times 100\ \mu m^2$ of antibody-activated area per minute per cell concentration in solution. The effects of the fimbriae expression level, antibody density, and immunosensor storing conditions on the cell capture rate are also discussed in this chapter. Chapter 4 discusses the use of the immunosensor for the detection of microbial contamination in Navy fuels. The findings show that our method offers a potential for on-site measurements that provide both real-time monitoring of bioprocesses and early, rapid, sensitive detection of microbial contamination in fuels. In addition, in this chapter possible future research directions related to the use of new technologies based on the immunoimmobilization method are outlined. Finally, Chapter 5 gives a summary and the general conclusions drawn from the thesis.

2. EXPERIMENTAL

Introduction

The immunoimmobilization of live bacterial cells on flat, polished solid surfaces in their physiological environment is a complicated process influenced by many factors, including material surface characteristics, surface chemistry, physiological medium and bacterial properties. To obtain efficient and reliable immunoimmobilization of live bacterial cells, attention must be paid to the careful preparation of bioactive surfaces that facilitate the capturing of targeted bacteria using specific ligand-receptor interactions, such as antibody-antigen interactions. A key element in the preparation of such surfaces is the efficient immobilization at high densities of oriented antibodies which target corresponding bacterial surface antigens, such as fimbriae, lipopolysaccharides (LPS), or flagella. Therefore, a reliable method for the preparation of a stable, active, high-yield antibody layer on a solid surface must be developed. It is critical that the proper linker molecules be employed and that the surface chemistry be carefully optimized to achieve the highest yield and reproducibility of the antibody layer.

Employing an appropriate surface chemistry is an essential step in surface preparation that effectively binds antibodies onto surfaces. Currently, two major approaches have evolved for antibody immobilization. The first approach is based on the physical adsorption of antibodies [16, 17]. In this approach, weak interactions, such as hydrogen bonding, van der Waals, and electrostatic interactions, take place between the antibody and the substrate surface. Although this approach is the easiest to prepare, antibodies immobilized in this way are not stable enough to overcome long incubation

times (hours, days) and thus are susceptible to detachment and being washed off from the surface. Furthermore, they are mostly randomly oriented on the substrate surface, yielding inconsistency in the activity of the antibody layer and the poor reproducibility of results [18]. The second approach provides more strongly bonded antibodies at the substrate surface by taking advantage of covalent linkage between the antibody and the linker layer of the substrate. Antibodies immobilized in this way not only preserve their integrity while the immunosensor is subject to static or flowing conditions, but also maintain high activity following attachment [19].

Various published reports focus on the use of self-assembled monolayers (SAMs) to attach antibodies to various substrates, such as silicon, glass, titanium, and polystyrene [20]. The formation of SAMs on these surfaces results from the covalent adsorption of surface-active molecules onto the substrate. Depending on the characteristics of the surface, these molecules contain reactive groups, such as −SH, −COOH, $-NH_2$, or −OH, which in turn are used to graft antibodies to the surface either directly or indirectly (i.e., through linker, or tether, molecules). In particular, the use of heterobifunctional molecules as tether molecules with functional groups on both sides has become important in recent years [21-25]. Unlike direct attachment, a tether molecule targets the amino acid residues located within the lower portion of an antibody for covalent attachment [22]. This region (the so-called Fc region) is located away from the antigen-binding site (i.e., paratope) of an antibody [26], so the antibody is left free to interact with the bacterial antigen of interest. Thus, a well-oriented antibody layer on the surface is achieved, which results in a high binding capacity [25].

The primary objective of this chapter is to describe the main ingredients for chemically modifying silicon surfaces for the covalent attachment of antibodies. A major part of this work is devoted to the investigation of the self-assembly process of silane molecules with amine ($-NH_2$) reactive groups on silicon surfaces. For this purpose, 3-aminopropyltriethoxysilane (APTES) molecules were employed. These molecules, if properly deposited, are capable of forming covalent bonds to the hydroxyl (–OH) groups of silicon surfaces and are hence perfectly suited to the immobilization of antibodies. The advantage of using n-[ß-maleimidopropyloxy]-succinimide ester (BMPS) as an intermediate tether molecule is also demonstrated in this chapter. A silicon substrate is modified in four steps: (1) cleaning, passivation, and patterning; (2) deposition of an APTES layer; (3) reaction of the APTES amine groups with BMPS; and (4) the immobilization of antibodies through the reaction of the maleimide groups of the cross-linker and the sulfhydryl groups of the antibodies. Each step in the functionalization of a silicon surface is characterized by surface-sensitive techniques, such as X-ray photoelectron spectroscopy (XPS), as described below.

Instrumentation

An effective step-by-step characterization of chemically modified surfaces is necessary to verify the chemisorption of each functional group to each monolayer of the activated surface. Thus, a number of spectroscopic and microscopic techniques have been used throughout the course of the work presented in this thesis, including X-ray photoelectron spectroscopy (XPS), time-of-flight secondary ion spectrometry (ToF-SIMS), scanning Auger electron spectroscopy (AES), atomic force microscopy (AFM),

and optical microscopy. XPS was used to characterize the silicon surfaces prior to and following each step of the chemical modification in order to obtain verification, quantification, and information about the chemical bonding of the elements on the surface of the sample; ToF-SIMS was used to create micropatterns on silicon surfaces for antibody immobilization; optical microscopy was used to detect and identify *in situ* live bacteria immobilized on antibody-modified micropatterns on silicon substrate; AES was used to image (map) spatial elemental distributions of antibody-modified micropatterns on silicon samples; and AFM was used to reveal the fimbriae on the surface of bacteria under study. In addition, ellipsometry and contact angle measurements were carried out to investigate the thickness and wettability, respectively, of silicon surfaces before and after the APTES silanization process. The overall aim of this section, however, is not to review all aspects of the instrumentation listed above, but instead to highlight a few important features of their working principles. This knowledge, along with a knowledge of surface and bulk chemistry, will help in understanding and interpreting the data presented in the subsequent sections.

X-Ray Photoelectron Spectroscopy

With its detection limit of about 0.1% of a monolayer, XPS is probably the most valuable surface-sensitive analytical technique. It is capable of identifying and quantifying all the elements, except hydrogen and helium, present in the uppermost atomic layers of a sample under study and determining their oxidation states. The basis of the technique consists of bombarding a sample with soft X-ray photons (~1.5 keV), which are capable of penetrating many microns into the bulk without destroying the

surface [27]. When the binding energies of core level electrons of some of the elements present in the sample are overcome by the incident photon energy, photon adsorption takes place, resulting in the ejection of core level electrons (i.e., photoelectrons). This is known as the photoelectron ionization process. The penetration depth of the photoelectrons and the secondary electrons they generate depends on their kinetic energy and is typically less than 10 nm [28].

The energy conservation of the photoelectron emission process can be expressed by

$$E_K = h\nu - E_B - \Phi \tag{2.1}$$

where E_K is the photoelectron kinetic energy, $h\nu$ is the incident photon energy, E_B is the core electron binding energy relative to the Fermi level of the analyzer, and Φ is a work function of the analyzer which is known or can be determined [29]. An electron energy analyzer is used to determine the kinetic energies of the photoelectrons, E_K, which lead to the binding energy E_B [27]. Thus, core electron binding energies can be determined from the energy conservation equation given above. Furthermore, during the photoelectron ionization process there is a probability that an electron from a high-energy orbital will make a transition to the empty state (a hole) in the core level left by the photoelectron process. The energy difference in this case can result in either the emission of an X-ray photon, which forms the basis for X-ray fluorescence (XRF) spectroscopy, or the ejection of another electron, i.e., a so-called Auger electron [30]. The Auger electrons that leave the surface also contribute to the kinetic energy spectrum, forming Auger peaks, which are easily distinguishable as they are broadened by nature [28] and the

kinetic energy positions of Auger electrons are independent of the primary X-rays (or electrons or ions) that produced them. The phenomenon described here is the fundamental principle of Auger electron spectroscopy (AES), another powerful surface-sensitive analytical technique. Most AES systems use focused electrons instead of X rays to create core holes. The subsequent decay and emission of Auger electrons are identical to those in the process described above. In AES, high spatial resolution is achieved when a low electron beam current is used (~2 nA). Also, high beam currents may induce surface damage to the sample. AES has not been used extensively in this thesis; hence the technique will not be described any more than what is given above. The interested reader can refer to the excellent publications in the literature [30-32].

Because core electron binding energies are well defined and unique to each element, the adsorbing atomic species in the photoelectron emission process can be readily identified from its energy position in an X-ray photoelectron spectrum. An example of such a spectrum, also referred to as a survey scan spectrum, is given in Figure 2.1. Here, all elements which are contained in the range from 0 to 600 eV in the as-received silicon wafer surface are demonstrated, providing a wealth of information about the different elements present on the surface of the sample.

The peak maxima of the photoelectron lines in a spectrum allow the binding energies to be measured accurately. As a consequence, the elements contained in the sample can be identified from the binding energy values. For example, the five intense lines in Figure 2.1, at binding energies of 532.6, 285.0, 150.2, 99.0, and 25.0 eV, are attributed to O 1s, C 1s, Si 2s, Si 2p, and O 2s, respectively. The shoulders (marked

with *) located at equidistant spacings from the binding energies of the main peaks, on the other hand, are attributed to multiple bulk-plasmon losses in Si [28].

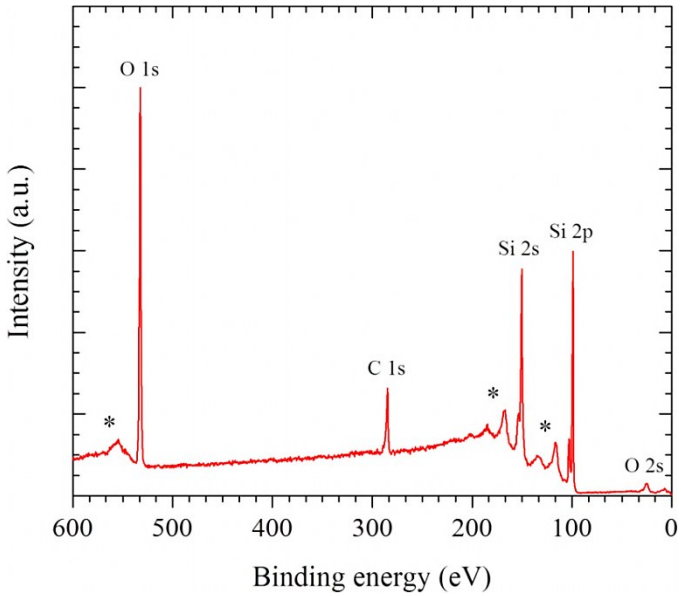

Figure 2.1. XPS spectrum of as-received silicon wafer surface. All elements are marked. The shoulders marked with * are attributed to multiple bulk-plasmon losses of Si.

It is important to emphasize here that the high intensity of the C 1s line in the figure above is due to a significant amount of carbon contamination on the sample surface. As we will discuss in the next section, this overlayer of carbon contamination buries the native oxide layer of the silicon, resulting in a low number of the hydroxyl (−OH) groups, which are essential for subsequent chemical modification, being available on the substrate. Thus, to reduce the concentration of this overlayer, ultrasonic cleaning followed by piranha etching (i.e., by etching the substrate surface with a concentrated sulfuric acid and hydrogen peroxide mixture) is applied in this study.

In addition to identification, the relative amount of a particular element present in a sample can be determined using a peak fit routine and the area under the peak after the

Shirley-type background subtraction [33], by taking into account relative sensitivity factors. In the simplest case, in which there is a homogeneous distribution of elements within the sample, the atomic concentration *C* of an element *X* in the volume sampled is given by

$$C_x = (I_x / S_x) / \sum_n (I_n / S_n) \tag{2.2}$$

where I_x is the intensity of the photoelectron line (area under the peak) attributed to element *X* and S_x is the sensitivity factor of the spectrometer to element *X*. The sum includes all *n* elements investigated in the XPS spectrum [27]. The sensitivity factors of the spectrometer for the various elements have been tabulated [34], and the ones used in this study, along with the relative atomic concentrations of elements in as-received silicon wafer surface (*see* Figure 2.1), are given in Table 2.1. The quantification provided by XPS is accurate to within ±10%. Within this limitation XPS is well suited to the quantitative elemental analysis of surfaces.

Element	*O 1s*	*N 1s*	*C 1s*	*Si 2p*
Sensitivity factor	0.711	0.477	0.296	0.339
Atomic concentration (%)	37.3	–	19.9	42.8

Table 2.1. Sensitivity factors and the relative concentrations of elements present in the clean silicon wafer.

Beyond the identification and quantification of the elements present on the surface of a sample, the acquisition of high-resolution spectra in binding energy regions of interest, followed by Shirley-type background subtraction and subsequent peak fitting, can provide additional information related to the local chemistry (oxidation states) of the

elements on the surface [28]. An example of a typical high-resolution spectrum is shown in Figure 2.2, in which C 1s acquired from as-received silicon wafer surface is shown.

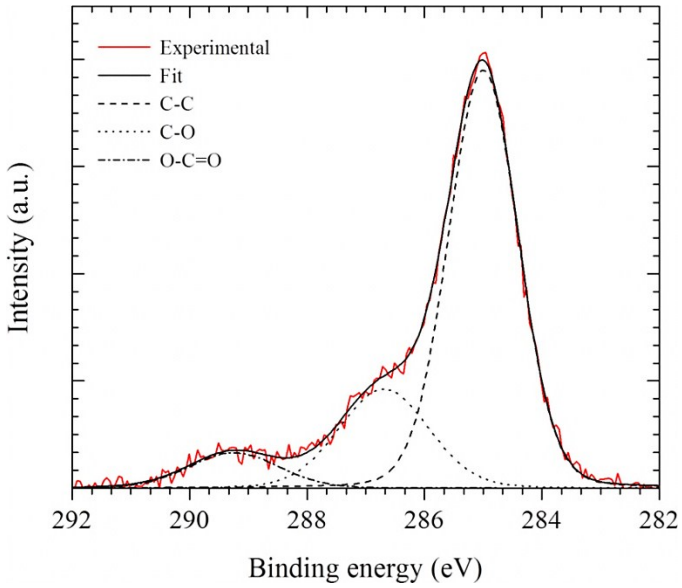

Figure 2.2. High-resolution XPS spectrum of C 1s of as-received silicon wafer surface. The experimental spectrum is the solid red line, and the fitted spectrum is the solid black line. The peak assignments of various oxidation states of C are indicated in the figure.

As described previously, following the background subtraction, the C 1s spectrum is resolved into three main component peaks. The binding energy values of the component peaks are determined from the peak maxima and are assigned to the various carbon bonds in the sample (e.g., 285.0 eV to C−H and C−C, 286.6 eV to C−O, and 288.6 eV to O−C=O) [28]. By convention, the component peak arising from the carbon in C−H and C−C bonds is assigned to a binding energy of 285.0 eV and the energy scale is shifted rigidly if the surface is charged.

The fact that the carbon in a C−O local configuration, being singly bonded to one electronegative oxygen atom, has a lower binding energy than the carbon in a −C=O configuration, which is bonded with a double bond to an electronegative oxygen atom, is

due to the difference in the electron density distribution surrounding these carbon atoms [28]. An excess electron around an atom raises the binding energy because of the electrostatic repulsion of e-e interactions. For example, the electron density is nearly evenly distributed between the two carbon atoms in a C−C bond, resulting in a higher binding energy compared to the other two C peaks in the spectrum. The reader should note here that, although the carbon atoms in C−H and in C−C bonds are in slightly different chemical states, the small difference in their binding energy positions (~0.4 eV) allows them to be attributed to a single component peak at 285.0 eV [28]. From here on this peak will be labeled only as the C−C peak, unless otherwise noted.

In addition to the various bonding types of an element, curve fits to a spectrum also yield the relative fraction of each bonding state. For example, the relative fractions of component peaks C−C, C−O, and O−C=O in Figure 2.2 are 70.8%, 21.5%, and 7.7% of the total area under the C peak, respectively.

In this work, all survey scan and high-resolution XPS spectra were collected using a Physical Electronics PHI 5600ci system equipped with monochromatized Al Kα X rays (1486.6 eV). The binding energies of adsorbed electrons were measured using a concentric hemispherical analyzer (CHA). For each sample, survey spectra were collected from 0 to 600 eV at a pass energy of 46.95 eV, whereas high-resolution spectra of O 1s, N 1s, C 1s, and Si 2p were acquired at a pass energy of 23.5 eV. Atomic concentrations were calculated from peak areas obtained after Shirley-type background subtraction of selected region scans of O 1s, N 1s, C 1s, and Si 2p using AugerScan software (RBD Instruments, USA). All spectra were referenced by setting the main

hydrocarbon peak (i.e., C 1s) to 285.0 eV. Charging problems were neutralized with an electron flood gun. The base pressure of the ultrahigh vacuum (UHV) analysis chamber was ~5×10^{-10} torr. Each step involved in chemical modification of an activated surface was analyzed on the same sample within a single study.

Time-of-Flight Secondary Ion Mass Spectrometry

ToF-SIMS is another leading surface-sensitive analytical technique with trace element sensitivity, capable of submonolayer depth resolution [35]. In this thesis, however, it was used for the purpose of creating micropatterns (from here on referred to as patterns) on silicon surfaces for antibody immobilization. This is why only the basic mechanism behind the patterning will be explained here. For general information on this instrument and its applications, the interested reader should refer to various documents published in the literature [36-42].

The basic mechanism behind the patterning is the sputtering process, which is depicted in Figure 2.3. In this process, a pulsed primary ion beam with an energy of ~12 keV hits the surface and penetrates the substrate to a depth of several nanometers below the surface. This penetration leads to an intense but short-lived collision cascade in the target, where the ion pulse transfers its kinetic energy to the atoms and molecules of the sample, thereby inducing a large-scale random collision process and bond breaking [35]. Most recoil particles have low energy; thus, only particles from the outermost layer with momenta directed toward the surface can overcome the surface binding energy and leave the target. Consequently, the removal of particles from the outermost layers of the sample erodes the surface [43], and forms patterns on the substrate surface.

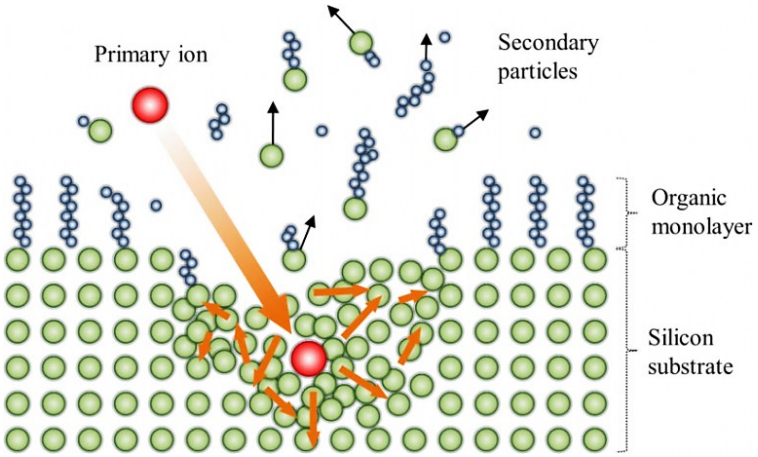

Figure 2.3. ToF-SIMS desorption of secondary particles from the outermost surface after excitation with primary ions with several keV of energy.

In this work, the microfocused liquid Ga^+ beam of a PHI-Evans triple focusing ToF-SIMS system was used to create patterned areas with a size of 100 × 100 μm^2 on silicon surfaces. The carefully adjusted sputter time was 10 seconds so that only a very thin layer (~2 nm) of the substrate surface would be removed. During the sputtering process, a beam energy of 15 keV relative to the ground was used. The target stage was biased at 3 keV. Thus, the primary ion impact energy was 12 keV. The direct Ga^+ ion current at the target position was measured to be 1.2 nA. The base pressure of the UHV analysis chamber was better than 1×10^{-9} torr.

Optical Microscopy

Optical microscopy was used for the purpose of detecting and identifying immunoimmobilized bacterial cells on patterned silicon surfaces *in situ*. The technique can be used to image samples in both ambient and liquid environments at a resolution of ~1 μm. In this system, light reflected or transmitted by the sample surface passes through lenses, creating a magnified image of the sample. It has two modes of operation:

reflection and epifluorescence. The reflection mode involves the reflection of visible light from the specimen. The epifluorescence mode, which is very common in biological applications, involves the illumination of a specimen stained with an appropriate fluorescence agent with light at a wavelength greater than that of the fluorescence. This results in the fluorescent specimen being highly visible against the dark background of the substrate surface.

In this work, all bright field and epifluorescence images were taken using an Olympus BX61 microscope, equipped with a motorized z-stage and a DP71 charge-coupled device (CCD) camera, either in reflection mode (for nonfluorescent strains) or in epifluorescence mode (for fluorescent strains). In both modes, immunoimmobilized bacteria were imaged in a liquid environment through a 60× water-immersion objective lens. Two filter sets, fluorescein isothiocyanate (FITC, excitation maximum 495 nm and emission maximum 521 nm) and tetramethyl rhodamine isothiocyanate (TRITC, excitation maximum 540 nm and emission maximum 605 nm), were used to image the green and red emissions of the fluorescent stains, respectively. The images were further processed with MicroSuite V software (Olympus, USA).

Scanning Auger Electron Spectroscopy

AES was used for the purpose of obtaining quantitative surface elemental distribution maps of antibody-modified patterns of silicon samples at high spatial resolution. Unlike in XPS, in AES electrons are excited from a solid by the impact of a focused electron beam. Because of this impact, the atoms in the sample are ionized, and electrons are liberated from the surface as a result of the electron transition from a higher

to a lower state in an atom. These electrons allow imaging of the elemental concentrations of the top few atomic layers of a solid. The brightness associated with each pixel in a produced image is proportional to the local concentration of the selected element at the corresponding spot on the surface of the sample. Furthermore, AES with a standard primary electron source has a lateral spatial resolution of ~0.3 to 3 μm and a depth resolution anywhere from sub-nm to 10 nm, depending on the kinetic energy of the Auger electrons [44].

In this work, a Physical Electronics PHI 660 system equipped with a lanthanum hexaboride (LaB_6) primary electron source was used to map the elemental compositions of antibody-modified surfaces on silicon surfaces. The system was equipped with a cylindrical mirror analyzer (CMA) energy analyzer. A 10-keV primary electron beam at 1.8 nA was used for the single-element map scans. During map scans, the base pressure of the UHV analysis chamber was ~5×10^{-10} torr. Auger data were analyzed using the AugerScan and AugerMap software of RBD Instruments, USA.

Atomic Force Microscopy

AFM [45] was used to image the fimbriae expression level of the bacteria under study. It measures forces between a sharp tip (with a nominal diameter of ~30 nm and a length of a few microns, positioned close to the free end of a well-calibrated cantilever) and a sample surface, which enables topographical mapping of a sample surface with nanometer spatial resolution. AFM has two primary modes of operation: contact and tapping modes. In contact mode, a constant force is applied to the tip, pushing the tip against the sample as it rasters over the sample surface. For imaging soft samples, such as

bacteria, this mode is not preferred since the constant force applied to the tip during the operation may damage or distort the surface. In tapping mode, however, the AFM cantilever oscillates across the sample surface near its resonance frequency. Thus, the tip only lightly touches the sample surface. As a consequence, tapping mode gives a more realistic topographical image of a soft sample surface.

Since the fimbriae of bacteria are surface antigens and among the key appendages of microorganisms, confirmation of their existence is central in our studies. Fimbriae on cell surfaces were revealed using a Veeco Multimode V AFM system in tapping mode with an E-type scanner and NSC18 AFM tips (MikroMasch, USA). Cells were immobilized on freshly cleaved mica surfaces by incubating ~100 μL of freshly grown bacterial culture on a mica surface for 30 minutes, followed by rinsing with water and slow drying in air. The fimbriae on the cell surfaces were seen clearly in the amplitude images, which were further analyzed with NanoScope software (Veeco, USA).

Ellipsometry

In this work, a Gaertner L116A ellipsometer was used to measure the thickness of APTES layers self-assembled on silicon surfaces. The light source was a He-Ne laser (632.8 nm) with a 70° angle of incidence from the normal plane. Data were taken at five distinct spots in air at 25 °C on each of three APTES-modified samples, to obtain an average thickness. The refractive index of an APTES layer was assumed to be equal to that of a native oxide layer of silicon (n = 1.465) [46]. Using software provided by the instrument vendor, the thickness of the native oxide layer of a silicon surface was measured to be 2.2 ± 0.1 nm. Consequently, in all measurements this value was used as a

reference and subtracted from the SiO_2/APTES layer of the substrate to yield the APTES layer thickness.

Contact Angle Measurements

In this work, a VCA 2500XE goniometer, equipped with a CCD camera, was used to measure the wettability of APTES layers self-assembled on silicon surfaces. Static probe drops were deposited on silicon surfaces using a microsyringe. The probe fluid was nanopure water. Data were taken at three distinct spots in air at 25 °C on each of three APTES-modified samples and further analyzed using VCA Optima XE software (AST Products, USA) to obtain the average contact angle values.

Materials and Methods

Chemicals and materials used in the work presented in this thesis are listed below. For detailed information on their use, the reader should refer to the appropriate sections in following chapters.

Chemicals

Phosphate-buffered saline (PBS, pH 7.4 at 25 °C), 3-aminopropyltri-ethoxysilane (APTES) and all other standard chemicals were purchased from Sigma-Aldrich (St. Louis, MO). N-(ß-maleimidopropyloxy)succinimide ester (BMPS) was purchased from Pierce Biotechnology (Rockford, IL), 5- and 6-carboxyfluorescein n-hydroxysuccinimide ester activated fluorescein (NHS-fluorescein, excitation maximum 495 nm and emission maximum 519 nm) was purchased from Sigma-Aldrich (St. Louis, MO), and 2-[methoxy-(polyethyleneoxy)propyl]trimethoxysilane (PEG-silane) was purchased from Gelest

(Morrisville, PA). All chemicals and solvents not mentioned above were of analytical grade and used as received.

Materials

Silicon wafers mirror-polished on one side (100 orientation, p-type, 1−10 Ω·cm resistivity, ~550 μm thickness) were purchased from Silicon Inc. (Boise, ID). Solid silica beads with a diameter of ~2 μm were purchased from Thermo Scientific (Rockford, IL). Quartz wools were obtained from Technical Glass Products (Painesville, OH). *Salmonella enterica* serovar Typhimurium (*S.* Typhimurium) strains H72-pBBS-cfa and H72-pBAD-cfa, wild-type enterotoxigenic *E. coli* H10407, colonization factor antigen I (CFA/I) fimbriae of *S.* Typhimurium and polyclonal anti-CFA/I antibodies raised against them were provided by Dr. Xinghong Yang of the Department of Immunology and Infectious Diseases at Montana State University in Bozeman, and wild-type enterohemorrhagic *E. coli* O157:H7 was obtained from the Center for Biofilm Engineering at Montana State University in Bozeman. Polyclonal antibodies raised against the LPS of O157:H7 were purchased from Santa Cruz Biotechnology (Santa Cruz, CA). Wild-type enterotoxigenic *E. coli* 3030-2 was obtained from the Veterinary Science Department at South Dakota State University, and polyclonal anti-K88ac antibodies raised against their F4 (K88ac) fimbriae were purchased from Novus Biologicals (Littleton, CO). Along with *Desulfoglaeba alkanexedens* ALDC^{T}, all Navy fuels (petroleum ultralow-sulfur diesel, petroleum low-sulfur diesel, petroleum JP-5, petroleum F-76, camelina-derived JP-5, algae-derived F-76, and soy-based biodiesel) and coastal Key West natural seawater were obtained from the Department of Botany and

Microbiology at the University of Oklahoma at Norman. Polyclonal antibodies raised against ALDC^{T} were provided by Dr. Xinghong Yang. Finally, diesel fuel was purchased from the ConocoPhillips gas station in Bozeman, MT.

Surface Preparation and the Characterization of Silicon Substrates

As we articulated in our previous publication [14], it is of paramount importance to establish a reliable method for the effective cleaning, passivation, and patterning of silicon surfaces prior to the deposition of the antibody binding layer, particularly when quantification of the bacteria immunoimmobilized on predefined areas of a substrate is desired. Thus, the cleaning and surface preparation methodology described in this section must be followed with care prior to any further modification of a silicon surface. Failure to adhere to this requirement can cause an unsuccessful deposition of the antibody binding layer, leading to poor immobilization of bacteria [14]. Through careful surface characterization we have achieved a high-density full monolayer of bacteria (limited only by the steric hindrance of the bacteria) immobilized on an activated area. It is our aim here to provide the reader with the procedures followed in this study to clean, passivate, and pattern silicon surfaces effectively prior to incubation with bacteria.

Cleaning

Earlier it was mentioned that the main goal of cleaning silicon substrate is to remove the overlayer of environmental carbon contamination from its surface and treat the native oxide layer of the substrate to generate a high density of hydroxyl (−OH) groups, which are anchoring points for covalently bound silane molecules, the first layer of the multilayer tether molecule structure. A wide variety of cleaning methods for silicon

oxide surfaces are described in the literature. The common procedures include wet chemical [47], ozone [48], and plasma [49] cleaning. Use of the wet chemical method is extensively reported for cleaning silicon surfaces in preparation for silanization [50, 51]. Various combinations of acids, bases, and organic solvents have been investigated at various temperatures in order to achieve optimal uniformity and reproducibility of the silanization process. The primary use of piranha solution, a concentrated sulfuric acid (H_2SO_4)/hydrogen peroxide (H_2O_2) mixture, with silicon wafer has been reported widely because of its effect of generating a high density of hydroxyl groups on substrate surfaces [52]. Therefore, in the course of the work presented in this thesis, piranha solution was used to clean organic contaminants off silicon surfaces effectively.

In our experiments, as-received silicon wafers were cleaved into ~1 cm × 1 cm specimens and cleaned ultrasonically in nanopure water and in absolute ethanol for 3 minutes to remove large particles from the surface. They were then immersed in piranha solution (a 4:1 by volume mixture of 95% H_2SO_4 and 35% H_2O_2) for 30 minutes at 25 °C to remove organic contamination and to increase the number of hydroxyl groups on the substrate surface (the reader should note here that piranha solution can be extremely dangerous and should be handled very carefully as it may result in skin burns). After being rinsed several times with nanopure water and absolute ethanol, the specimens were dried with nitrogen gas. After the surface cleanness (see below) was confirmed using XPS, the cleaned silicon wafers were stored in a high-vacuum chamber where the base pressure was kept at ~10^{-6} torr.

Immediately after cleaning, XPS survey and high-resolution scans were

performed on the silicon surfaces to reveal the effect of the cleaning procedure on the substrate cleanness: the decrease in the C 1s intensity (from 19.9% to 7.3%) in the XPS spectrum of the clean silicon, shown in the top panel of Figure 2.5, compared to the survey scan XPS spectrum of the as-received silicon (*see* Figure 2.1), indicates that the overlayer of carbon contamination is minimized, while the increases in the O 1s intensity (from 37.3% to 40.9%) and the Si 2p intensity (from 42.8% to 51.8%) reflect the high density of hydroxyl groups exposed on the substrate surface. As a final remark, we note that a small but persistent amount of carbon is always present on silicon surface as an indication of environmental contamination. Exposure to air makes it impossible to prevent such trace contamination on silicon surface.

Passivation

In order to prevent antibodies from adsorbing to regions on the silicon surface where they are not wanted, the method developed by Papra *et al*. [53] was applied to passivate silicon surfaces prior to patterning. As described in their report, the method relies on depositing low molecular weight (460−590) poly(ethylene glycol) (PEG) molecules on silicon surface by liquid-phase self-assembly via covalent coupling using the single-step procedure depicted in Figure 2.4. Upon the condensation of PEG-silane on the surface, one of the three methoxy ($-OCH_3$) groups of PEG molecules interacts with a hydroxyl (−OH) group at the substrate surface and a stable −Si−O−Si− covalent linkage is produced [54]. As opposed to the other common passivation methods, which involve two or more deposition steps, this method offers stable, smooth, and homogeneous surface coverage with a PEG monolayer with a thickness ranging from 10 to 17 Å [53].

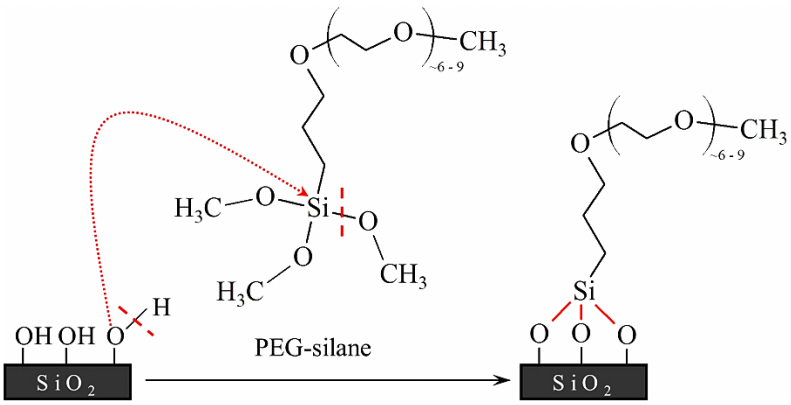

Figure 2.4. Coupling reaction of PEG-silane molecules on clean silicon wafer surface. The solid red lines represent new bonds formed in this reaction. Statistically, a more realistic picture would show only one of the three bonds of the silane molecule coupling to the surface.

The adhesion of antibodies to locations outside the patterned areas of the silicon surface is not desirable, since this can cause the indiscriminate immobilization of antibodies in these areas and result in a false quantification of captured bacteria [14]. The covalent coupling of PEG molecules to silicon surfaces is a suitable choice for preventing this for two reasons. First, these molecules, if properly deposited, are known to have protein-repellent characteristics in aqueous environments. Although the mechanism of repulsion is unclear [54], PEG has been found to be the most effective protein-repellent polymer. Second, covalently coupled PEG molecules are expected to be more stable in aqueous environments. Hence, for prolonged incubation times little or no loss in functionality of PEG films is expected [55].

In our experiments, freshly cleaned silicon wafers were soaked in a 3 mM solution of PEG-silane in toluene with 80 μL of added concentrated hydrochloric acid (HCl) as a catalyst for 90 minutes at 25 °C. Following rinsing with nanopure water and absolute ethanol, the modified chips were dried with nitrogen gas, analyzed with XPS,

and stored for further use in a high-vacuum chamber where the base pressure was kept under 10^{-6} torr.

Immediately after PEG deposition, it is very useful to perform XPS survey scans to ascertain the presence of PEG molecules on the surface of the silicon substrate. For example, the survey scan spectra for cleaned and PEG-modified silicon surfaces depicted in Figure 2.5 clearly illustrate the C 1s and Si 2p intensities of the silicon surface before PEG deposition (top panel) and after PEG deposition (bottom panel).

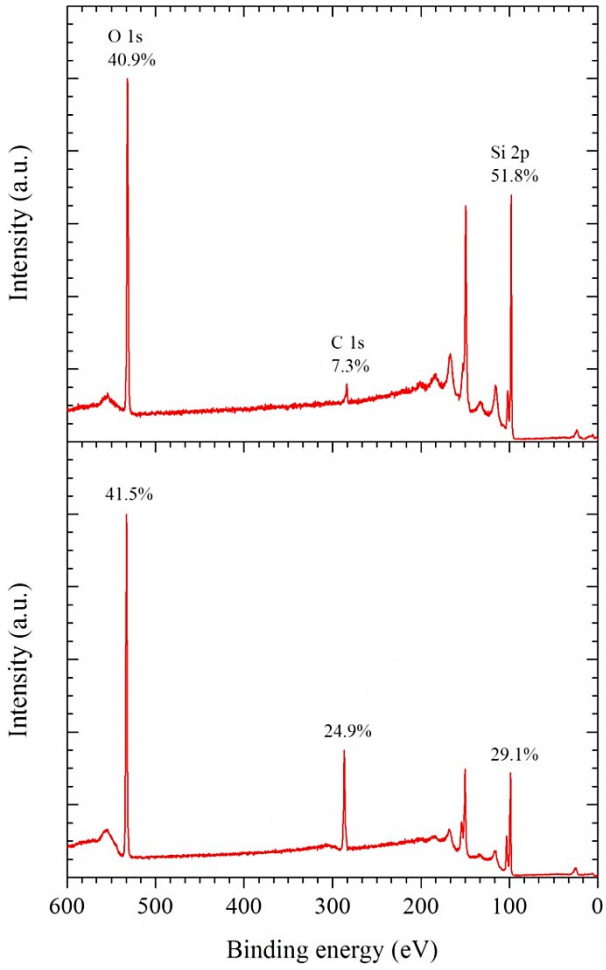

Figure 2.5. Survey XPS spectra of cleaned (top) and PEG-modified (bottom) silicon wafer surface from 0 to 600 eV. Notice the increase in C and the decrease in the Si signal following PEG modification.

As can be seen, there is a sharp increase in the C 1s peak (from 7.3% to 24.9%) and a decrease in the Si 2p peak (from 51.8% to 29.1%) for the PEG-modified silicon surface, suggesting the successful deposition of PEG molecules onto the silicon surface. The slight increase in O 1s (0.6%) is attributed to the oxygen atoms in the PEG molecule.

A typical high-resolution C 1s spectrum of PEG-modified silicon is shown in the bottom panel of Figure 2.6.

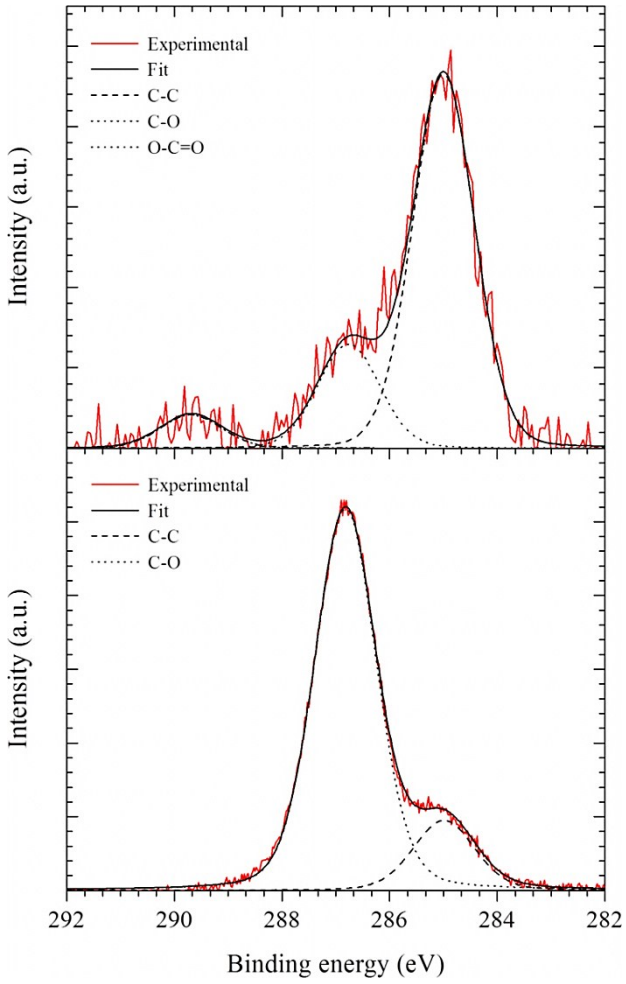

Figure 2.6. High-resolution C 1s spectra of clean (top) and PEG-modified (bottom) silicon wafer surface. The experimental spectra are plotted as solid red lines, and the fitted spectra are plotted as solid black lines. The peak assignments of various oxidation states of C are indicated in the figure.

After the background was subtracted, the C 1s peak was resolved into two components. The intense peak (compared to the C 1s spectrum of the clean silicon in the top panel) at 286.8 eV (84.5%) is attributed to the carbon in the C−O bonds of the PEG molecules and is a characteristic of successful PEG coupling to silicon surface [55]. The smaller peak at 285.0 eV (15.5%) is related to the carbon in C−C bonds which are apart from PEG's silane terminal groups [54]. As discussed earlier in this chapter, the presence of this peak also indicates, to some extent, the hydrocarbon contamination of the sample surface which, as a matter of fact, is found in all samples, including clean silicon. Finally, the absence of the carbon peak at 288.9 eV (labeled as the O−C=O peak) on PEG-modified silicon surface is not significant.

Patterning

While establishing methods for the quantification of immobilized bacteria, it is important to have antibody patterns with clearly defined regions [14]. For accurate estimation of the detection limit and the time required to achieve it, it is essential that only the patterned areas on silicon surface be available for bacterial immobilization. Thus, a reliable method for effectively removing preselected portions of PEG-passivated areas so that these sites are available for the deposition of an antibody-binding layer, and hence for antibody attachment, is needed.

In our experiments, the microfocused Ga^+ beam of a ToF-SIMS instrument was used to remove preselected portions of the PEG layer from silicon substrates so that patterned areas with a size of $100 \times 100\ \mu m^2$ were created. The bright area in Figure 2.7 corresponds to such a pattern.

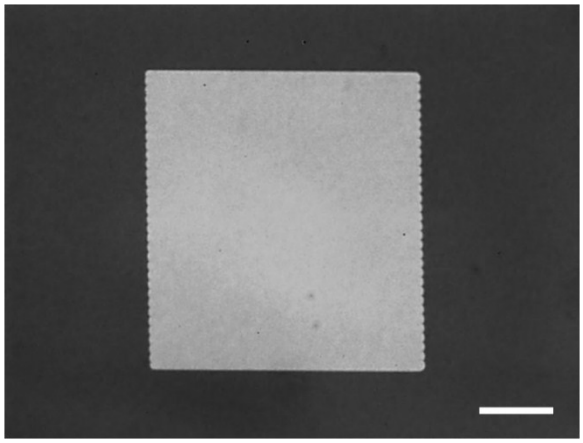

Figure 2.7. A 100 × 100 μm^2 pattern (bright area) etched on a silicon wafer surface using a ToF-SIMS focused ion beam. The scale bar is 25 μm.

To ensure effective removal of the PEG layer, careful adjustment of the etching time was carried out by measuring the depth of 18 × 18 μm^2 areas using tapping mode AFM as a function of sputter time. Figure 2.8 shows such a calibration curve.

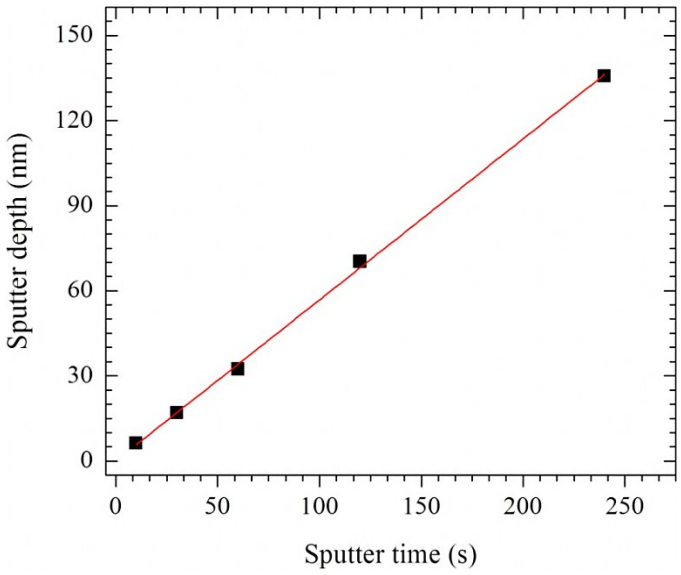

Figure 2.8. ToF-SIMS sputter depth calibration on Si wafer. The red line represents the linear least-squares fit to the experimental data. From the slope, the sputter rate of the ion beam on the silicon surface was determined to be 0.59 ± 0.01 nm/s. Thus, for all samples the etching time for creating 100 × 100 μm^2 patterned areas on silicon surfaces was chosen to be 10 seconds so that only a very thin layer (approximately 20 Å) of the substrate would be removed.

Once these areas are patterned they are available for the covalent attachment of antibodies to the substrate. The method for immobilizing antibodies on the substrate relies on the execution of linker chemistry using silane and coupling molecules: one end of the linker is anchored to a patterned area of the silicon surface while the other end is linked to an antibody, all via covalent bonds. Meanwhile, the PEG-modified regions of the surface are immune to chemical reactions, including all the linker chemistry steps, so ideally the passivated regions are expected to be unaffected by the chemical reactions taking place on the etched areas. The basic design of covalently attaching antibodies to patterned areas of silicon surface through linker molecules is depicted in Figure 2.9.

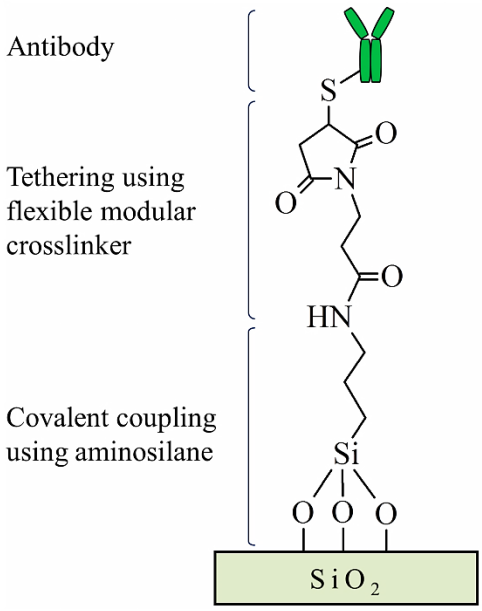

Figure 2.9. Elementary steps associated with the linker chemistry of immobilizing antibodies on patterned silicon wafer surface.

The ultimate goal of this design is to produce a high-density antibody-binding layer on patterned areas of a silicon substrate that has long-term stability in aqueous environments. As we will demonstrate later in this thesis, this approach allows antibodies

to retain their antigen-binding activities for prolonged incubation times in solution. The following two sections of this chapter are devoted to details of the attachment of linker molecules to silicon surfaces. XPS was used mainly to characterize silicon surfaces quantitatively after each chemical treatment.

Self-Assembly of APTES on Silicon Surfaces

APTES is currently one of the most commonly used aminosilanes for preparing SAMs through the silanization process on silicon surfaces having a layer of adsorbed water [56]. APTES can be introduced onto the surface in either of two ways: either by vapor deposition—a vacuum is created on APTES by suction, which is allowed to evaporate and condense on the surfaces of interest—or by insertion of the surface into a low APTES concentration (~0.5 wt. %) solution of a fairly pure (99.5%) organic solvent, such as toluene. We have tried both approaches, but most of the work in this thesis was conducted using the organic solvent approach. The chemical reactions described in this section involve hydrolysis reactions with water, either the water adsorbed on the solid substrate surface or the trace water dissolved in the toluene.

The APTES molecule has three ethoxy ($-OCH_2CH_3$) groups attached to a silicon atom. Through hydrolysis, one of these ethoxy groups is cleaved to allow the Si on the APTES to form a covalent bond with a hydroxyl ($-OH$) group on the substrate surface to produce a stable $-Si-O-Si-$ linkage. The reactive amine ($-NH_2$) group at the opposite end of the APTES can interact with an appropriate linker molecule to facilitate the attachment of an antibody to a flexible tether molecule. Upon deposition, therefore, it is desirable to have these amine groups directed away from the surface (Figure 2.10).

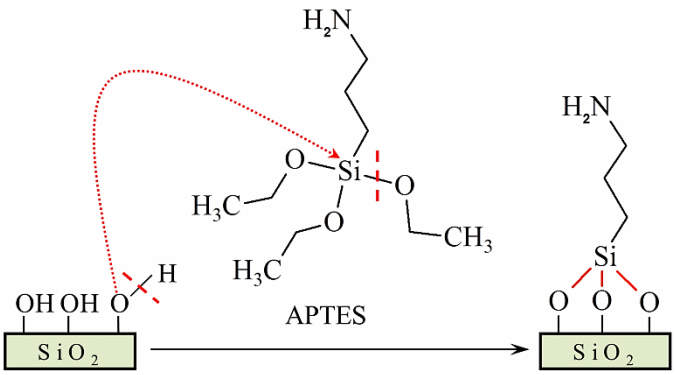

Figure 2.10. Coupling reaction of APTES with an amine terminus on clean silicon wafer surface. The solid red lines represent new bonds formed in this reaction.

In the presence of water, however, these amine groups have a tendency to interact with surface hydroxyl groups and neighboring silane molecules via covalent, hydrogen, van der Waals and electrostatic interactions. This results in polymerization of the APTES both in the vertical and the horizontal directions [57]. The amine moieties tend to incorporate protons from the environment, forming protonated ($-NH_3^+$) groups [56]. The polymerization of APTES molecules is problematic during the preparation of silane films, since the availability and reactivity of the surface amine groups are crucial to many applications, including the construction of the bioactive areas presented in this thesis. In addition, hydrogen bonding interactions with the surface hydroxyl groups may result in weakly attached silane moieties on the silicon surface, which in the long run may lead to the loss of adhesion of the aminosilane films [57].

Under ideal conditions the reaction mechanism leading to the formation of SAMs on a substrate during the silanization process with APTES takes place in four steps (*see* Figure 2.10). First, APTES molecules are physisorbed onto a hydrated surface. Second, the silane ethoxy (EtOH) groups are broken in the presence of water nearby through the

process of hydrolysis. Third, these broken bonds lead to the formation of silanols (−Si−O−Si−) on the substrate surface. Fourth, the silanols, through further interaction with the neighboring molecules, give rise to a polysiloxane network in the plane of the substrate [58].

The self-assembly of APTES in the liquid phase on various substrates has been widely studied [59-63]. The stability of these SAMs is crucial to the overall immuno-immobilization process. Hence, a large number of studies have been reported on the quality of this APTES layer and its dependence on the organic solvent, trace water content, silane concentration, incubation time and reaction temperature. Annealing at elevated temperatures in air has also been shown to affect the end quality and structure of the adsorbed layer [59, 62]. It has been speculated that annealing silanized surfaces for a period of time (~1 hour) immediately after the silanization process improves the silanization because of (a) heat promoting the conversion of protonated groups to reactive amino groups [64] and (b) heat liberating the loosely bound protonated groups through evaporation [56]. Longer annealing times and annealing at higher temperatures, on the other hand, have been reported to cause reduction of the amine groups through oxidation [60, 64].

In our experiments, APTES SAMs were prepared by placing patterned silicon samples in a toluene solution containing 0.5 wt. % APTES molecules for 45 minutes at 25 °C, similar to the procedure described in reference [59]. After silanization, the substrates were sonicated in absolute ethanol for 5 minutes to remove loosely bound APTES molecules from the surface, dried with nitrogen gas and placed in an oven for 30

minutes at 100 °C. Surface characterization using XPS was carried out after sample cooling. In addition, the overall long-term stability of these samples in an aqueous environment was investigated by immersing them in PBS buffer for 24 hours at 25 °C. Ellipsometry was used to characterize the thickness, and contact angle measurements were used to characterize the wettability of APTES films prior to and after immersion. Afterword, silanized samples were stored for further use in a high-vacuum chamber where the base pressure was kept under 10^{-6} torr.

In the deposition of an antibody-binding layer, the initial step of forming amine-terminated surfaces on the silicon substrate is the most critical step. Thus, the ultimate requirement is to have a silanized surface which is stable in an aqueous environment for a long period of time and has as many reactive amine groups as possible. For this reason, several survey scan and high-resolution XPS measurements were performed to confirm the presence of chemical bonding between the APTES and the silicon surface. Figure 2.11 shows the resulting survey XPS spectrum of APTES-modified silicon (bottom panel). The presence of a N 1s peak (3.1%) on the silanized silicon which was not on the clean (unmodified) surface (top panel) reveals that APTES has been successfully introduced onto the silicon surface. Also, the increase in the C 1s peak (from 7.3% to 30.2%) is due to carbon-associated APTES molecules, while the significant decrease in the Si 2p peak (from 51.8% to 33.3%) is consistent with bonding between the ethoxy groups of APTES and the hydroxyl groups of silicon surface. The slight reduction in O 1s (8.1%), on the other hand, is attributed to (a) the presence of the APTES layer on the Si oxide surface and (b) low-level cross-reactivity between APTES molecules [65].

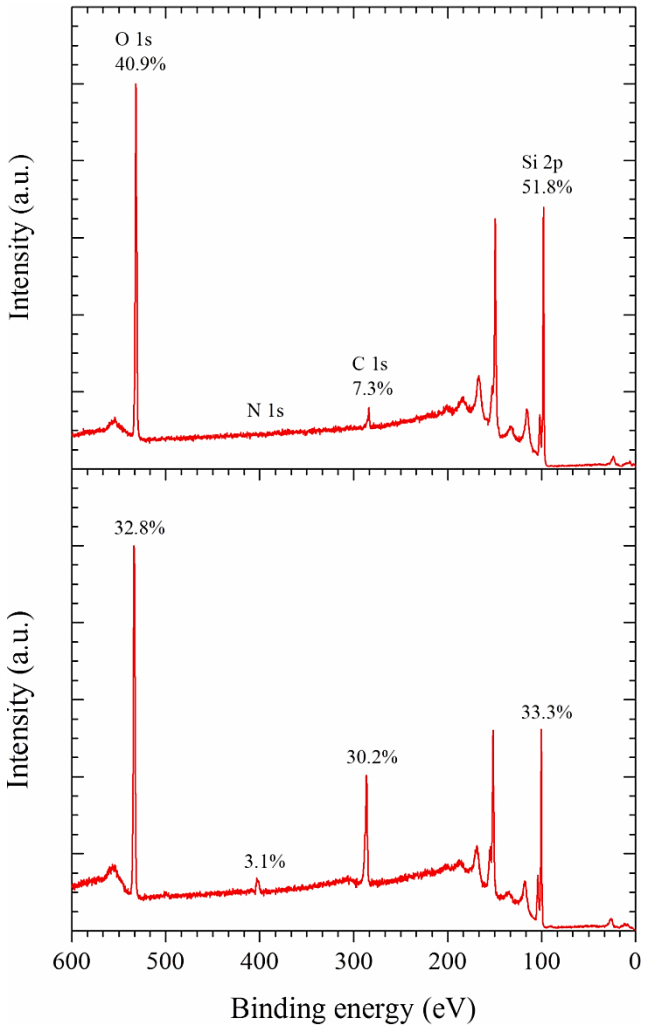

Figure 2.11. Survey XPS spectra of cleaned silicon wafer surface (top) and of silicon wafer surface modified with APTES with an amine terminus (bottom) from 0 to 600 eV.

High-resolution XPS spectra were taken to investigate further the oxidation states of APTES films on silicon substrate. The top panel of Figure 2.12 shows such a spectrum of C 1s which, after the background was subtracted, was resolved into three component peaks: a large peak centered at 285.0 eV (64.5%), a smaller peak centered at 286.4 eV (26.8%), and a well-separated peak centered at 288.5 eV (8.7%) [63, 66].

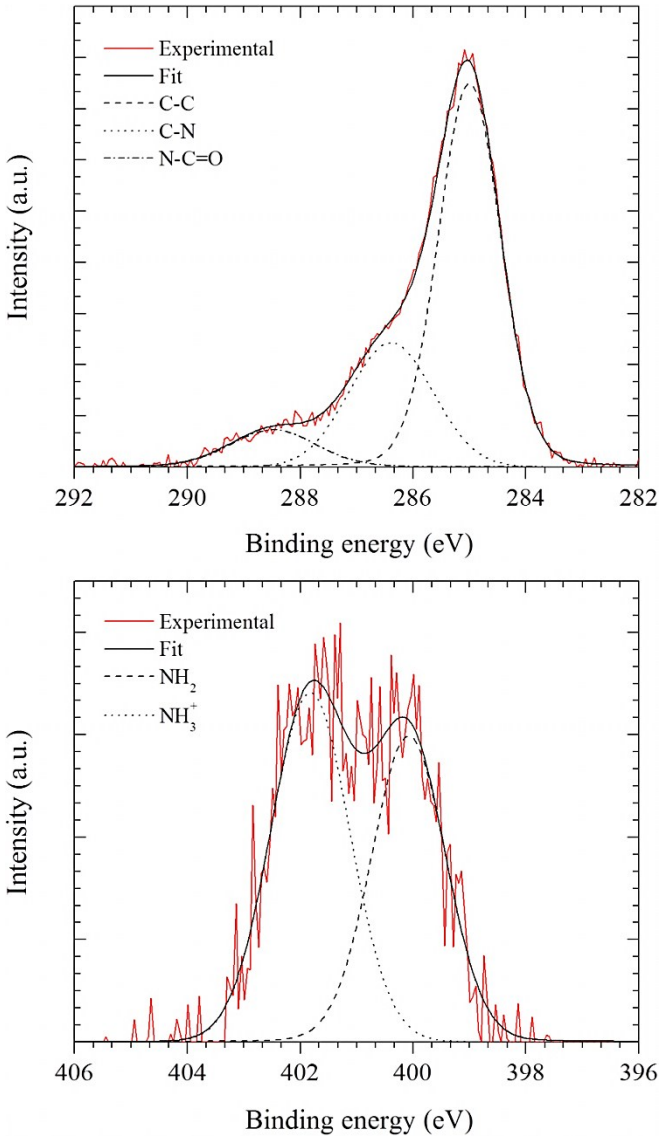

Figure 2.12. High-resolution C 1s (top) and N 1s (bottom) spectra of silicon wafer surface modified with APTES with an amine terminus. The experimental spectra are plotted as solid red lines, and the fitted spectra are solid black lines. The peak assignments of various oxidation states of C are indicated in the figure.

As described previously, the main carbon peak at 285.0 eV is characteristic of the carbon in the C−C bonds of the APTES molecules as well as indicative of hydrocarbon contamination of the sample surface. The peak at 286.4 eV is assigned to carbon in C−N bonds (*see* Figure 2.10). The increasing and broadening of this peak, compared to that of

clean silicon (*see* Figure 2.6, top panel), strongly suggest that the self-assembly of APTES on the silicon surface was successful, although in making a quantitative argument one has to take into account the presence of a small amount of C contamination on the clean surface. Finally, the peak at 288.5 eV is attributed to the formation of N−C=O [65].

Nitrogen 1s is a good indicator of successful silane deposition. Hence, analysis of the N 1s spectrum supports the conclusion reached from analyzing the C 1s spectrum regarding the success of the APTES deposition. As shown in the bottom panel of Figure 2.12, the N 1s spectrum has two peaks, centered at 400.1 eV (45.4%) and 401.8 eV (54.6%), indicating the presence of the nitrogen atoms of APTES on the silicon substrate [63, 66]. The peak at 400.1 eV is assigned to the nitrogen in the reactive amine ($-NH_2$) groups. This peak is used to monitor subsequent modifications of silicon substrate with BMPS. It is reactive to biomolecules because of its lone pair of electrons [67]. The peak at the higher binding energy is attributed to protonated nitrogen ($-NH_3^+$) groups and is not reactive [58]. The two peaks are separated by ~1.7 eV, in agreement with the published literature [63].

The presence of protonated groups on the silanized silicon surface suggests that not all ethoxy groups of APTES molecules react with the hydroxyl groups of silicon surface. This observation is also consistent with the high ratio of the relative atomic concentrations of C 1s and N 1s, shown in the bottom panel of Figure 2.11. The ellipsometry measurements revealed that the ~0.8-nm measured thickness of the silane film (Table 2.2) was consistent with previously published results for an APTES monolayer [59]. These observations, together with the ~1:1 ratio of the two resolved peak

areas of N 1s, suggest that there is no vertical polymerization of the APTES on the silicon surface but rather that there is horizontal polymerization, indicating inhomogeneity of the silane layer. The decrease of the thickness of the silane layer to ~0.5 nm after immersion in PBS for 24 hours at 25 °C (*see* Table 2.2) clearly indicates that there is a loss in the thickness of the layer due to the detachment of weakly coupled silane molecules from the silicon surface; this leaves a more homogeneous and robust layer on the substrate surface.

Exposure to PBS	*Thickness (nm)*	*Contact Angle (deg)*
Before	0.8 ± 0.1	64.6 ± 1.9
After 24 hours	0.5 ± 0.1	59.4 ± 2.1

Table 2.2. Thickness and water contact angle measurements of APTES layers before and after exposure to PBS for 24 hours at 25 °C.

This hypothesis is further supported by the contact angle data given in Table 2.2 for silanized silicon samples before and after immersion in PBS, although the 64.6° water contact angle measured for silanized silicon surfaces before immersion constitutes a discrepancy with previously published data. It has been reported that because of the hydrophilic nature of the reactive amine groups of APTES, contact angles of < 15° are expected for well-organized monolayers with amine groups pointing away from the surface [58, 68]. However, in their study Firestone *et al*. [69] reported a large contact angle (75°) for silanized surfaces and they attributed this to a densely packed, highly ordered silane film. In any case, the observed contact angle of 59.4° after immersion in PBS suggests that the loss from the silane layer is due to the detachment of loosely bound amine groups of the APTES. This leaves its undetached reactive amine groups available

for further BMPS modification, as is explained in the next section.

Treatment of Amine-Terminated Surfaces with BMPS

Heterobifunctional cross-linkers are often used as tether molecules to attach proteins to amine-terminated surfaces covalently. These molecules, if properly deposited, serve as (a) flexible modular cross-linkers between the antibodies and the silanized silicon surface and (b) physical spacers which provide freedom of motion to the tethered antibodies, facilitating antibody-antigen interactions [70]. A number of cross-linkers are commercially available, with each molecule synthesized for specific end groups for use in protein conjugation [71]. We use the ones having an end group reacting with amines on one end and an end group reacting with sulfhydryl groups on the other. BMPS is an example of such a linker molecule, and throughout the course of this work BMPS is used as an intermediate linker molecule forming a rigid covalent bridge between the amine-terminated APTES on the surface and the sulfhydryl groups on antibodies.

The deposition of BMPS molecules on amine-terminated silicon substrates relies on the fact that the two reactive groups within the molecule are designed for site-specific coupling. The succinimide group (bottom end of BMPS in Figure 2.13) is specifically designed to couple with the reactive amino groups of silane molecules through an amide (N−C=O) linkage (*see* Figure 2.13), leaving the moiety of the other end (the maleimide group) available to couple with the sulfhydryl groups of proteins (such as antibodies) through a thiol (C−S) linkage (*see* Figure 2.9). As stated clearly by Mattson *et al*. [71], in aqueous environments the succinimide group of the BMPS molecule hydrolyzes more rapidly than its counterpart, thus reacting faster with the surface silanols.

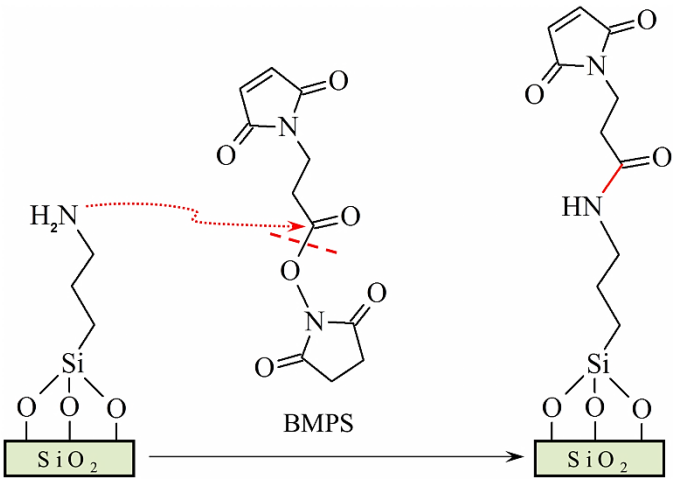

Figure 2.13. Coupling reaction of BMPS on amine-terminated silicon wafer surface. The solid red line represents a new bond formed in this reaction.

Also, according to Partis *et al*. [72] the interaction between maleimide groups and sulfhydryl groups tends to be very specific and rapid (1000 times faster than the interaction between maleimide groups and the N-terminal groups of proteins) at neutral pH and below. Consequently, the use of BMPS provides an excellent route to tethering antibodies covalently to silanized silicon substrates in an oriented fashion and at high concentrations [22, 25]. Additional considerations [71] in choosing this cross-linker include its stability below pH 7.5 [73], its simplicity, and its rigidity (spacer-arm length of 5.9 Å).

In our experiments, following the formation of the APTES layer on the silicon surface, the silanized substrates were incubated in a solution of BMPS in PBS (3 mg/mL) for 30 minutes at 25 °C [74]. Afterward, samples were thoroughly rinsed with nanopure water and dried with nitrogen gas. Following the surface characterization using XPS, samples were stored until use in a high-vacuum chamber where the base pressure was kept under 10^{-6} torr.

XPS analysis was performed on BMPS-modified silicon surfaces to ensure the presence of maleimide groups, and results are shown in Figure 2.14.

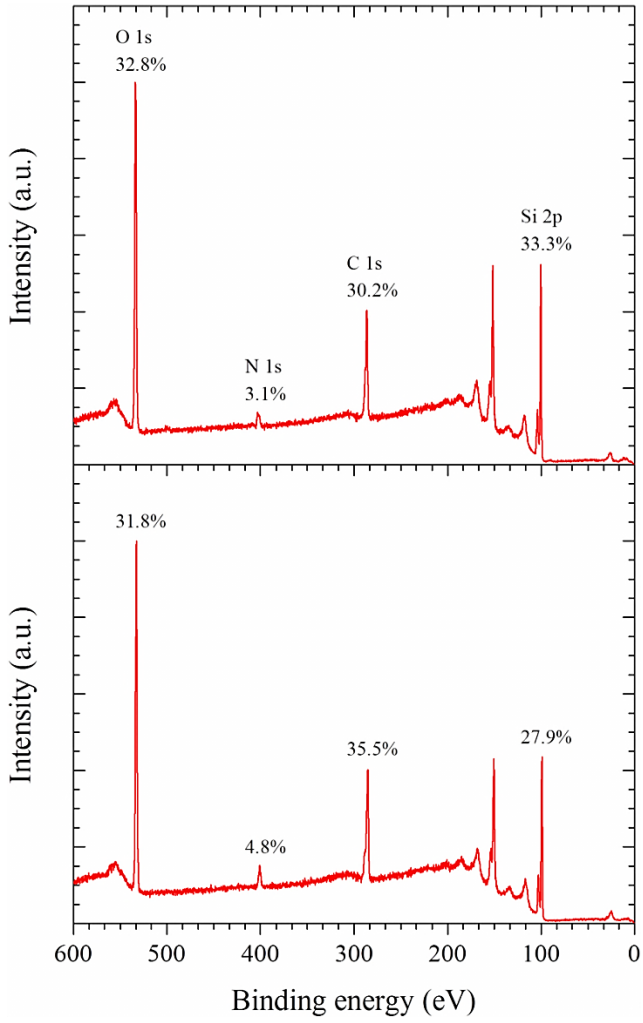

Figure 2.14. Survey XPS spectra of silicon wafer surface modified with APTES (top) and BMPS (bottom) from 0 to 600 eV.

Compared to the survey scan spectrum of APTES-modified silicon in the top panel of Figure 2.14, both the increases in the N 1s and C 1s intensities and the decrease in the Si 2p peak depicted in the bottom panel of the figure demonstrate that BMPS molecules had been successfully introduced onto silanized silicon surfaces.

Figure 2.15 shows high-resolution XPS spectra of C 1s (top panel) and N 1s (bottom panel) after BMPS deposition.

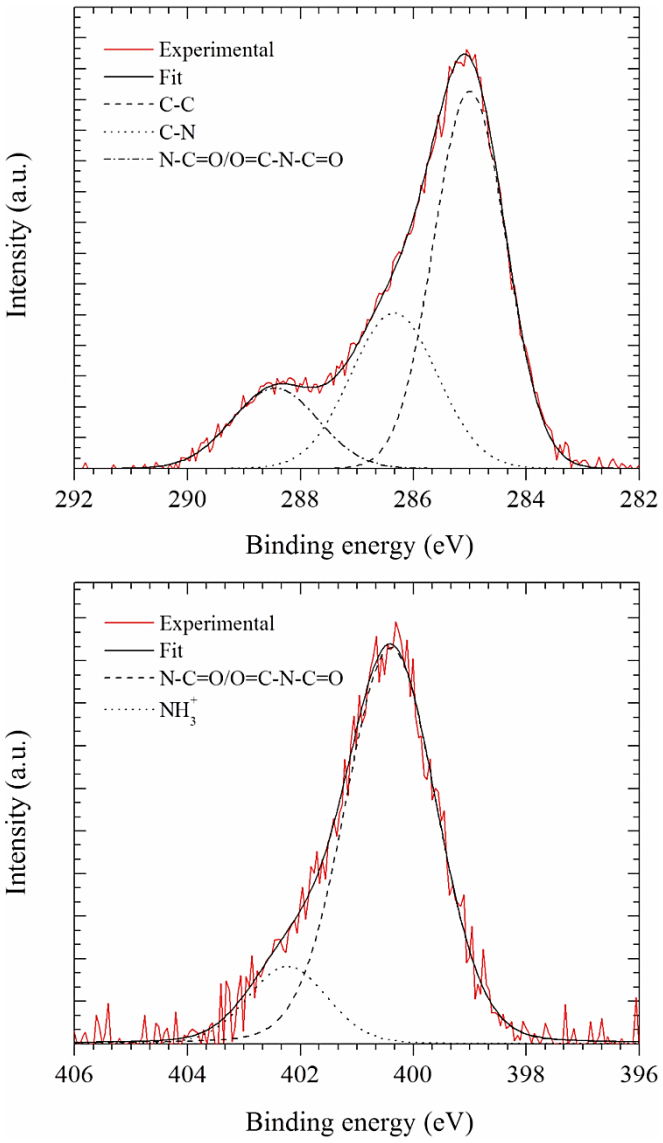

Figure 2.15. High-resolution C 1s (top) and N 1s (bottom) spectra of BMPS-modified silicon wafer surface. The experimental spectra are plotted as solid red lines, and the fitted spectra are solid black lines. The peak assignments of various oxidation states of C are indicated in the figure.

As before, the main peak at 285.0 eV (57.2%) in the C 1s spectrum is assigned to carbon in C−C bonds, while the peak centered at 286.3 eV (28.3%) is attributed to carbon in

C−N bonds. The intense peak around 288.5 eV (14.6%) is characteristic of maleimide groups and confirms the formation of amide (N−C=O) and imide (O=C−N−C=O) bonds. The ~3.5-eV difference between this peak and the main carbon (C-C) peak is very close to previously reported values [65]. N 1s, on the other hand, shows two different peaks. The more intense and broadened peak at 400.4 eV (85.5%) points to the presence of maleimide groups on the sample surface, as expected. The ~0.3-eV shift in this peak compared with the $-NH_2$ peaks in silanized samples (*see* Figure 2.12) is attributed to the formation of amide and imide bonds. Here, the more electronegative N shifts the peak toward a higher binding energy than the C−N bonds in the amine groups [65]. The second peak at 402.2 eV (16.1%), however, indicates the presence of $-NH_3^+$ groups on the sample surface, which remained intact.

Antibody Immobilization

Our aim in developing the chemistry for covalently bonding antibodies onto patterned areas of silicon substrates was to decorate these patterns with antibodies at a high density while preserving the activity of the antibodies towards the bacterial antigens against which they were raised. Our expectation is that antibodies immobilized in this way will maintain a high binding efficiency with antigens via antibody-antigen interactions involving both arms of the Y-shaped antibodies [26] so that an ideal immobilization efficiency and density of bacterial cells can be achieved. As described previously, maleimide-activated surfaces tend to interact rapidly with the sulfhydryl groups of antibodies at neutral pH and below; thus they offer a good strategy for the site-directed immobilization of antibodies onto patterned silicon surfaces. In this protocol, the

double bond in the C=C group of the maleimide moiety of a BMPS molecule (*see* Figure 2.13) undergoes a selective reaction with the sulfhydryl group present in the lower portion of the antibody's Fc region, which leaves the two antigen-binding arms (Fab region) of the antibody oriented towards the sample surface [75]. As a result, the antigen-binding sites (i.e., paratope) located in the Fab region of the antibodies are available and free to interact with the corresponding bacterial antigens (*see* Figure 2.9). An added advantage of using BMPS molecules is their rigidity, which results in a well-oriented and stable antibody layer on the substrate surface [69].

In our experiments, mostly polyclonal anti-CFA/I antibodies were used to demonstrate the effectiveness of the immunoimmobilization method discussed in this thesis. These antibodies were affinity-purified towards the CFA/I antigen of *S.* Typhimurium [14]. This means the majority of the proteins in the antibody solution were CFA/I antibodies. In choosing an antibody against a surface antigen, purity of the antibody is highly desirable.

In the final step of substrate preparation, concentrated antibody solutions were first diluted to 100 times (1 μg/mL) using PBS. Afterward, they were deposited onto maleimide-activated surfaces as ~2-μL droplets by means of micropipettes for 45 minutes at 25 °C. During this time, samples with antibody droplets were kept in a humidity chamber in order to (a) allow the covalent linking of the antibodies, and (b) prevent evaporation of the antibody solution. Finally, the excess antibody solution was removed from the surface by washing the samples with PBS. Specimens prepared thus far were then kept in PBS in petri dishes for further bacterial incubation.

Figure 2.16 shows the survey XPS of an antibody-covered surface which was incubated onto a maleimide-activated surface using 1 μg/mL of antibody solution.

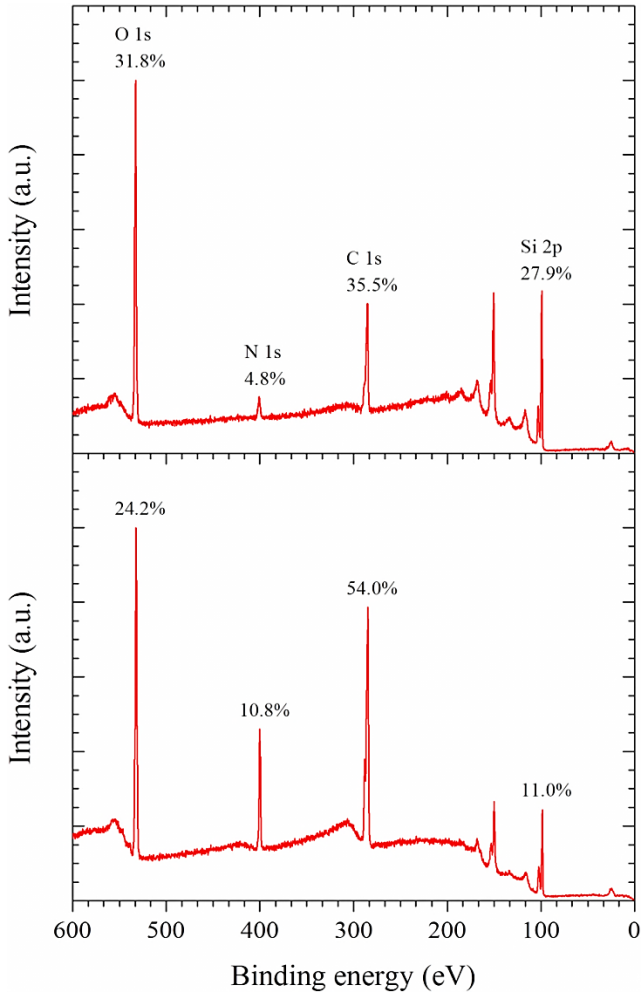

Figure 2.16. Survey XPS spectra of silicon wafer surface modified with BMPS (top) and anti-CFA/I antibody (bottom) from 0 to 600 eV.

Compared to the survey scan spectrum of BMPS-modified silicon in the top panel of Figure 2.16, we observe increases in the N 1s (from 4.8% to 10.8%) and C 1s (from 35.5% to 54.0%) intensities as well as decreases in the Si 2p (from 27.9% to 11.0%) and O 1s (from 31.8% to 24.2%) peaks, depicted in the bottom panel of Figure 2.16. This is consistent with the presence of antibodies on maleimide-activated silicon surfaces.

High-resolution XPS spectra of C 1s (top panel) and N 1s (bottom panel) after antibody immobilization are shown in Figure 2.17.

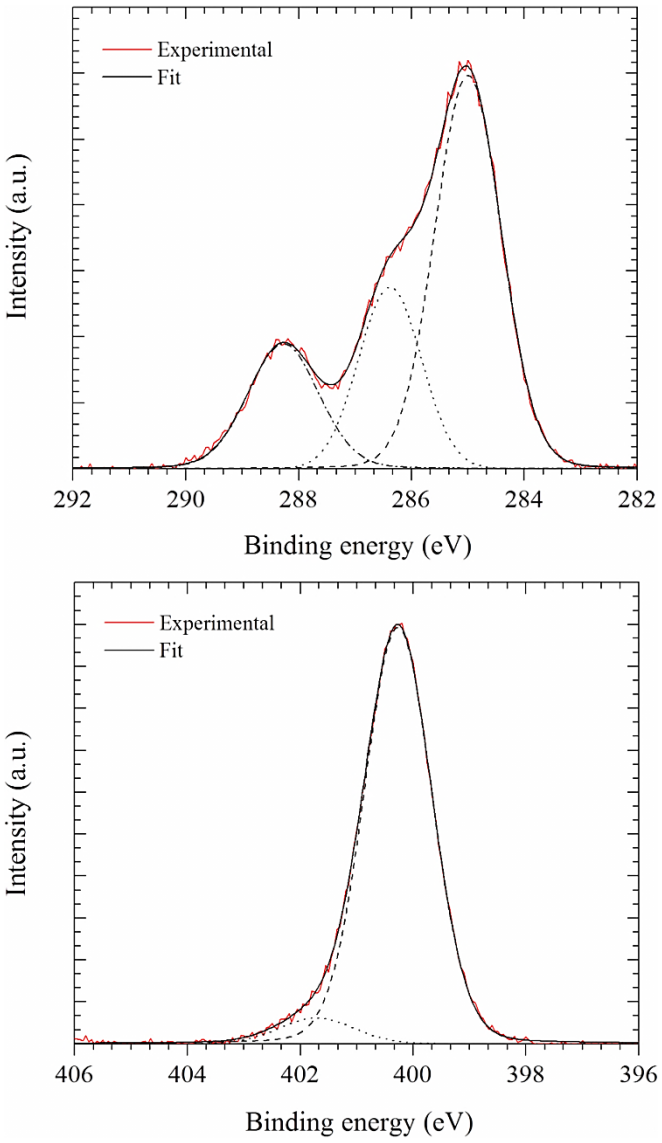

Figure 2.17. High-resolution C 1s (top) and N 1s (bottom) spectra of silicon wafer surface modified with anti-CFA/I. The experimental spectra are plotted as solid red lines, and the fitted spectra are solid black lines.

Here, no significant chemical shifts from BMPS-modified surface are observed. However, the significant increases of the relative peak areas of N 1s at 400.3 eV and of

C 1s at 288.3 eV show the successful attachment of antibodies through maleimide groups of BMPS. The presence of a relatively small peak at 401.7 eV, on the other hand, is attributed to the protonated amines of the silanized surface, suggesting that the antibody layer is not fully covering the surface. Finally, the amounts of sulfur present in C−S bonds between the maleimide groups of the BMPS and the sulfhydryl groups of the antibodies are very negligible and thus not detectable using XPS [61].

Antibodies are costly to produce, and the amounts available are limited. This is why one needs to verify that the antibody solution is sufficiently concentrated to provide a full coverage of the antibody, one which will lead to an effective immobilization of bacterial cells on the substrate surface. In this study, the loading capacity, i.e., the amount of saturated antibody adsorption, on maleimide-terminated surfaces was monitored using XPS to ensure that for a given antibody concentration a full coverage of immobilized antibodies on the surface was achieved. In three independent runs under identical conditions of substrate preparation, maleimide-activated silicon surfaces were incubated with series of antibody concentrations ranging from 0.004 to 4 μg/mL, and the atomic concentrations of N 1s were used to track the saturation of the surface as a function of antibody concentration. The findings of this experiment are shown in Figure 2.18. It is clearly seen that the surface capacity is saturated at an antibody concentration of ~1 μg/mL. Increasing the solution concentration to 4 μg/mL is simply a waste of valuable antibodies because the extra antibodies in the solution do not improve the surface antibody coverage [76].

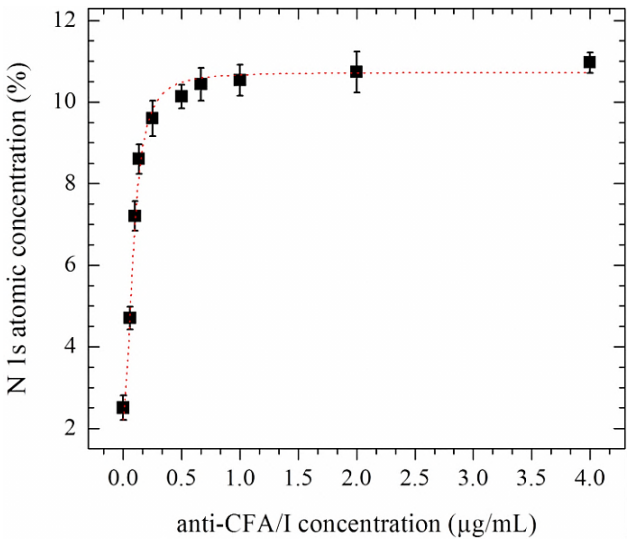

Figure 2.18. Determination of the antibody-loading capacity of the maleimide-activated silicon wafer surface. The graph indicates the normalized N 1s atomic concentration as a function of the concentration of anti-CFA/I in PBS.

In previous studies no attention was paid to characterizing antibody-activated surfaces for antibody immobilization efficiency. As a result, high concentrations of antibody solutions have been reported for the preparation of surfaces for bacterial immobilization, ranging between 15 µg/mL and 2.5 mg/mL [74, 76-79]. Some of these solutions are more than three orders of magnitude more concentrated than necessary: almost all of the antibodies are simply wasted. Of course, there may be some applications in which higher antibody concentrations are acceptable, such as adsorbing antibodies onto a plastic microtiter plate, where the relatively large ratio of surface area to sample volume allows binding of the excess antibodies [80]. Nevertheless, our experimental data suggest that in the preparation of antibody-activated substrates using the linker chemistry developed in this thesis, a concentration of no more than 1 µg/mL is needed for effective and reproducible immunoimmobilization results.

The existence of a dense antibody layer on the patterned area of a silicon substrate

can be confirmed from a N chemical map acquired with scanning Auger mapping (Figure 2.19). In the image in the left panel we see clearly the 2-D distribution of the antibodies on the activated area. Here, the brightness associated with each pixel is proportional to the local concentration of N on the antibody-modified area of the surface and hence confirms the dense, continuous and homogeneous antibody coverage on the patterned areas of the silicon substrate. Finally, it is worth noting that the passivation outside the patterned areas appears not to be perfect: This is most likely due to the low Auger signal generating a noise background. It could also be due to antibodies finding ways to attach to passivated regions of the silicon surface, either by physical adsorption or via covalent bonding due to imperfections in the passivation of the surface. This has been observed occasionally; however, it is a rare occurrence.

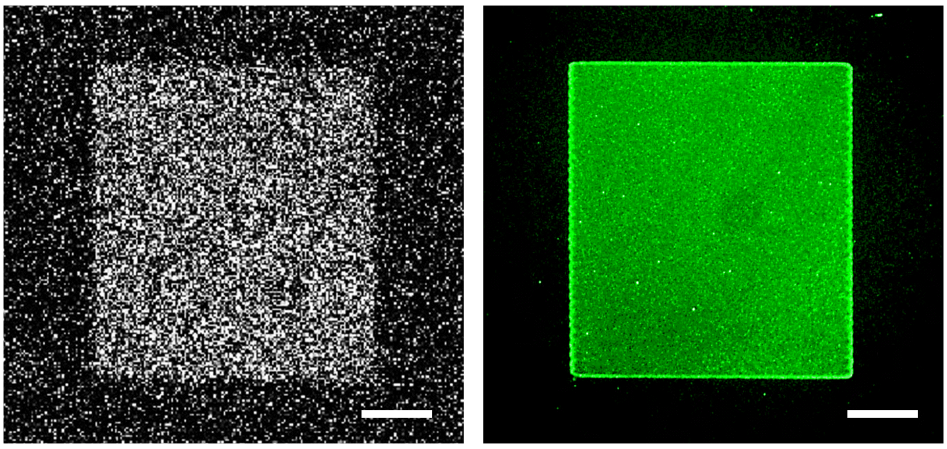

Figure 2.19. Auger N KLL chemical map of a pattern modified with anti-CFA/I antibody (left panel). Antibodies labeled with NHS-fluorescein on the pattern (right panel). The scale bar is 25 μm.

To further verify the surface concentrations and orientations of the antibodies on the patterned areas, we evaluated the accessibility of the antigen-binding sites of the antibodies by labeling them with NHS-fluorescein. A characteristic of this molecule is

that it specifically binds to the Fab arms of the antibody [81]. In our experiments, antibody-activated silicon surfaces were incubated in a solution of 1 mg of NHS-fluorescein in 400 μL of dimethylformamide (DMF) in the dark for one hour at 25 °C to allow covalent linkage between the succinimide groups of the NHS-fluorescein and the N-terminal groups of the antibodies located in the Fab region. Following this, the samples were washed with water to remove loosely bound dyes. Subsequently, specimens were immersed in dye-free water in petri dishes and analyzed with an optical microscope in epifluorescence mode using FITC. The green fluorescence signal in the image shown in the right panel of Figure 2.19 clearly indicates that antibodies have been reliably immobilized with high density and specificity on the patterned regions (green areas). As expected, the passivated regions on the silicon surface (black areas) exhibit little or no specific or nonspecific antibody binding.

To conclude, simple, effective, reproducible, and reliable linker chemistry with a three-step reaction has been developed to link antibodies covalently, with high density and activity, onto patterned areas of silicon substrate. These surfaces are now available for implementing bacterial immobilization.

Bacteria

Selection

The detection of wild-type pathogenic strains of *E. coli* and genetically modified *S. enterica* with antibody-based methods has been extensively reported (*see* Chapter 3 for reference). For this thesis, we particularly focused on live *Salmonella enterica* serovar Typhimurium (*S.* Typhimurium) strain H72-pBBS-cfa and wild-type enterotoxigenic *E.*

coli strain H10407, both of which express CFA/I fimbriae, and used them as model bacteria to demonstrate the *in situ* detection and quantification of these pathogens in aqueous environments (PBS, seawater and Navy fuels). In addition, we used wild-type enterohemorrhagic *E. coli* strain O157:H7 to demonstrate the applicability of the method to quantifying bacteria immobilized with antibodies which target LPS on the bacterial surface. Finally, we used wild-type enterotoxigenic *E. coli* strain 3030-2 expressing F4 (K88ac) fimbriae to demonstrate, together with H10407, the feasibility of the immuno-immobilization method for simultaneously detecting and identifying by sorting the mixed bacterial strains present in fuels. AFM images of these bacterial strains are shown in Figure 2.20.

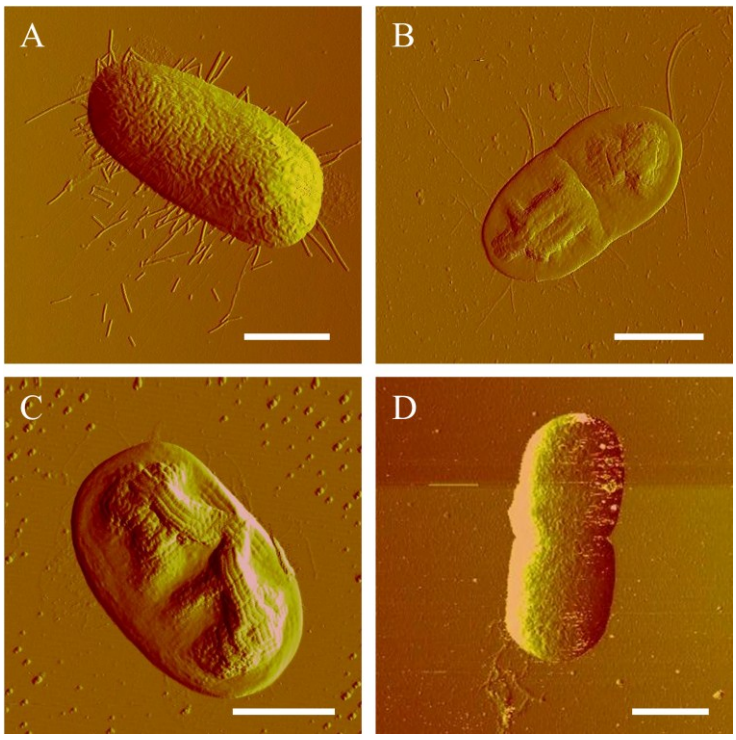

Figure 2.20. High-resolution atomic force microscope images of (A) *S.* Typhimurium H72-pBBS-cfa [14, 15], and of *E. coli* strains (B) H10407 [9], (C) 3030-2 [9], and (D) O157:H7. Panels A, B, and C clearly reveal the fimbriae on the surface of the bacteria. The scale bar is 1 μm.

Growth and Enumeration

Pure bacterial cultures kept as stock at −80 °C were used to inoculate separate Luria-Bertani (LB) plates and grown at 37 °C overnight. Afterward, each isolate was cultured in 3 mL of LB liquid medium and incubated on an orbital shaker (135 rpm) for three hours at 37 °C. Following 10-fold serial dilutions with PBS, the viable cell number in each dilution was determined by spreading 0.1 mL of the diluted solution onto an LB plate for overnight incubation at 37 °C. Dilutions showing at least 30 colonies per plate were used to determine the average viable cell number in cells per milliliter (cells/mL), sometimes referred to as colony-forming units per mL, or cfu/mL.

Immobilization, Detection and Counting

Specific surface antigens associated with common pathogenic strains of *S.* Typhimurium and *E. coli*, such as fimbriae and LPS, and the corresponding antibodies were used for the efficient immobilization of intact, viable bacteria from a culture solution. The capture efficacy of the immunosensor was tested in the following way: first, the immunoimmobilization of live bacterial cells was carried out by pipetting 1 mL of a freshly prepared serially diluted bacterial culture onto an antibody-activated silicon surface under ambient conditions; next, the capturing of bacteria on $100 \times 100\ \mu m^2$ antibody-activated patterns on silicon substrates was evaluated *in situ* using an optical microscope in reflection mode (starting from the first minute of bacterial incubation, optical images were taken every second for 90 minutes); and finally, the manual counting of captured cells in the acquired images was carried out with ImageJ software (National Institutes of Health, USA).

Surface Preparation and Bacterial Immobilization

To investigate the effects of surface characteristics on bacterial immobilization, several experiments were conducted using silicon substrates with different chemical compositions. In these experiments, silicon surfaces were first cleaned, passivated, and patterned according to the procedure described earlier in this chapter. Afterward, 10-fold serially diluted bacterial cultures of *S.* Typhimurium H72-pBBS-cfa (*see* Figure 2.20) were used to inoculate (a) nonmodified, (b) APTES-silanized, and (c) BMPS-activated patterned surfaces, which were incubated with concentrations of about 3×10^7 cells/mL of *S.* Typhimurium for 60 minutes at 25 °C. After the specimens were washed with PBS in petri dishes, they were investigated under an optical microscope in reflection mode. The results are presented in Figure 2.21.

Clearly, for each set of experiments described above the results indicate that only a few sparsely attached cells populated the patterned areas on the silicon surface. We hypothesize [14] that the reason for this failure of direct immobilization (i.e., without the use of antibodies) is that the sites available for nonspecific bacterial capture (unpassivated areas) on the silicon surface are occupied by proteins present in the bacterial culture before living bacteria have a chance to interact with them: under stationary conditions the diffusion coefficient of proteins tends to be much higher than that of bacteria [82]. Since proteins (such as yeast) are always present in bacterial cultures, their complete removal is out of the question. Furthermore, the extracellular polysaccharide (EPS) capsule surrounding each cell will prevent the bacterium from interacting directly and rapidly with such a surface [14].

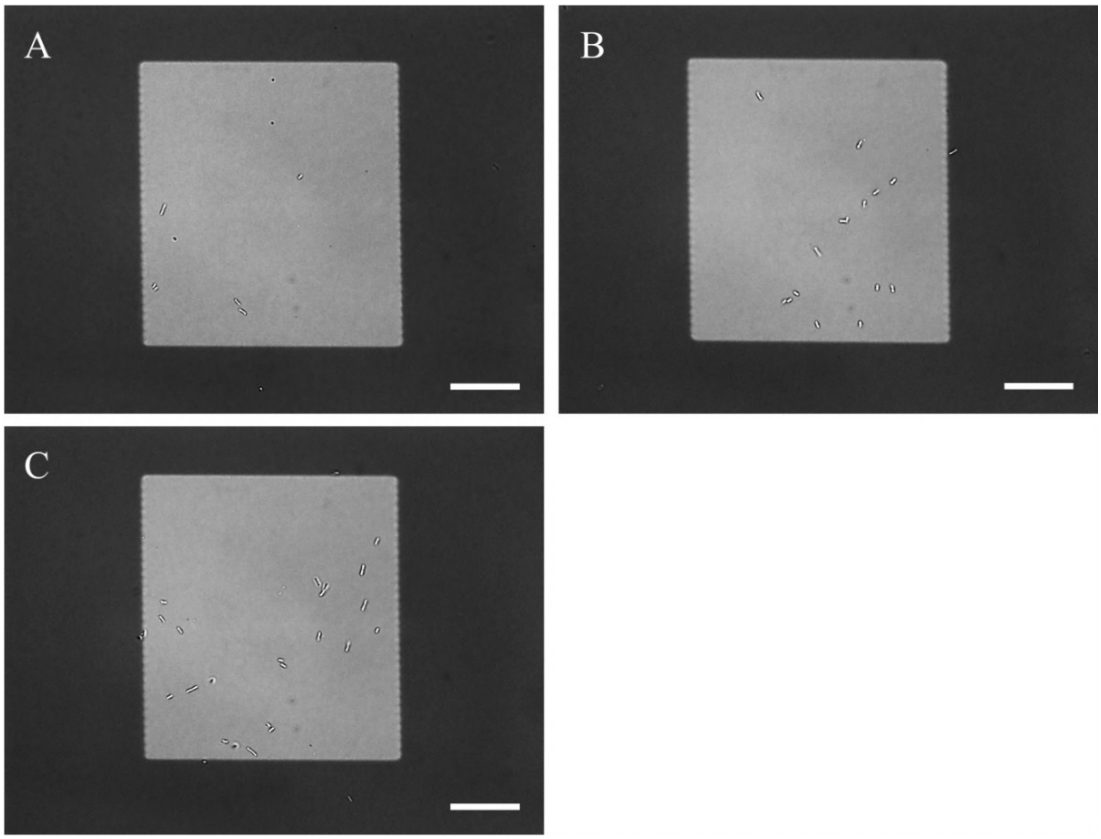

Figure 2.21. Optical images of (A) etched, (B) APTES-modified, and (C) BMPS-activated patterns on silicon substrates after exposure to a concentration of ~3 × 10^7 cells/mL of *S.* Typhimurium for one hour. Only a few sparsely attached cells were observed in each of these patterns, confirming that without an antibody the immobilization of bacteria is not possible. The scale bar is 25 μm.

We also tested the immunoimmobilization efficacy of antibodies immobilized directly onto (a) nonmodified, (b) amine-terminated (after APTES silanization), and (c) maleimide-activated (after BMPS deposition) patterned surfaces. Under identical conditions the samples were incubated with suspensions of 10-fold serially diluted bacterial cultures of *S.* Typhimurium H72-pBBS-cfa for 60 minutes at 25 °C. This corresponds to a cell concentration of ~3 × 10^7 cells/mL. We then analyzed these surfaces under an optical microscope in reflection mode. The results are shown in Figure 2.22.

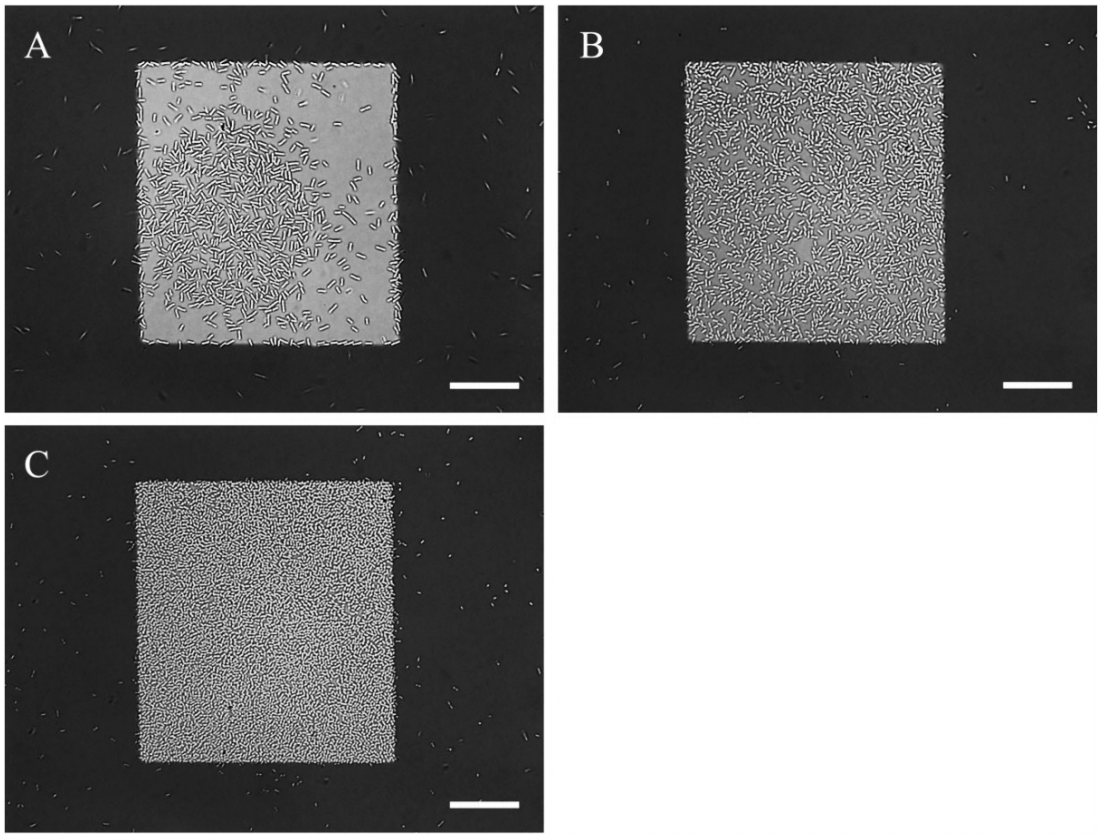

Figure 2.22. Optical images of antibody-activated patterns on silicon substrates exposed to *S.* Typhimurium cells at a concentration of ~3 × 10^7 cells/mL for one hour: (A) antibodies are physisorbed on patterned areas, without linker chemistry; (B) antibodies are covalently linked to APTES-silanized patterned areas, without tether molecules; and (C) antibodies are anchored to APTES-silanized patterned areas using BMPS as a cross-linker. A dense monolayer of bacteria filled the patterned areas when linker chemistry was used to immobilize the antibodies. Panel C clearly demonstrates the ultimate in immunoimmobilization (limited only by the steric hindrance of bacteria), leaving no available space in the activated area for a new organism to attach. In fact, the majority of these organisms are standing up, giving rise to the maximum possible surface coverage [14]. This is the highest coverage density reported [14] in the literature to this date. The scale bar is 25 μm.

It is not surprising that the best immobilization of bacterial cells was achieved with antibodies anchored to maleimide-activated patterned areas (Panel C). As can be seen in the image, a dense monolayer of cells was achieved in these areas, indicating successful antibody immobilization with high density and activity. Furthermore, most of

the cells are standing up and thus packing in the maximum possible number of bacteria per unit area of the monolayer (~7300 cells), which is the highest immobilized cell density reported in the literature to this date [14]. The second best immobilization was achieved with antibodies anchored to amine-terminated patterned areas as shown in panel B. Although the cell density in this case was not as high, this approach can be still be viable in cases where the extra step of coupling antibodies through tether molecules is not desired. Finally, the least effective way of immobilizing bacteria is shown in panel A. In this method antibodies are allowed to adsorb nonspecifically and noncovalently onto patterned areas without linker molecules. As expected, the immobilization of antibodies was the least effective on these areas but was effective nevertheless. Another interesting observation is that the bacteria lined up against the edges of the patterned areas. It seems that the antibodies preferentially and nonspecifically formed a dense layer along these edges. Nonetheless, the results demonstrate that a high density of oriented antibodies on the sample surface is a fundamental prerequisite for the successful immobilization of bacterial cells.

Another consideration which arises from the optical images in Figure 2.22 concerns the attachment of cells to locations outside patterned areas because of the inperfections in substrate passivation. So far we have demonstrated that the majority of cell immobilizations require antibody-antigen interactions at the substrate surface. It is safe to state that almost all the cell immobilizations outside the patterned areas are also due to antibody-antigen interactions (*see* Figure 2.22). This is confirmed by (a) the presence of N 1s on the PEG-passivated regions of silicon following the deposition of the

antibodies using the linker chemistry (*see* Figure 2.23), and (b) movies made of these immobilized bacteria.

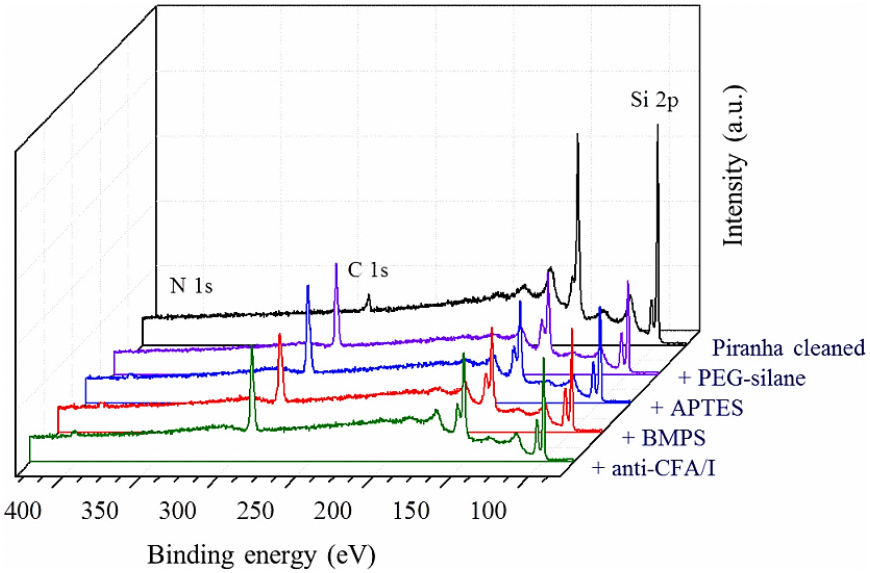

Figure 2.23. Imperfections in passivation: XPS spectra associated with the cleaning, surface passivation, and subsequent exposure to the steps used in the linker chemistry for antibody modification of the passivated area. The variations in N 1s suggest that the PEG-passivated regions of silicon wafer are affected by the chemical reactions associated with antibody activation. However, this is not too serious, as is indicated by Figure 2.22. A very small fraction of the immobilized bacteria are located on the passivated regions.

Moreover, as is shown in Figure 2.24, washing silicon chips with PBS after 60 minutes of incubation does not alter the monolayer formation of cells inside patterned areas where the linker chemistry was applied properly (panel B). However, for substrate with antibodies directly deposited nonspecifically onto patterned areas, the majority of cells are washed away, demonstrating that the attachment is not robust enough to withstand the washing process (panel A).

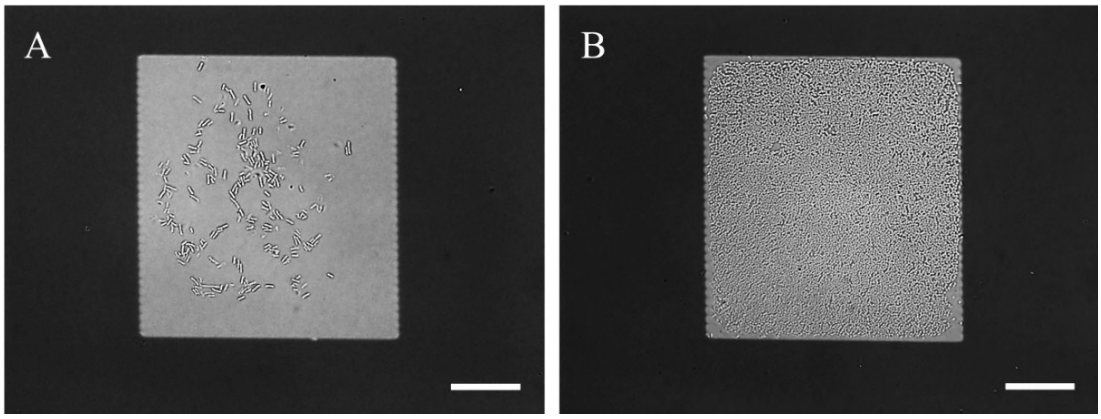

Figure 2.24. Optical images showing the effect of washing on the incubated silicon chips shown in Figure 2.21: (A) cells immobilized by antibodies physisorbed on etched patterns on silicon surface detach during washing, but (B) cells immobilized by antibodies covalently anchored to silicon surface through linker chemistry do not detach during washing, proving that they are attached strongly to the surface. The scale bar is 25 μm.

It is important that we describe the washing procedure to clarify (a) the purpose of washing incubated silicon substrates and (b) the procedure that needs to be followed for the washing to be effective and reproducible. The purpose of rinsing incubated silicon substrates is to remove the excess and loosely attached bacteria from the medium and from the sample surface so that we observe only the remaining cells, which are immobilized through antibody-antigen interactions at the substrate surface. Hence, to prevent any loss of information, the washing procedure should be as follows: after the desired incubation time, samples inoculated with bacterial cultures should be gently rinsed inside their petri dishes by simply introducing ~3 mL of PBS in a counterclockwise circular motion and disposing of the leftover medium from the container. Rinsing incubated samples outside their petri dishes, as described in our previous report [15], is not recommended since taking these surfaces out of the solution will subject the bacterial cells to large surface tensions, which will overcome the

antibody-antigen interaction forces and result in the removal of some of the attached cells from the surface.

Capture Efficiency of Dead Bacterial Cells

Many of the antibody-based systems have been used to quantify captured heat-killed bacterial cells (*see* Chapter 3 for reference). To test this we conducted a series of experiments in which we tested the cell capture efficiency of antibodies deposited onto maleimide-activated patterned surfaces for specimens which were incubated for 60 minutes at 25 °C in 10-fold serially diluted cultures at concentrations of about 3×10^7 cells/mL of *S.* Typhimurium H72-pBBS-cfa which was first killed (a) in a 100 °C oven or (b) with 2% by volume glutaraldehyde solution in PBS buffer. The findings of these experiments are shown in Figures 2.25 and 2.26.

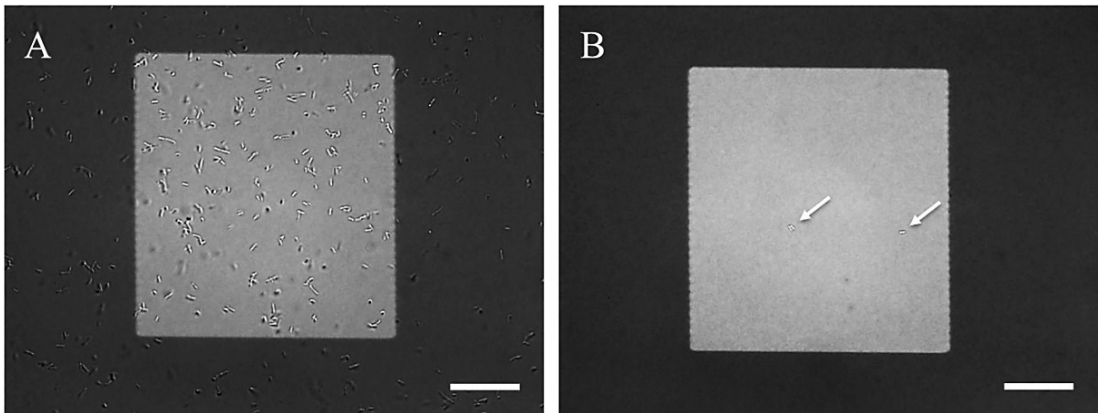

Figure 2.25. Immunoimmobilization efficiency for heat-killed *S.* Typhimurium at a concentration of ~3×10^7 cells/mL that (A) before and (B) after the incubated samples were washed. The attachment of heat-killed cells through antibody-antigen interactions was not robust enough to prevent them from being washed off the surface. The scale bar is 25 μm.

Clearly, the immunoimmobilization method did not work well for heat-killed bacterial

cells, as the patterned area in panel A of Figure 2.25 shows sparsely attached cells. From the image, it is obvious that, compared with the results for live bacteria, only a small fraction of the dead bacteria were successfully immobilized. Furthermore, these cells could not withstand the washing procedure described above, indicating possible detachments of their fimbriae from the cell surfaces (panel B). It is obvious that heat-killed bacteria are not immobilized as effectively as living cells.

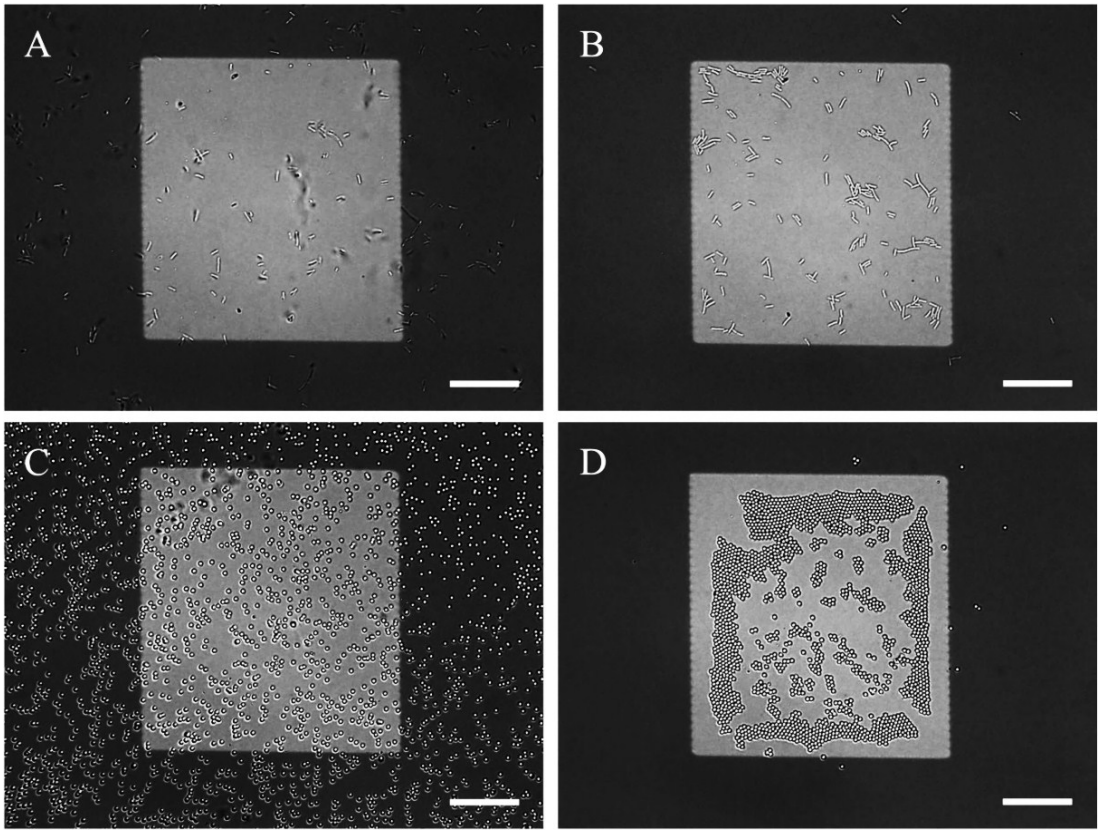

Figure 2.26. Immunoimmobilization efficiency for *S.* Typhimurium cells at a concentration of ~3×10^7 cells/mL that were glutaraldehyde-killed (A) before or (B) after the incubated samples were washed. As opposed to heat-killed bacteria, the attachment of glutaraldehyde-killed cells through antibody-antigen interactions was robust enough to prevent the cells from being washed off the surface. (C) To mimic the experiments with dead bacteria, CFA/I-modified silica beads were allowed to interact with antibody-activated patterns on silicon surface. (D) The accumulation of the beads on the patterned area after washing suggests that the majority of the fimbriae on the surfaces of the beads were effective at preventing the beads from washing off. The scale bar is 25 μm.

The bacteria killed with glutaraldehyde showed comparable results (panel A in Figure 2.26), with the exception that after the samples were washed with PBS there was an accumulation of cells in the antibody-patterned areas (panel B). It is possible that during the washing process some of the planktonic cells in the bulk had a chance to interact with the surface, thus leading to the accumulation of cells in the patterned areas. This behavior was also confirmed for CFA/I-modified silica beads (panel C) that were attached using the linker chemistry and used to mimic killed bacteria. After the samples were washed with PBS, similar behavior was observed on the patterned areas (panel D).

3. DETERMINATION OF INITIAL RATE OF CAPTURE IN THE IMMUNOIMMOBILIZATION PROCESS

Introduction

Currently there is no technique for assessing the rate of cell capture during the immunoimmobilization process for a given antibody-antigen pair of a given strain of bacteria. This chapter describes our method developed to determining this quantity for living *Salmonella enterica* (*S. enterica*) and *Escherichia coli* (*E. coli*) in an aqueous environment under the conditions described in Chapter 2. The quantity we are interested in is the initial rate of attachment in terms of the number of cells immobilized per unit time per unit area per cell concentration in the solution for a given antibody-antigen pair and a given strain of bacteria. Many of the previously reported antibody-based detection methods [74, 76-79, 82-87] rely on correlating the number of cells attached to an activated surface with a signal measured by optical, electrochemical, mechanical, or other means [88]. Although these methods offer great promise for continuous environmental monitoring in real time, there is a possibility, especially at low cell concentrations, that such indirect measurements can lead to false positive results and thus overestimation of the number of cells attached to a surface: environmental contaminants such as sand, clay, and pollen in solution may contribute to the detection signal [89].

Several methods, such as electron [79, 90], optical [74, 78, 79, 85-87], and atomic force [86] microscopy, have been used to confirm positive signals by verifying the presence of captured bacteria on the antibody-modified areas of a substrate surface visually. Prior to imaging, a washing and drying procedure is applied to the samples.

With regard to the limit of detection of the sensor, large uncertainties can be introduced into measurements by variations in the handling and washing off of excess bacteria. As explained in Chapter 2, some of the immobilized cells may be washed off of the surface prematurely if careful attention is not paid during this procedure. Direct approaches based on polymerase chain reaction (PCR) [91] are used to determine the surface density of the cells attached to the sensor surface, without a need for culture or enrichment steps. However, these approaches are unsuitable for field applications since they require extra time and skilled personnel to analyze samples. Most of these determinations have been conducted on heat-killed bacteria; very little published work focuses on quantifying immobilized living bacteria. Furthermore, in all the published work on antibody-antigen-based bacterial capture, antibodies raised against whole bacterial cells were used, which cannot guarantee an optimum efficiency in every case. For example, Premkumar *et al.* [85] exposed anti-*E. coli* activated glass slides to a 2×10^8 cells/mL concentration of live *E. coli* for more than 30 minutes and could not increase the captured cell density on a flat surface beyond $\sim 10^5$ cells/cm^2. In fact, there was no significant improvement in the captured cell density on the antibody-activated surface beyond $\sim 10^5$ cells/cm^2 ($\sim$10 cells/(100 μm)^2) even when the concentration of the solution of live *E. coli* was increased from 2×10^6 to 2×10^8 cells/mL. As described in this and the next chapter, we have always been able to increase the captured cell density with time and with an increased cell concentration in the solution until the activated surface was fully saturated, reaching concentrations of thousands of organisms per (100 μm)^2 area as shown in Figures 3.1 and 3.4.

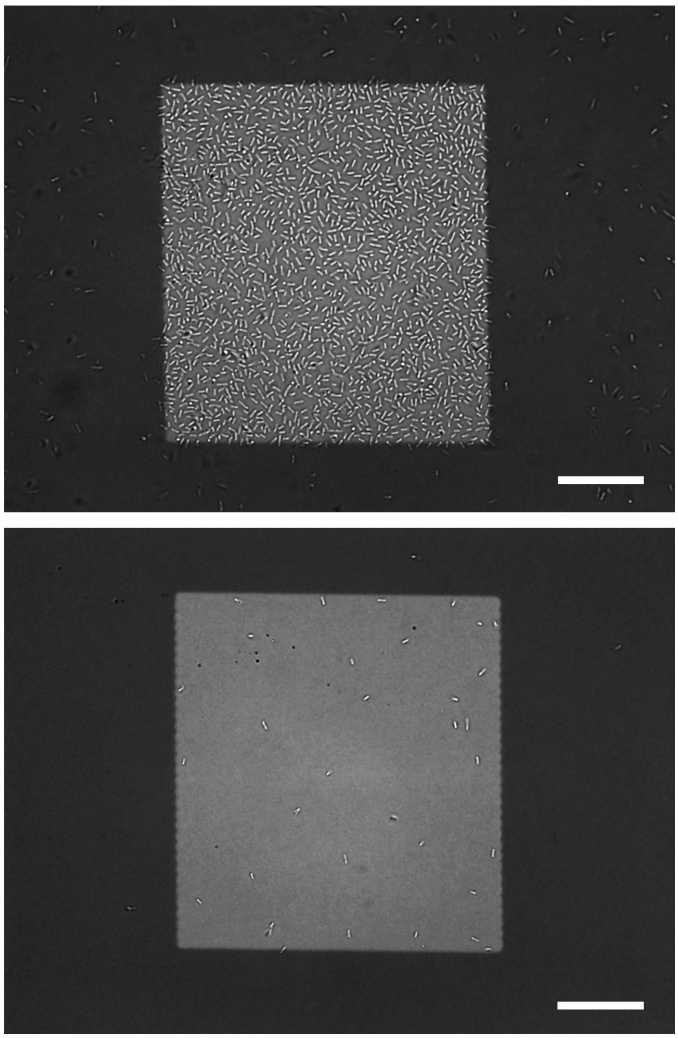

Figure 3.1. Optical images of 100 × 100 μm^2 antibody-activated patterns on silicon substrates exposed to *E. coli* H10407 cells at solution concentrations of (5.9 ± 0.3) × 10^7 cells/mL (top panel), and (6.1 ± 0.2) × 10^5 cells/mL (bottom panel). During the 30-minute incubation period, 1899 cells attached to the patterned area on top, and 34 cells attached to the one on the bottom. The scale bar is 25 μm.

This proves the need for surface characterization using surface-sensitive techniques. Such characterization is one of the key requirements for the reproducible, successful activation of these surfaces. In the case of Premkumar's work [85] mentioned above, either their activated surface had a low density of antibodies, which were saturated with immobilized bacteria early in the incubation, or the activated surface was not prepared properly

because of a lack of surface characterization techniques. A similar work was reported by Duplan *et. al.* [86] in which the density of the *E. coli* captured using a solution concentration of ~10^6 cells/mL was similar to ours; however, they did not show a surface that was fully saturated with captured bacteria cells similar to those in Figures 3.1 and 3.4 when they used a more concentrated solution of cells nor did they mention the error bars in their capture rates. It is expected that the initial rate of capture by a properly activated surface will be proportional to the concentration of the bacteria in the solution, as presented in this thesis.

In our publications during the course of this thesis work [9, 14, 15] and in Chapter 2 we reported rapid, reliable, simple, specific, sensitive, and label-free detection of living *Salmonella enterica* serovar Typhimurium (*S.* Typhimurium) and *E. coli* cells in an aqueous environment by means of immunoimmobilization on patterned silicon surfaces. In Chapter 2, we explained that the preparation of such surfaces involves depositing antibodies onto aminofunctional silanes with heterobifunctional cross-linkers as a reactive intermediate and requires careful surface-sensitive characterization to ensure efficiency of the antibody coverage. One of the key requirements for efficient immobilization is a proper choice of antibody-antigen pairs [9, 14, 15]. The general rule for selection is (a) to use affinity-purified antibodies and (b) to target the surface antigens of the bacterium. In our previously reported studies, we carried out systematic experiments to evaluate and compare the immobilization efficiencies of immunoglobulin G (IgG) antibodies raised against four different types of surface antigens of *S.* Typhimurium and *E. coli*. These are the fimbriae, lipopolysaccharides (LPS), and flagella

and a capsular protein [9, 15]. The results showed that, with the exception of the capsular protein, all the surface antigens can in principle be targeted to achieve a fairly high degree of immobilization. Among the various surface antigens, targeting the fimbriae resulted in the highest immobilization efficiency. This is not surprising, since these appendages are long and protrude outside the cell body. Consequently, a monolayer of bacteria is achieved on antibody-patterned areas within a short amount of time, provided that the solution concentration of the bacteria is high enough [15]. Capturing live organisms has the added advantage that after cell division the daughter cell, too, remains on the antibody-activated surface. Thus, an immunosensor based on the immuno-immobilization approach not only captures living bacteria but also facilitates their multiplication, growth and self-enrichment on the antibody-activated areas. Furthermore, the optical imaging approach used here has a high degree of detection sensitivity: a single bacterial cell within a 200 × 200 μm^2 field of view can easily be spotted and followed in time using a high-end optical microscope without a need for extra steps such as tagging bacteria with fluorescent agents [82], provided that a highly polished silicon wafer or a glass surface is used as the activated surface.

Here we describe a new approach to assessing the capture efficiency of the immunosensor for living bacteria. The study employed two model bacteria, both expressing colonization factor antigen I (CFA/I) fimbriae: *S.* Typhimurium H72-pBBs-cfa and wild-type enterotoxigenic *E. coli* H10407 (*see* Figure 2.20). Our systematic work on the rate of capture of living bacteria involved solution concentrations of cells ranging from ~3×10^4 to ~3×10^7 cells/mL. In addition, we tested the application of this method

to *E. coli* O157:H7 (*see* Figure 2.20) by using antibodies raised against the LPS of those organisms.

Experimental Setup

The methods used for the *in situ* quantification of immunoimmobilized bacteria include the direct counting of captured cells based on images acquired with an optical microscope operated in reflection mode within the first ten minutes of bacterial exposure. For all silicon substrates, surface preparation and characterization and the covalent attachment of polyclonal anti-CFA/I antibodies to patterned areas were carried out by the procedure described in Chapter 2.

Prior to each set of experiments, *S.* Typhimurium H72-pBBs-cfa and *E. coli* H10407 were cultured in 3 mL of LB liquid medium and incubated on an orbital shaker (135 rpm) for 3 hours at 37 °C in order to yield a final cell concentration of approximately 3×10^8 cells/mL. Following serial dilutions using PBS, 1-mL amounts of serially diluted cultures with solution cell concentrations ranging from $\sim 3 \times 10^4$ to $\sim 3 \times 10^7$ cells/mL were pipetted onto a silicon surface with 100×100 μm^2 antibody-activated areas facing up in a petri dish. Thus, the Si substrates being completely immersed in the bacterial culture marked the beginning of the time for the inoculation processes. These specimens were immediately placed under an optical microscope using a 60× water-immersion objective lens to follow the development of the bacterial immobilization process over time. High-resolution digital images were taken at one-second intervals over an incubation period of 90 minutes starting after the first minute of incubation. At the end of the incubation period, the silicon chips were washed with PBS

inside the petri dishes as described in Chapter 2 to remove loosely bound cells from the substrate surface and from the solution medium, which was replaced with pure PBS. This reduced the density of the cells in the medium, which in this thesis is referred to as cell-free PBS medium, even though there might still be some low level of cells in the medium. The chips thus prepared were then kept in cell-free PBS inside petri dishes at 25 °C for further optical investigation.

For a given cell concentration, captured bacterial cells within the $100 \times 100\ \mu m^2$ antibody-activated area were counted as a function of incubation time at one-second intervals and recorded as part of the captured cell density at that time, as cells/$(100\ \mu m)^2$. Thus, the rate of initial attachment for a given cell concentration was determined from the slope of the captured cell density versus incubation time curve, taking into account that the initial rate of attachment is expected to be linearly related to the incubation time for the solution concentrations of interest.

The rates of capture of the two different bacteria, *S.* Typhimurium and *E. coli*, are presented below. For both of these bacteria the antibodies raised against the CFA/I of *S.* Typhimurium were used. Even though these antibodies were developed against the CFA/Is isolated from the genetically engineered *S.* Typhimurium H72-pBBs-cfa strains, the original gene for the CFA/I enrichment of *S.* Typhimurium was isolated from *E. coli* H10407 strains [9]. For this reason the *E. coli* strain was expected to interact with the antibodies raised against the *Salmonella* CFA/I antigens. However, as the results below prove, *E. coli* strains do not interact with these antibodies as strongly as the *S.* Typhimurium strains do.

Determination of the Initial Cell Capture Rate

In determining the cell capture rates of the two strains of bacteria, it is important to limit the count to the bacteria captured in the 100 × 100 μm^2 antibody-activated areas in the first ten minutes of bacterial incubation in order to avoid oversaturation of the activated area by immobilized bacteria and to avoid overestimating the number of immobilized bacteria because of cell division. With prolonged incubation times, captured bacteria start dividing and populating the available antibody-activated areas (under optimum growth conditions cells can divide every 20 minutes) [9].

Figure 3.2 shows examples of such experiments in which *S.* Typhimurium was used as the model bacterium. Here, the results of two different experiments are presented: two samples with 100 × 100 μm^2 antibody-activated areas were inoculated with *S.* Typhimurium solutions with concentrations of (3.2 ± 0.6) × 10^7 (top panel) and (6.7 ± 0.6) × 10^5 cells/mL (bottom panel). Each experiment lasted 90 minutes and involved the production of over 5000 frames of high-resolution pictures so that we could observe the dynamics of the immunoimmobilization process. The data in Figure 3.2 were obtained from the subset of these pictures focusing on the first ten minutes of bacterial incubation. The findings suggest that, for a given cell concentration, the captured cell density increases linearly ($r^2 > 0.98$) with the incubation time (best fit to $y = ax$, with the substrate placed in cell-free PBS medium prior to bacterial inoculation). For the bacterial concentrations given above, the recorded capture rates (the slopes of the increases over time) were 240 ± 5 cells/[min·(100 $\mu m)^2$] (top panel) and 7.2 ± 0.2 cells/[min·(100 $\mu m)^2$] (bottom panel), respectively, suggesting that the slopes of these curves are highly

dependent on the cell concentrations of the solutions.

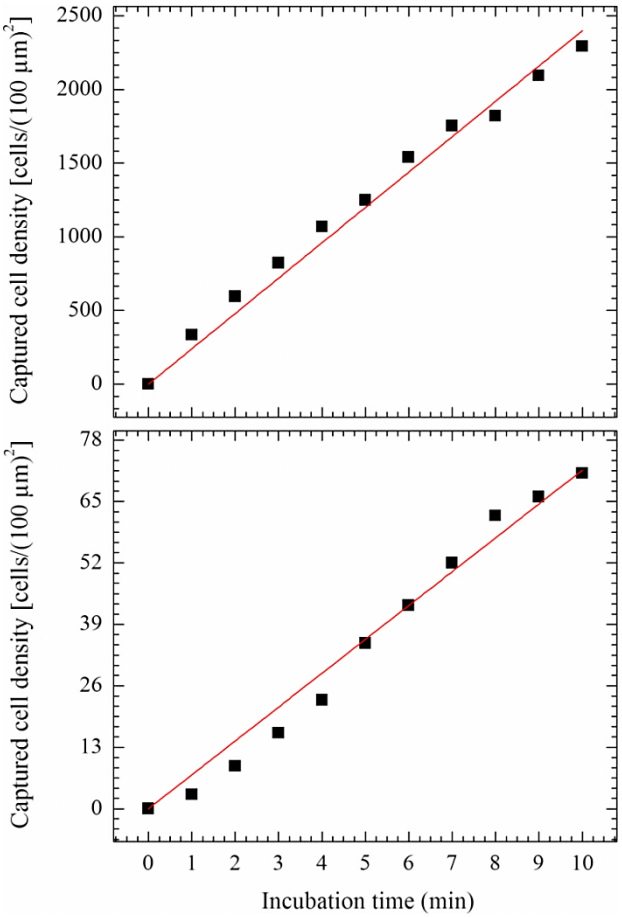

Figure 3.2. Captured *S.* Typhimurium cell density vs. incubation time for two different concentrations of cells in solution: the top panel corresponds to (3.2 ± 0.6) × 10^7 cells/mL; the bottom panel, to (6.7 ± 0.6) × 10^5 cells/mL. For a given concentration of bacteria in a culture solution, the rate of the initial attachment of the bacteria is determined by a direct counting of the immobilized cells using high-resolution optical images of the 100 × 100 μm^2 antibody-activated area. This is plotted as a function of time for the first 10 minutes of bacterial incubation. The density of the immobilized bacteria appears to increase linearly (r^2 > 0.98) with the incubation time, as shown above. The slopes of this increase give rates of 240 ± 5 cells/[min·(100 μm)^2] (top panel) and 7.2 ± 0.2 cells/[min·(100 μm)^2] (bottom panel).

The top panel of Figure 3.3 shows the variation in the captured cell density of *S.* Typhimurium as a function of prolonged incubation times for a cell concentration of (3.2 ± 0.6) × 10^7 cells/mL.

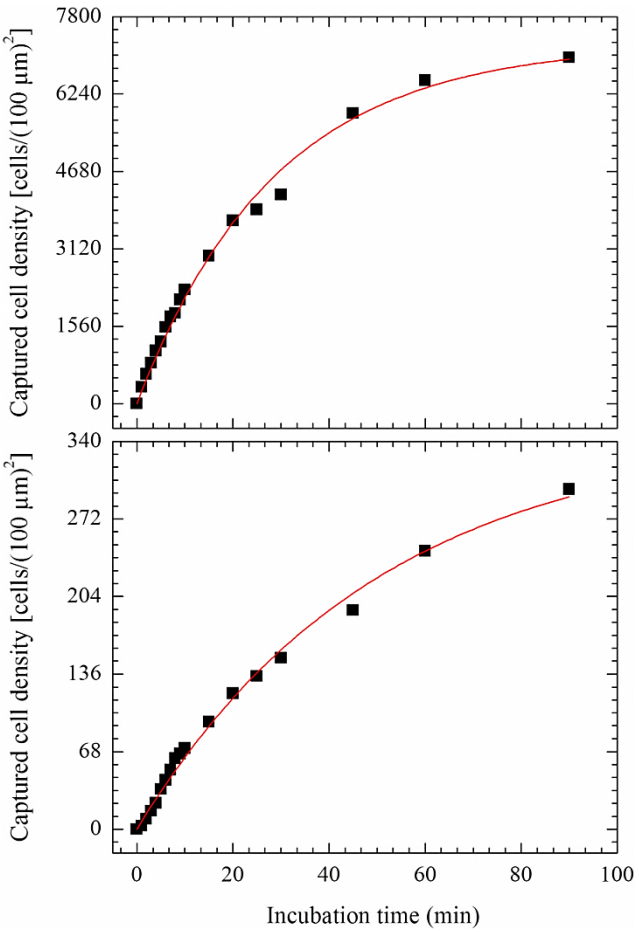

Figure 3.3. Saturation of captured cell density at two different concentrations of incubated bacteria: $(3.2 \pm 0.6) \times 10^7$ cells/mL (top panel) and $(6.7 \pm 0.6) \times 10^5$ cells/mL (bottom panel). It is clear the capture rate starts deviating from its linear behavior after the first 15 minutes of incubation. The full lines are Langmuir isotherm plots fitted to the experimental data points ($y = a\left[1 - \exp\left(-bx\right)\right]$).

The results suggest that after 15 minutes of incubation, captured cells start saturating the antibody-activated areas, until all the available spots on the 100×100 µm^2 squares are covered by a monolayer of bacteria (*see* Figure 3.4, top panel). Some of the bacteria immobilized in the top panel of Figure 3.4 presumably originate from the division of immobilized bacteria.

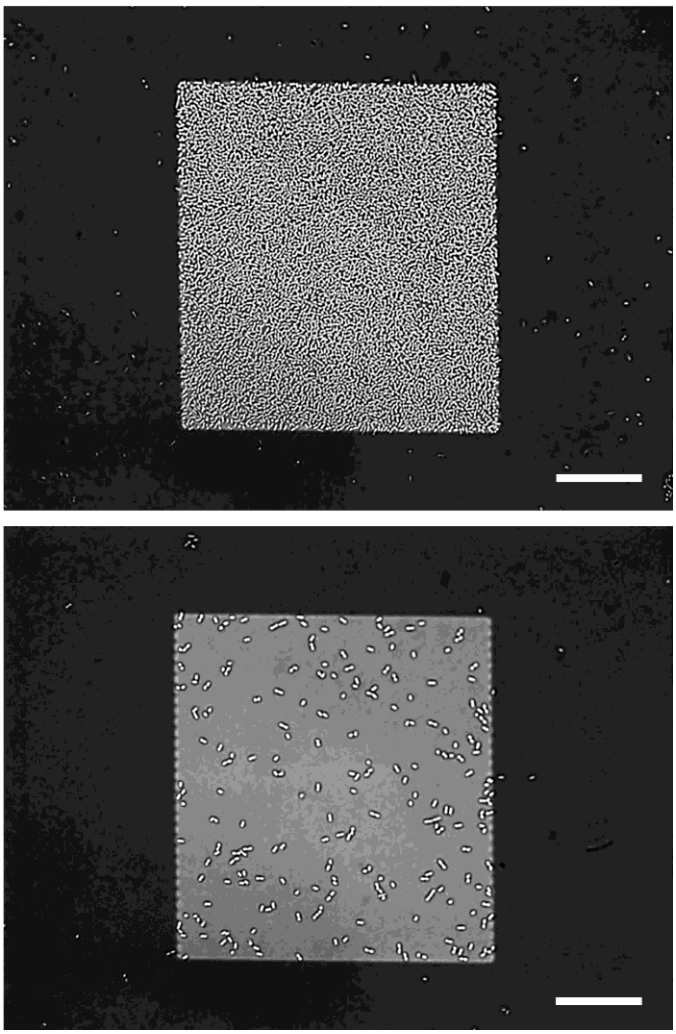

Figure 3.4. Optical images showing 100 × 100 μm^2 antibody-activated squares exposed to cultures of *S.* Typhimurium H72-pBBs-cfa at (3.2 ± 0.6) × 10^7 cells/mL (top panel) and (6.7 ± 0.6) × 10^5 cells/mL (bottom panel) for 90 minutes at 25 °C. The image at the top shows a full monolayer coverage of captured bacteria, totaling ~7300 cells inside the white square, whereas the image on the bottom shows ~350 cells inside the white (activated) area. The scale bar is 25 μm.

In our experiments the incubation of bacterial cultures with antibody-activated substrates was conducted in PBS at 25 °C. At this temperature bacterial cells divide every 40 to 60 minutes [8], which is less than the 90 minutes of total incubation time reported here. Mathematical fits to the experimental data using a Langmuir isotherm plot [92] level off

at ~7300 cells/(100 μm)^2, as shown in the top panel of Figure 3.3. An image associated with this saturation is presented in the top panel of Figure 3.4. A similar fit to the data is shown in the bottom panel of Figure 3.3, which represents cell capture on an activated surface incubated with the same bacteria in a solution having a concentration of (6.7 ± 0.6) × 10^5 cells/mL. This resulted in a saturation cell concentration of ~350 cells/(100 μm)^2. A view of this cell coverage is shown in the bottom panel of Figure 3.4. As observed in Figure 3.3 and also presented in our previous publication [9], captured cell density vs. incubation time starts deviating from its linear behavior after the first 15 minutes of incubation. This is particularly evident for solution concentrations higher than 1 × 10^6 cells/mL. This is not surprising, considering that a large fraction of the activated areas are covered rapidly in the early period of incubation, reducing the chance of a planktonic organism finding an activated surface with which to interact [9, 78]. On the other hand, the saturation observed for low solution concentrations (lower panel of Figure 3.3) is puzzling to us. At this time we have no convincing explanation for this behavior. We speculate that antibodies are blocked by fimbriae (pili) shed by bacteria in solution, reducing the activity of the antibody-covered areas; however, this hypothesis is yet to be proven.

To examine the ranges in which the immunosensor can be used for the detection of microbial contamination and to investigate the relation between the cell capture rate and the bulk concentration, a number of serial dilution experiments were conducted using our model bacteria, *S.* Typhimurium H72-pBBs-cfa and *E. coli* H10407. In order to verify the reproducibility of the results, series of three independent runs were carried out

under identical conditions (substrate preparation, temperature, growth of bacteria and incubation time) with solution concentrations varying from ~1 × 10^5 to ~3 × 10^7 cells/mL. For each concentration of cells in solution a cell capture rate was determined from the slope of the cell density vs. the incubation period, as described in Figure 3.2. These extremely time-consuming and challenging experiments require extreme attention to detail at every stage of the experiment. The results of a single series of experiments with *S.* Typhimurium are shown in Figure 3.5.

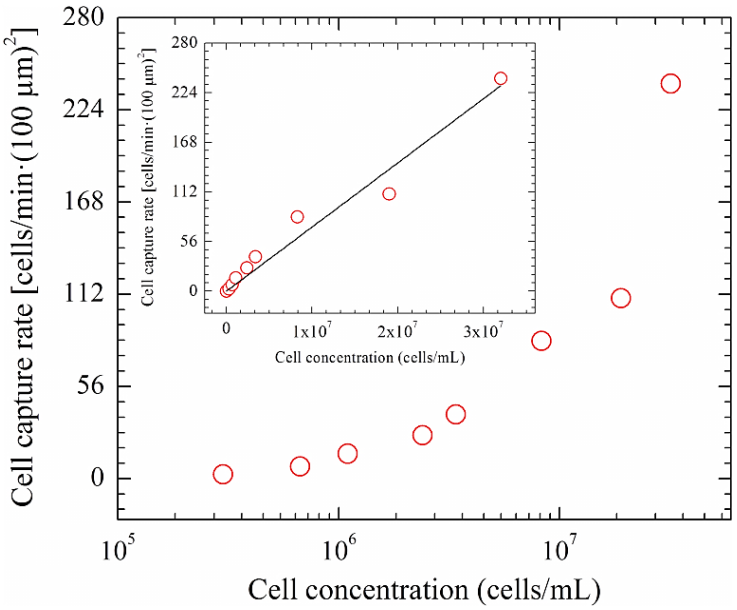

Figure 3.5. The semilogarithmic graph in the figure and the linear graph in the inset show the initial rate of capture as a function of the cell concentration in the bulk solution. The determination of the initial capture rate for a given solution concentration is explained in Figure 3.2. This graph suggests that the initial rate of capture is a linear function of the cell concentration in the solution. The slope of this increase, shown in the inset, is 7.2 ± 0.4 × 10^{-6} cells/(min·(100 μm)^2)/(cells/mL).

The rate of capture as a function of solution cell concentration is plotted in a semilogarithmic scale in the figure and in a linear scale in the inset. From the linear plot (inset in Figure 3.5) it is clear that the initial capture rate on a 100 × 100 μm^2 antibody-

activated area increases linearly ($r^2 = 0.98$) with the cell concentration in the solution. A similar linear relationship was obtained between the initial capture rate and the cell concentration in the bulk solution in the series of three runs for each isolate of *S.* Typhimurium or *E. coli*, as shown in Figure 3.6.

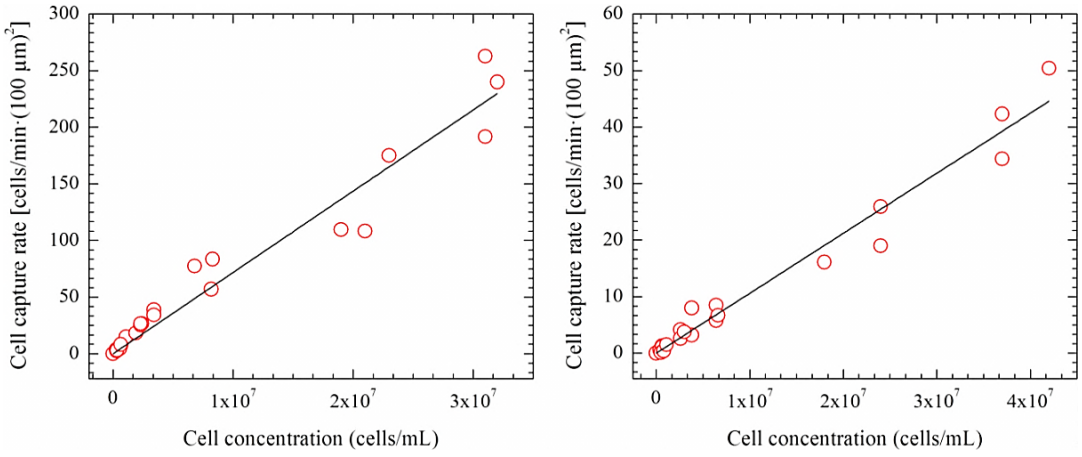

Figure 3.6. The initial rate of capture as a function of the cell concentration in the solution for *S.* Typhimurium H72-pBBs-cfa (left panel) and *E. coli* H10407 (right panel). For a given bacterial strain and antibody the rate of capture increases linearly ($r^2 > 0.97$) with the cell concentration in the solution. The slope of this increase, however, depends on the interactions of a particular strain of bacteria with the corresponding antibody. The slope of this line is a measure of this interaction; the slope of the line on the left is $(7.2 \pm 0.3) \times 10^{-6}$ cells/(min·(100 μm)^2)/(cells/mL) for *S.* Typhimurium, and the one on the right is $(1.1 \pm 0.1) \times 10^{-6}$ cells/(min·(100 μm)^2)/(cells/mL) for *E. coli*.

For both cell cultures, the initial cell capture rate increased linearly ($r^2 > 0.97$) with solution concentrations ranging from ~1×10^5 to ~3×10^7 cells/mL. For *S.* Typhimurium the slope of this increase was determined to be $(7.2 \pm 0.3) \times 10^{-6}$ cells/(min·(100 μm)^2)/(cells/mL) (top panel), and that for *E. coli* was found to be $(1.1 \pm 0.1) \times 10^{-6}$ cells/(min·(100 μm)^2)/(cells/mL) (bottom panel). These results suggest that the rate of attachment of *S.* Typhimurium is about seven times greater than that of *E. coli*. The difference in the initial capture rate may, as speculated above, result from the fact

that the antibodies were prepared against fimbriae of *S.* Typhimurium and not *E. coli* [9].

The current method for determining the initial cell capture rate is also applicable to quantifying bacteria immobilized with antibodies targeting other surface antigens, such as the LPS of a bacterium. A proof of concept experiment on this was conducted using *E. coli* O157:H7, a highly pathogenic strain of *E. coli* [93]. In this experiment, a patterned area (squares) on silicon was decorated with polyclonal antibodies raised against the LPS (O-antigens) of the bacterial strain. Figure 3.7 shows the results of these studies.

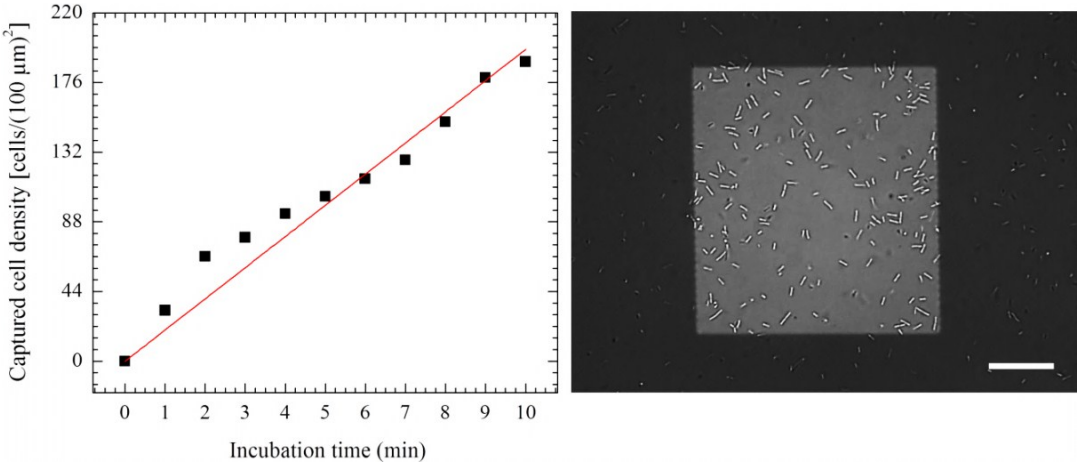

Figure 3.7. Left panel: change in the captured cell density of *E. coli* O157:H7 in the first 10 minutes of bacterial incubation as a function of incubation time. Right panel: An optical image of a 100 × 100 μm^2 activated square with ~189 cells immobilized on the square at the end of 10 minutes. Silicon surfaces were incubated in a culture with a cell density of ~7 × 10^7 cells/mL. The square areas were activated with antibodies raised against the LPS (O-antigens) of the cells. As expected, the cell density increased linearly (r^2 = 0.99) with incubation time. The slope of this increase gives the initial rate of capture, 19.7 ± 0.7 cells/[min·(100 μm)^2], for a cell density of ~7 × 10^7 cells/mL. The scale bar is 25 μm.

For a cell concentration of (6.8 ± 0.6) × 10^7 cells/mL, the initial cell capture rate was found to be around 19.7 ± 0.7 cells/[min·(100 μm)^2]. Correspondingly, the number of cells attached to antibody-activated squares was observed to be around 189 cells in the

first ten minutes of incubation (right panel). The initial rate of attachment of *E. coli* involving anti-LPS antibodies was a factor of almost forty (40) times smaller than those involving anti-fimbriae antibodies. These rates appear to be a function of both the bacterial strain and the choice of antibody.

The results presented thus far demonstrate that, regardless of the bacteria and the surface antigens and corresponding antibodies used, the relationship between the captured cell density in a $100 \times 100\ \mu m^2$ antibody-activated area and the incubation time is linear in the first ten minutes of incubation, and that the rate of capture increases linearly with the cell concentration. There are additional factors that affect the cell capture rate, including the antibody purity and the clone type, as discussed in our earlier publication [14]; however, we did not pursue these factors in this thesis work any further than what is presented in our publications.

Self-Enrichment of Immunoimmobilized Bacteria

When developing an immunosensor, it is desirable to have not only a low detection limit but also a short period of detection. The immunoimmobilization method described in this thesis offers the possibility of detecting individual cells in a relatively short period of time. For example, for cell solution concentrations of $\sim 1 \times 10^5$ cells/mL and above, an incubation time of only a couple minutes is required to detect a single bacterium in the aqueous environment. On the other hand, the time needed to detect a single cell in a solution containing $\sim 3 \times 10^4$ cells in 1 mL of liquid is between 8 and 30 minutes. Below concentrations of $\sim 3 \times 10^4$ cells/mL, detecting a bacterium becomes

increasingly difficult and depends on the chances of one getting close to the active area for antibody-antigen interactions to take place [84].

As shown in the left panel of Figure 3.8, for a concentration of ~3 × 10^4 cells/mL we were able to detect as few as five cells attached to the patterned area of the silicon surface after one hour of incubation.

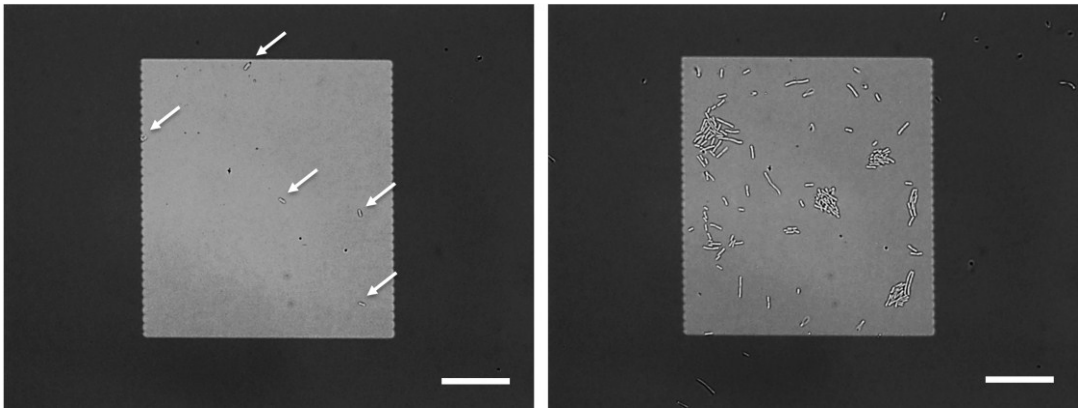

Figure 3.8. Optical images demonstrating the limit of detection of ~10^4 cells/mL of *S.* Typhimurium H72-pBBs-cfa: five cells were captured on the antibody-activated patterns within one hour of incubation time (left). For longer incubation times (~20 hours) the same area became more populated partly because of additional capture events but mostly because of cell division of the captured bacteria (self-enrichment). The scale bar is 25 μm.

Eventually, for longer incubation times (~20 hours), this area became populated by the division of living bacterial cells. As suggested by the image in the right panel of Figure 3.8, we attribute this cell accumulation partly to additional captures of bacteria by the antibodies on the patterned areas but mostly to cell division of the captured bacteria resulting in captured daughter cells at the locations of the original immobilized cells (see arrows in the left panel). These new cells add to the density of immunoimmobilized bacteria in the activated areas (self-enrichment) [9]. This self-enrichment process

continues until the activated areas are totally covered with immobilized bacteria.

We also observe additional factors contributing to cell captures at low concentrations (~10^4/mL), which at this time we cannot explain. This is shown in Figure 3.9, which plots the captured cell density on a 100 × 100 μm^2 antibody-activated area as a function of incubation time over a period of 125 minutes.

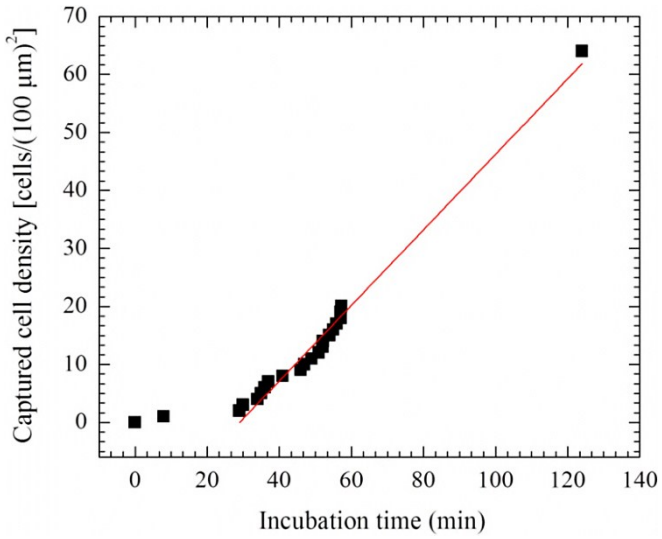

Figure 3.9. Accumulation of captured cells on a 100 × 100 μm^2 antibody-activated pattern on silicon substrate when the substrate was incubated with *S.* Typhimurium H72-pBBs-cfa culture (~10^4 cells/mL). From the slope shown (r^2 = 0.99), the capture rate was (0.65 ± 0.02) cells/[min·(100 μm)^2]. This is one of a handful of observations we could not explain. Notice that there is no visible capture in the first 30 minutes and then a fast rate of capture is suddenly initiated. Is this the onset of a quorum sensing? This result was not reproducible!

As shown in the figure, there is only one cell capture in the first 29 minutes of incubation, but suddenly, after 29 minutes, the capture process starts and increases linearly for the next 90 minutes at a rate of (0.65 ± 0.02) cells/[min·(100 μm)^2]. This is too fast a process for cell division; besides, as shown in Figure 3.8 it is easy to differentiate cell division populations because they are localized around the mother cells. Therefore, this sudden

increase in cell capture is an enigma at this time. Is this an onset of quorum sensing? We were not able to reproduce Figure 3.9. However, we have on several occasions noticed unusual densities of bacterial capture at low solution concentrations, which remains unexplained at this time.

Obviously, it is safe to state that antibody-modified patterns on silicon substrates serve as clean platforms not only for the efficient capturing of bacteria, but also for the promotion of their growth after capture. As a result, the concentrating of bacteria captured by immunoimmobilization can be used as an alternative for the standard culture methods [2], which are time-consuming. Also, it can give sufficient support to the viability and progression of bacteria, especially when changes over time of viable but non-culturable bacteria are to be studied. Furthermore, bacteria immobilized on a flat surface can be a platform for testing the efficacy of an antibiotic on captured bacteria before its actual use. Similar cultivation methods have been reported previously [91, 94-96]. However, none of the existing techniques come close to the practicality and high-throughput applicability of the immunoimmobilization method described in this thesis, which relies on the specificity of the antibody-antigen interactions making it possible to identify the locations of pathogenic bacteria on immunosensor surfaces.

Discussion

Early Saturation of Captured Cell Densities

The results shown in the bottom panel of Figure 3.3 warn us of some of the serious issues which have not been resolved in this thesis. One of these issues is variations in the saturation densities of immunoimmobilized bacteria. As we articulated

above, the saturation of captured cell densities at intermediate cell concentrations (3×10^5 to 3×10^7 cells/mL) of bacteria is a challenging issue. In fact, it relates to the issue of reproducibility. The following results show this clearly. In two sets of experiments, antibody-functionalized surfaces were incubated in PBS inoculated with 1 mL of a solution of *S.* Typhimurium cells. One of the solutions had a bacterial density of ~3×10^5 cells/mL; the other, ~3×10^7 cells/mL. The experiments were conducted under identical conditions to those presented in Figure 3.3. As described previously, immediately after the first minute of incubation optical images were obtained in order to assess the change in captured cell density within a 100×100 μm^2 antibody-activated area as a function of the incubation time over a period of only 10 minutes. The results are shown in Figure 3.10. It is clear that at fairly low incubation times the captured cell density starts deviating from its linear behavior and begins to saturate, at ~1100 cells for the medium with a bacterial cell density of ~3×10^7 cells/mL (top panel) and at ~24 cells for the medium with ~3×10^5 cells/mL (bottom panel). This happens within the first 10 minutes of bacterial incubation. This does not happen often, but we are puzzled about these observations and compelled to report them here as part of this thesis. We have also noticed that if we have a reproducibility issue associated with a group of observations it typically turns up repeatedly around the same time while we are carrying out a series of experiments. That is to say, whatever causes this reproducibility issue is triggered by a common cause affecting that series of experiments. For example, as far as we are concerned the series of experiments whose results are shown in Figure 3.10 was supposed to be identical to those whose results are shown in Figure 3.3 in every sense of the word,

yet the results are drastically different. The activated field was saturated at ~1100 cells instead of at ~7300 cells for the solution with ~3 × 10^7 cells/mL, and the lower panel in Figure 3.10 predicts a saturation count of ~24 cells for the solution with ~3 × 10^5 cells/mL, as opposed to ~350 cells.

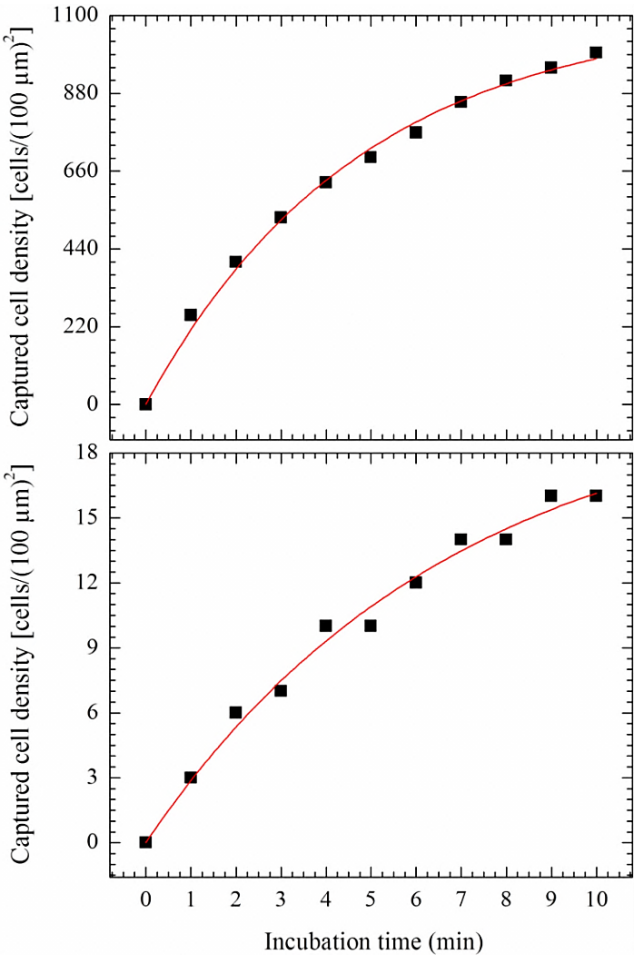

Figure 3.10. Early saturation of captured cell density at two different cell concentrations of incubated *S.* Typhimurium H72-pBBs-cfa: ~3 × 10^7 cells/mL (top panel) and ~3 × 10^5 cells/mL (bottom panel). At fairly short incubation times the captured cell density deviates from its linearity and begins to saturate antibody-covered patterns, at ~1100 cells for the concentration of ~3 × 10^7 cells/mL (top panel) and at ~24 cells for the concentration of ~3 × 10^5 cells/mL (bottom panel) within the first 10 minutes of bacterial incubation. The full lines are Langmuir isotherm plots fitted to the experimental data points ($y = a\left[1 - \exp\left(-bx\right)\right]$).

We could not dismiss these observations. Although they were observed less than 10% of the time, there were no special circumstances leading us to dismiss these results. Although not explained, a similar early saturation has been reported in the literature [85, 87]. As discussed above and in Chapter 2, the early saturation of the captured cell density may result from free-floating antigens (e.g. pili shed by bacteria) in the solution that block the antibodies on the activated areas, reducing the density of the active antibodies in these areas. Under stationary conditions the diffusion coefficient of these free antigenic proteins is much higher than that of bacteria [82]. It is thus possible that the antibody-activated areas are occupied by these proteins before bacteria have a chance to reach the surface to interact with antibodies.

Dependence of Cell Capture Efficiency on CFA/I Expression Level

Environmental stresses, such as variations in temperature, and the growth medium are known to alter the physiological activity and antigen expression level of bacteria [97]. Bacteria encode general stress proteins (GSP) which affect the cell surface structure, leading to changes in their antigen expression level [98]. Thus, in order to ensure the reliable bacteria capture, the dependence of the immunoimmobilization on the antigen expression level should be examined and understood first.

We carried out systematic experiments to investigate how the cell capture efficiency is dependent on the fimbriae expression level of the targeted bacteria [9]. In these experiments, we used genetically modified strain *S.* Typhimurium H72-pBAD-cfa [99] as a model bacterium that allows us to control its CFA/I expression level by

adjusting the arabinose concentration in the growth medium. By immobilizing cells grown at various arabinose concentrations (0, 0.3, 1, and 3 μg/mL), as shown in Figure 3.11, we investigated the capture efficiency of the antibodies with respect to the fimbriae expression level of the bacteria.

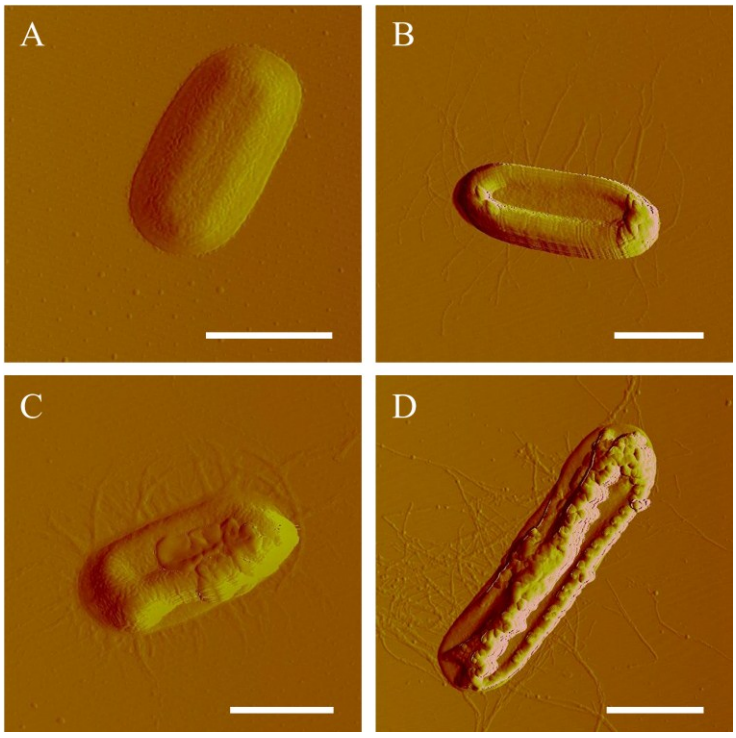

Figure 3.11. Atomic force microscope images of *S.* Typhimurium H72-pBAD-cfa grown in media with different arabinose concentrations. The dependence of the CFA/I expression level on the concentration of added arabinose is demonstrated in the images: (A) at 0 μg/mL, no visible fimbriae are observed; at (B) 0.3 μg/mL and (C) 1 μg/mL, enhanced CFA/I expression is observed; and (D) at 3 μg/mL, overexpressed CFA/I expression is observed. The scale bar is 1 μm.

The outcomes of these experiments are shown in Figure 3.12. In these experiments antibody solutions were deposited onto activated silicon surfaces as small droplets (~1 μL in volume) such that the antibody molecules covered only part of the substrate surface and a sharp boundary was formed between the antibody-modified area

and the unmodified area [15]. As shown in the optical images, the immobilized *S.* Typhimurium cells, grown at different arabinose concentrations, demonstrated a distinct division at this boundary. The blank areas in the upper right corners of the images were blocked from binding protein using bovine serum albumin (BSA) [100] and therefore serve as a negative control.

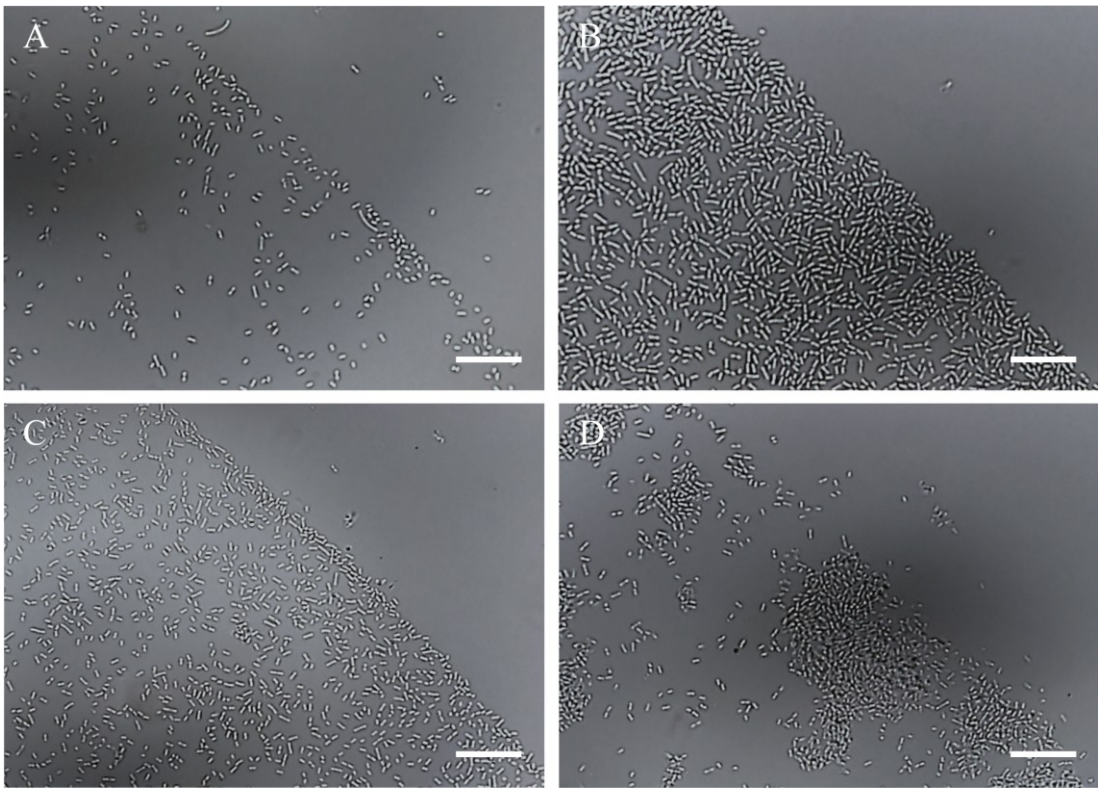

Figure 3.12. Optical images showing the dependence of cell capture efficiency on the fimbriae expression level of *S.* Typhimurium H72-pBAD-cfa. (A) Bacteria grown in a medium without added arabinose (0 μg/mL) had a minimal amount of CFA/I expression, providing a low capture efficiency. Bacteria grown in media containing arabinose at concentrations of (B) 0.3 and (C) 1 μg/mL, respectively, had enhanced CFA/I expression, providing high capture efficiency. (D) Bacteria grown in a medium containing arabinose at a concentration of 3 μg/mL produced clump formations. The scale bar is 25 μm.

For each of the arabinose concentrations listed above, the CFA/I expression level of the bacteria was investigated with AFM (Figure 3.11). As expected, when there was no

arabinose no visible fimbriae were observed on the bacterial cells (*see* Figure 3.11A). Consequently, the amount of CFA/I per cell increased as the result of an increase in the arabinose concentration (0.3, 1, and 3 μg/mL), as shown in Figure 3.11B-D. Under identical conditions of substrate preparation, temperature, growth of bacteria and incubation time, the lowest immobilization efficiency occurred at the lowest fimbriae expression level, which in this case was found in the growth medium with no arabinose added to the broth (Figure 3.12A). Arabinose concentrations of 0.3 and 1 μg/mL, on the other hand, produced much higher densities of immobilized cells (Figures 3.12B&C). An interesting observation was made at the arabinose concentration of 3 μg/mL: clumps of bacteria formed on the substrate (Figure 3.12D). Eventually, these cells tended to form colonies on the substrate. Most likely overexpressed CFA/Is led to oversaturation of the medium with loose fimbriae pieces, which blocked the antibody-covered areas as discussed above and deactivated them.

Dependence of Cell Capture Rate on Antibody Coverage

Several experiments were conducted in an effort to investigate the effect of antibody density on the capture efficiency of the immunosensor. In Chapter 2 we demonstrated that the antibody-binding layer is highly efficient and deposits antibody molecules on silicon surface at high density. It is expected that having a large number of antibody molecules available to bind the fimbriae of bacteria will result in a high capture efficiency [9]. To test this hypothesis, antibody solutions at five different concentrations—0.05, 0.07, 0.13, 0.25, and 1 μg/mL—were deposited on 100 × 100 μm^2

activated areas of silicon samples. In addition, one sample was prepared as a control on which no antibody molecules were deposited. As before, for each sample XPS was used to determine the relative atomic concentration of N. The samples were then incubated in a *S.* Typhimurium H72-pBBs-cfa solution (~3 × 10^6 cells/mL) and the corresponding cell capture rates were determined as described above. Figure 3.13 gives the dependence of the cell capture rate on the N concentration.

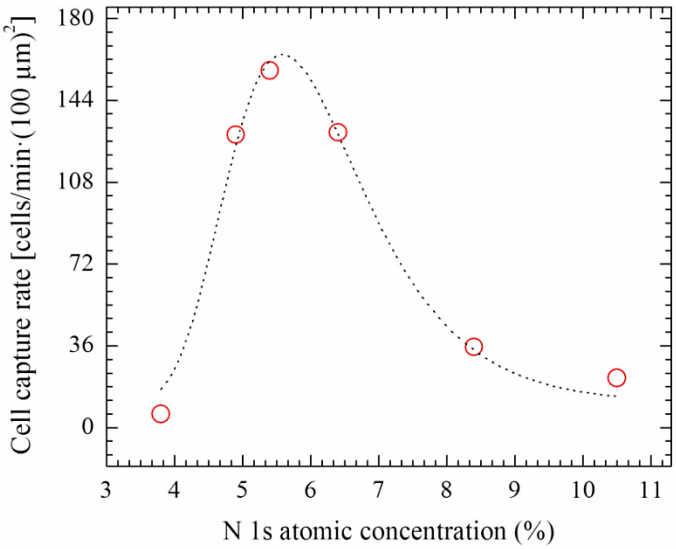

Figure 3.13. Dependence of the cell capture rate on the antibody density for a solution containing ~3 × 10^6 cells/mL of *S.* Typhimurium H72-pBBs-cfa. The highest yield of bacterial immobilization was achieved at a N concentration of ~5.6%, which corresponds to an antibody concentration of ~0.08 μg/mL.

As is apparent in the figure, the capture rate passes through a maximum and then decreases with increasing N atomic concentration. Surprisingly, the highest level of bacterial immobilization was achieved at a N concentration of ~5.6%, which corresponds to an antibody concentration of ~0.08 μg/mL. This observation needs to be interpreted carefully. Several other factors play a role here, including the physiology of the bacteria and the expression level of the CFA/I fimbriae. It is possible that at an antibody

concentration of ~0.08 μg/mL on silicon surface the antibody molecules are less tightly packed together than those at high antibody concentrations (~1 μg/mL); high antibody concentrations might result in conformational changes in the antibodies [76] that result in a reduced interaction efficiency.

Dependence of Cell Capture Rate on APTES Annealing and Storage in PBS

The linker chemistry we have used thus far relies on the efficient deposition of APTES, which couples to the −OH groups on the silicon surface to bind antibody molecules covalently through BMPS. As demonstrated in Chapter 2, APTES coupling to silicon surfaces in some cases does not exhibit long-term stability in an aqueous environment. Despite our efforts to produce stable silanes, ellipsometry and contact angle measurements showed that in some cases seemingly attached APTES does come off of silicon surface under prolonged exposure to PBS. Annealing silanized silicon samples at an elevated temperature (~100 °C) for a short time (~30 minutes) in air appeared to improve the stability of the silane layer. As stated before (*see* Chapter 2 for details), longer annealing times and annealing at higher temperatures are not recommended since they can cause a decrease of the amine groups through oxidation. This, of course, will result in less antibody coverage on the silicon surface and consequently in a lower capture efficiency. To test this, we conducted experiments in which we annealed silanized silicon samples for 0.5, 2, and 12 hours at 100 °C in air. Following BMPS deposition, we spotted antibody molecules (at a concentration of 1 μg/mL) onto these samples to allow covalent attachment. Immediately afterward, we incubated these

samples with *S.* Typhimurium H72-pBBs-cfa (~3 × 10^6 cells/mL) and determined the corresponding cell capture rates.

Figure 3.14 shows the effect of annealing APTES for prolonged times on the capture rate of the immunosensor. Based on the slight drop in the cell capture rate from 26 to 22 cells/(min·(100 μm)^2) for longer APTES annealing times (up to 12 hours), the results suggest that even at prolonged APTES annealing times the immunosensor can be used as an effective way to capture bacterial cells.

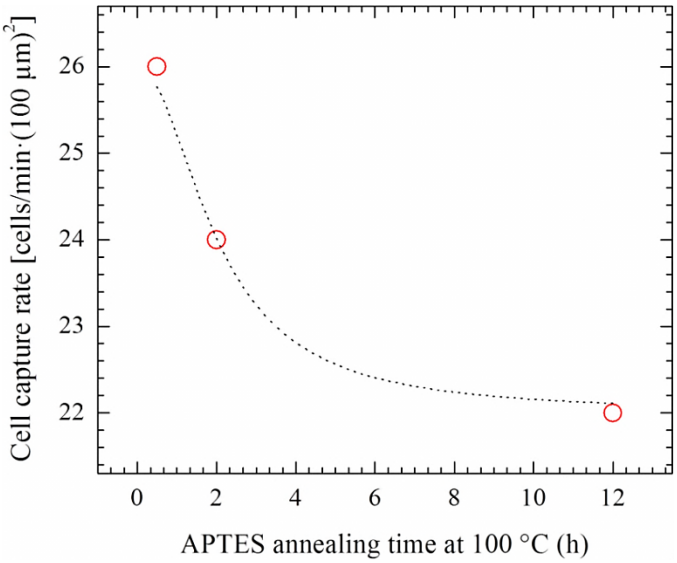

Figure 3.14. Correlation of cell capture rate of immunosensor with the APTES annealing time at 100 °C.

To test the dependence of antibody activity on the storage time in an aqueous medium we conducted a series of experiments on APTES-covered silicon samples that had been first annealed for 12 hours at 100 °C. The annealed APTES-functionalized surfaces were first activated with antibodies through BMPS, then stored in a cell-free PBS medium for 0, 6, 24, 33, 49, or 78 hours at 25 °C and incubated with a *S.*

Typhimurium H72-pBBs-cfa solution (~3 × 10^6 cells/mL). The dependence of the cell capture rate on the storage time of the immunosensor in PBS is shown in Figure 3.15. Here, the capture rate appears to pass through a minimum and then increase steadily with increasing storage time. As explained earlier, it is possible that during longer incubation times in PBS some APTES molecules come off of the silicon surface. However, the good news is that the activity of the antibodies was not adversely affected by the storage time; if anything it improved with the storage time. At this time, we have no explanation for this improvement in the capture rate.

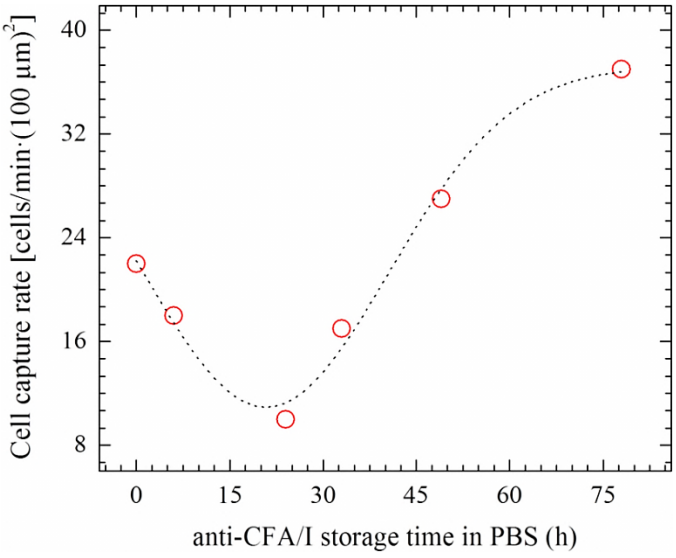

Figure 3.15. Dependence of capture rate on the storage time of anti-CFA/I modified silicon samples in cell-free PBS at 25 °C. Prior to antibody deposition, each one of the samples was annealed for 12 hours at 100 °C after incubation with APTES. The highest level of bacterial capture was achieved after 78 hours of storage in PBS, which nearly doubled the cell capture efficiency.

4. THE USE OF IMMUNOIMMOBILIZATION FOR THE DETECTION OF BACTERIA IN FUELS

A Brief Overview of Microbial Contamination in Fuels

Hydrocarbon fuels can be a plentiful source of nutrients for some bacteria and fungi. Therefore, the inevitable presence of water in fuel storage tanks can encourage microbial growth in fuels. For example, in their recent study Raikos *et al.* [101] demonstrated that a water content as low as 2% by volume can support the growth of bacterial isolates in fuels. Similarly, in their report Yemashova *et al.* [102] suggested that 5−80 ppm of water is adequate to preserve the growth of bacterial spores in a fuel environment.

Water can come from many sources. Most fuels contain significant amounts of dissolved water, which, during long-term storage in storage tanks, may condense because of changes in temperature, pressure, or both and remain in liquid form as droplets on tank walls [103]. Moisture contained in air can also enter fuel storage tanks through breather hoses by condensation, and, to a lesser degree, through seal leaks. On ships, seawater is intentionally added to fuel storage tanks as ballast to maintain ship stability while fuel is used [104]. Once seawater enters a fuel storage tank, because its specific mass is larger than that of the fuel it will accumulate at the bottom of the tank. Hence, under appropriate conditions microbial growth will occur either at the fuel/seawater interface and in its immediate vicinity (approximately ±1 mm of the interface), where the oxygen concentration is relatively high (an excellent environment for fungi and aerobic bacteria), or at the deep bottom of the storage tank, where the oxygen levels are completely

depleted (an environment for facultative anaerobic bacteria) [103]. The negative consequences of such microbial growth [105] include the degradation of fuel hydrocarbons [106], the production of biomass and nonvolatile metabolic by-products [107] and microbially influenced corrosion (MIC) on the surfaces of fuel tanks [108].

Although the water phase is essential for microbial growth, there are some circumstances in which microorganisms that can form spores or are confined within water droplets can still disperse into the fuel phase and retain their viability [103]. For example, measurements of the distribution of viable microorganisms in a fuel storage tank filled with diesel fuel revealed a concentration of 117 cells/mL in the middle of the tank. This number increased tremendously in other locations, reaching the highest concentration, 1.9×10^8 cells/mL, at the fuel/water interface [102]. It should be noted here that this type of poor survival of some microbes in the fuel phase may be problematic because of operational problems they cause, such as filter plugging [103]. Furthermore, diagnostic tests for possible contamination of the fuel phase may result in underestimating the microbial contamination [103].

Any detectable microorganism in the fuel and/or water phase is a cause for concern, although concentrations ranging from 1×10^3 to 1×10^5 cells/mL in the water at the bottom can be acceptable if all other storage conditions, such as temperature and concentration of biocides, are at normal levels [101, 109]. Since the elimination of water from fuel storage tanks is impractical and not cost-effective, it is important to employ a rapid and sensitive method to detect and quantify microbial contamination in fuels before they reach the end user. The following sections of this chapter investigate in some detail

the applicability, under both aerobic and anoxic conditions, of the immunoimmobilization method described in this thesis as a tool for the rapid, sensitive, and simultaneous detection and identification of microbial contamination in fuels using model bacteria.

Immunoimmobilization as a Tool for the Detection of Bacteria in Fuels

Introduction

As discussed above there is a need for a rapid, sensitive method for detecting and identifying the contaminants in fuels, particularly biofuels. Biofuels are an inescapable component of future fuels, and they are more susceptible to biodegradation than their fossil counterparts [110]. Molecular approaches such as real-time polymerase chain reaction (PCR) amplification seem well suited to the identification and characterization of microbial communities isolated from fuels. These techniques are fairly effective because (a) the methods for isolating DNA from targeted microbes are matured, (b) hybridization probes based on 16S ribosomal RNA (16S rRNA) have been developed and tested for many bacterial species, and (c) libraries of 16S rRNA have been created [102, 111, 112]. Furthermore, these methods are very sensitive ($10-10^3$ cells/mL) and specific [113, 114]. However, it is essential to realize that these molecular methods have a major drawback: they are laborious and time-consuming. Standard microbiological methods, such as cultivation, staining, and physical testing [115] are very labor-intensive, time-consuming (from 18 hours up to 5 days), and not necessarily very precise [116, 117].

A number of other contemporary methods have also been employed to detect

microbial contamination in fuels, including bioluminescence and immunofluorescence methods. The former method mainly correlates the intracellular adenosine triphosphate (ATP) with the plate and/or direct viable count method and estimates bacterial concentrations within minutes. Thus, this method offers a fast enumeration of bacterial populations in fuels; however, it needs some minimum concentration of cells [118]. It should be emphasized here that the lack of specificity of this method is a drawback. Immunofluorescence offers rapid (within hours) and specific detection and quantification of pathogens in fuels [119], but it requires extra steps, such as the labeling of reporter antibodies with fluorescent molecules or enzymes.

Commercially available test kits could be considered as an alternative. They are field-deployable, generally easy to use, simple to interpret, and sensitive, giving results comparable to the standard plate counts. They can be used to detect and enumerate total bacteria, fungi and yeasts, and sulfate-reducing bacteria (SRB) in fuels [120]. The majority of these "dip-stick" kits rely on microbiological testing, e.g., on the use of either slides covered with suitable agar mediums or pads enriched with nutrients, for the detection and enumeration of microbes. However, they generally require two to seven days to produce results, are susceptible to human error, and are not specific.

This brings us to one of the practical merits of the immunoimmobilization method described in this thesis. The method offers rapid (within hours), sensitive and specific detection (up to ~10^4 cells/mL) within four hours of exposure at 25 °C without a need for cell concentration. The sensitivity can be further improved by increasing the time: as few as ~10^2 cells/mL can be detected upon prolonged exposure times of up to 24 hours.

In the upcoming sections some proof of concept experiments will be presented in some detail, including studies of the feasibility of the immunoimmobilization method performed in a range of fuel environments contaminated with model aerobic bacteria. In addition, this method can be readily employed to sort specific bacterial strains from mixed cultures of bacteria in fuels, provided that appropriate antibody-antigen pairs are available. It will also be demonstrated that, using the immunoimmobilization concept on model SRB species, the method is applicable to detecting, under anoxic conditions, the presence of facultative anaerobic bacteria in fuels. To the best of our knowledge, this is the first time an antibody-based method has been applied for a rapid, sensitive and simultaneous detection of bacteria present in fuels. Finally, at the end of this chapter a new procedure for entrapping and concentrating the species present in fuel environments at low concentrations will be proposed. This procedure takes advantage of antibody-activated surfaces of microfibers of quartz wool, a cheap and widely available material.

Experimental Setup

We used fuels of interest to the Navy, including petroleum ultralow-sulfur diesel (ULSD), petroleum low-sulfur diesel (LSD), petroleum JP-5 (petro JP-5), petroleum F-76 (petro F-76), camelina-derived JP-5 (camelina JP-5), algae-derived F-76 (algal F-76), and soy-based biodiesel (soy biodiesel) [121, 122] as model fuels to test the immuno-immobilization concept. We also used commercial diesel (diesel) as a model fuel. The first question that needed to be answered was whether or not antibodies could survive in a fuel environment. Prior to use, all fuels and coastal Key West natural seawater (from here on referred to as seawater) were filter-sterilized using filters with a pore size of 0.45 μm

and stored in sterile centrifuge tubes at 25 °C to avoid any cross contamination.

Serial dilution experiments were carried out to investigate the ranges in which patterns modified with the anti-CFA/I antibody on silicon substrates can be used for the detection of *E. coli* H10407 cells (*see* Figure 2.20) in each of the fuels mentioned above. The method of activating silicon substrates with antibodies and growing and enumerating bacteria was similar to that described in Chapter 2, with the exception that serial dilutions of H10407, with concentrations ranging from ~10^2 to ~10^7 cells/mL, were prepared in seawater instead of PBS buffer. Prior to incubation, 100 μL of an *E. coli* solution in seawater with the appropriate cell concentration was used to inoculate 900 μL of fuel, which was then shaken gently with a vortex to ensure the uniform distribution of cells in the seawater/fuel solution. Immunoactive patterned surfaces prepared ahead of time were immersed immediately in these solutions and incubated for (a) 4 hours at 25 °C for cell concentrations ranging from ~3×10^3 to ~3×10^7 cells/mL or (b) 24 hours at 25 °C for a cell concentration of ~3×10^2 cells/mL to allow bacterial capture on the antibody-activated patterns on silicon substrates. Finally, the same experiments were carried out in seawater and PBS environments as controls.

Sorting experiments were conducted for the purpose of demonstrating the applicability of the immunoimmobilization method to simultaneously detecting and identifying (with minimal cross-reactivity) mixed bacterial strains present in fuels. The protocol followed for the surface preparation of silicon substrates and the growth and enumeration of bacteria was the same as that described in Chapter 2, with the exception that antibody deposition was carried out using a microplotting system (Bio-Rad,

VersArray Chipwriter Compact System) at 25 °C with the humidity inside the system chamber adjusted to 90%. The tip diameter of the quill pins was ~30 μm. Antibody micropatterns were created using two different polyclonal antibodies, anti-CFA/I and anti-K88ac, to target two different strains of *E. coli*, H10407 and 3030-2, respectively (*see* Figure 2.20). Each antibody was plotted as a row of spots. Each spot had a diameter of ~100 μm and was separated from other spots by a distance of ~250 μm, center to center. Afterward, the substrates with antibody droplets were kept in a system chamber with 98% humidity for 45 minutes at 25 °C to allow the covalent linking of antibodies to the substrate. Subsequently, these surfaces were treated with 1% by volume bovine serum albumin (BSA) [100] in PBS for 20 minutes at 25 °C to block the nonspecific binding sites on the substrate. After washing off with PBS to remove excess antibodies from the surface, activated surfaces were incubated with mixed cultures of H10407 and 3030-2, suspended in two different liquid environments, fuel and seawater, at equal concentrations for one hour at 25 °C. The reader should note here that, prior to incubation, each strain was diluted to ~3×10^7 cells/mL in seawater and then 100 μL of each solution was used to inoculate 800 μL of each of (a) camelina JP-5 and (b) seawater, which were then shaken gently with the vortex to ensure the uniform distribution of cells within the environments. Also, as described in our previous report [9], to differentiate the cells visually and examine cross-reactivity after their immobilization, each *E. coli* strain was genetically modified to express fluorescent proteins for sorting experiments: the H10407 strain was modified to express red fluorescent protein, while 3030-2 was modified to express green fluorescent protein.

In both preparation methods, after cell capturing the silicon substrates were washed with PBS using the washing procedure presented in Chapter 2 to remove loosely bound and excess cells from the substrate surface and medium. Subsequently, the cells that remained on the patterned areas of the silicon substrates were imaged in cell-free PBS medium using the optical microscope in (a) reflection mode and (b) epifluorescence mode, to image the whole bacterial population and the fluorescent strains, respectively. As before, using optical images each captured bacterial cell within a 100 × 100 μm^2 antibody-activated pattern was counted and recorded as part of the captured cell density (cells/(100 $\mu m)^2$). Subsequently, the readouts from four such identical antibody-activated squares on the same silicon surface were averaged and standard deviations were calculated. The quality of each step of the chemical modification and the antibody deposition on the silicon substrates was monitored before incubation with bacteria as described in Chapter 2.

The Utility of Immunoimmobilization Demonstrated

Figure 4.1 depicts the overall process of immobilizing bacteria on antibody-activated patterns on silicon substrate in a fuel environment. The fuel/water mixture is represented with blue for water and orange for fuel. The water bubbles in fuel (a) preserve the integrity and functionality of the antibodies deposited on the silicon surfaces (the black Y shapes) and (b) maintain the viability of the bacteria (green ovals) in the fuel environment. Because the density of bacteria is slightly higher than that of fuel, given enough time, bacteria suspended in fuel will eventually settle on solid surfaces and colonize them [103]. Whether driven by gravity, motility or sheer chance, the

bacteria will have a chance to interact with the activated silicon surface, where they will encounter antibodies and some will be immunoimmobilized, provided the antibodies have maintained their functionality.

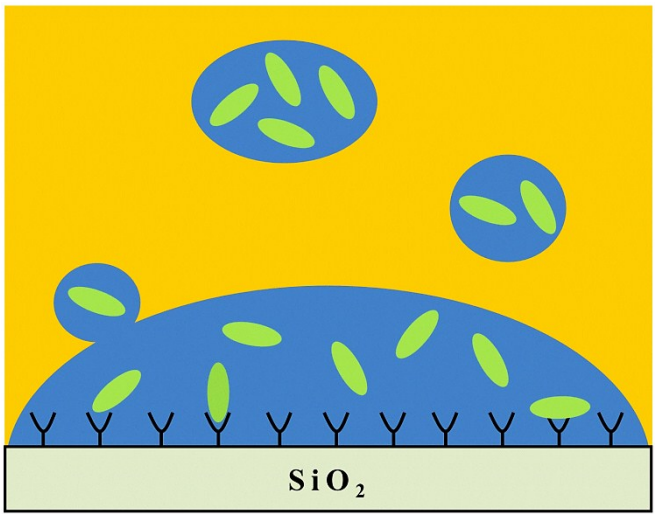

Figure 4.1. Schematic representation of the immunoimmobilization method applied to the detection and identification of bacteria (green ovals) present in a fuel (orange) environment. The presence of water (blue) in fuel is inevitable, which enables the preservation of (a) the integrity and functionality of antibodies (black Y shapes) and (b) the viability of bacteria.

Preliminary proof of concept studies suggest that the immunoimmobilization method described in this thesis maintains its efficiency in the fuel environment, allowing the patterning of live bacterial cells on antibody-activated areas of silicon substrates. An example of such bacterial patterning is shown in Figure 4.2: model bacteria *E. coli* H10407 were immobilized on antibody-activated patterns on silicon substrate in petro F-76 fuel under aerobic conditions. From this image it is clear that, given sufficient time (up to 12 hours), the immobilization of bacterial cells in these areas works very effectively. Notice that the chemically activated areas are covered to their maximum capacity with a monolayer of tightly packed bacteria, supporting the hypothesis that

antibodies maintain their integrity and functionality during prolonged exposure (~12 hours) to a fuel environment.

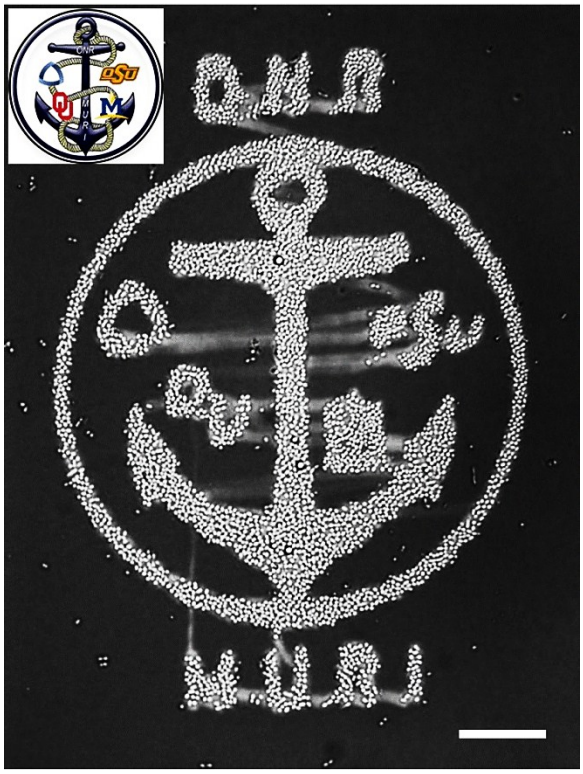

Figure 4.2. Immunoimmobilized *E. coli* H10407 cells patterned on an ONR MURI logo (inset) etched using a focused ion beam on a silicon substrate. The experiment was conducted in a petro F-76 fuel environment, illustrating that antibodies preserve their integrity and functionality inside fuels. The scale bar is 25 μm.

The capture efficiency for *E. coli* H10407 on activated silicon surfaces has been studied in a number of fuels using the techniques described in Chapter 3. The results prove that immunoimmobilization can be an efficient tool for targeting a specific bacterial contamination in fuel. As shown in Figure 4.3, in all tested fuels the sensitivity achieved for the detection of bacteria was comparable to that obtained in a PBS environment (Chapter 3): the limit of detection of this method without any concentration is ~3×10^4 cells/mL, provided that the incubation time is ~4 hours.

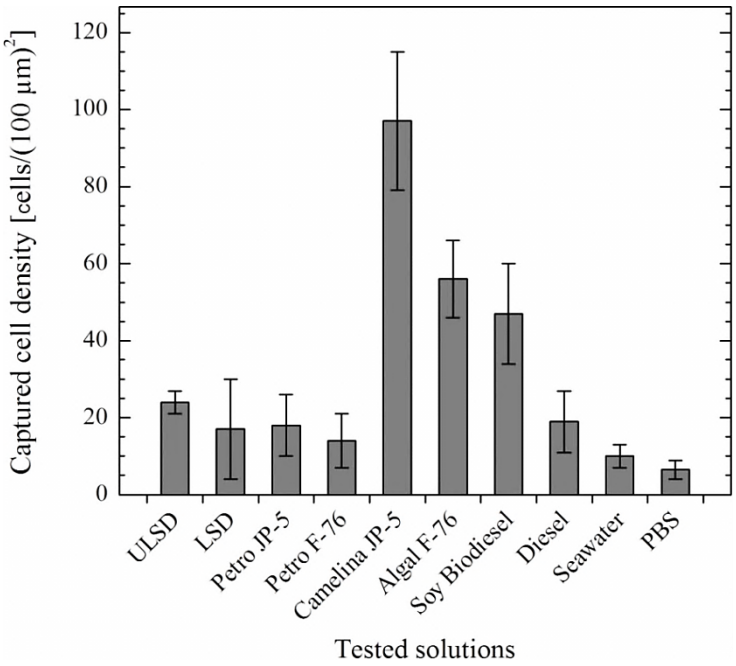

Figure 4.3. Captured *E. coli* H10407 cell densities in various fuels: *E. coli* cell count on an activated 100 × 100 μm^2 area after ~4 hours of incubation at 25 °C as a function of the solution type, identified along the x-axis. In all measurements the suspended *E. coli* H10407 cell density was kept at ~3 × 10^4 cells/mL.

Another consideration that arises from the data in Figure 4.3 is the variation in the captured cell density on the 100 × 100 μm^2 antibody-activated patterns on silicon substrate. Within the 4-hour incubation time, the numbers of cells attached to the patterned areas varied from as many as 97 cells in camelina JP-5, to as few as 10 cells in seawater (*see* Figure 4.4) and 7 cells in a PBS environment. This behavior is difficult to explain at this time, and because of time constraints we have not repeated the experiments. The averages and standard deviations shown in Figure 4.3 were obtained from four different readings from identical activated squares (bright areas in Figure 4.4) on the same silicon surface. The large standard deviations are explained by the bacteria not being dispersed evenly: they were, after all, in water bubbles in fuel. However, the

variability in the capture efficiency is difficult to explain at this time. For example, it is clear that the capture efficiency in camelina JP-5 is almost one order of magnitude higher than that in PBS. This could be a coincidence or a fact. These questions are left for future studies.

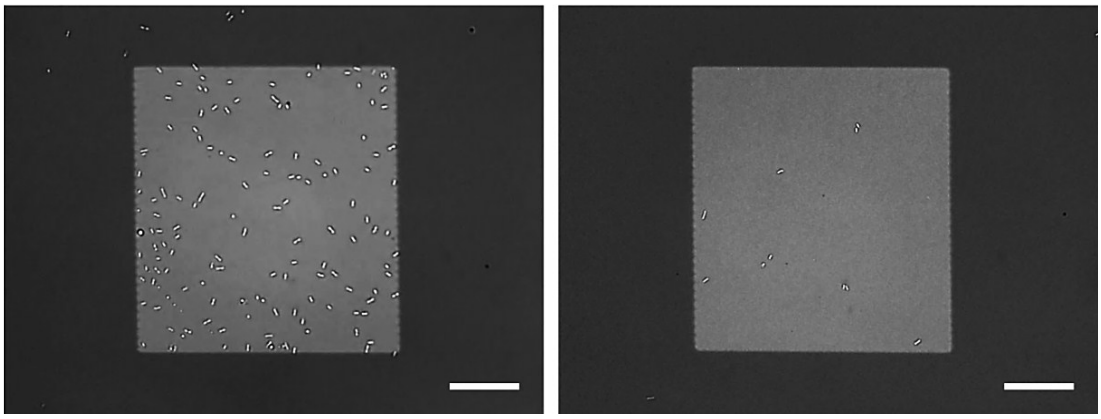

Figure 4.4. Detection limit for *E. coli* H10407 in camelina JP-5 (left) and seawater (right). The suspended cell concentration was ~3.0×10^4 cells/mL. The immobilized cells in the images can be counted in the patterned areas: 97 cells were attached in the camelina JP-5 environment, and 10 cells were attached in the seawater environment during the 4-hour incubation time. The scale bar is 25 μm.

At first glance, the bacterial incubation time may seem to be especially long. In practice it is advantageous to conduct a reliable measurement in a short period of time. However, this issue can be solved by pre-concentrating the bacteria. As was demonstrated in Chapter 3, there are three different concentration ranges of bacteria, for which different incubation times are used: for cell concentrations of ~1×10^5 cells/mL and above, the incubation time can be reduced to as little as 1 minute. In contrast, at least 30 minutes of incubation time is necessary to detect bacterial contaminations ranging from ~1×10^4 to ~1×10^5 cells/mL. For low cell concentrations, on the other hand, longer incubation times are needed to ensure an accurate determination of the bacterial

contamination level. In our experiments, prolonged incubation times (up to 24 hours) allowed for the detection of as few as 300 cells in 1 mL of fuel. However, this would lead to large uncertainties in results. As is discussed briefly at the end of this chapter, we have developed a practical new method for capturing and concentrating bacteria from low-level concentrations (~10/mL) to a level where we can easily use the immuno-immobilization approach described here.

Stability of Immunosensors

In Chapter 3 it was demonstrated that the binding affinity of antibodies can vary depending on the storage conditions of the antibody-activated surfaces prior to use. We designed a set of experiments to ascertain the stability of immunosensors for a period of time under ambient conditions. These experiments were conducted using antibodies patterned onto 100 × 100 μm^2 areas on silicon substrates, similar to those described in Chapter 3. Here, patterns activated with anti-CFA/I antibody were first kept in cell-free PBS medium for 17 hours at 25 °C. Following incubation with *E. coli* H10407 (at a concentration of ~3 × 10^7 cells/mL) for 4 hours at 25 °C, the incubated specimens were washed with PBS and imaged under an optical microscope. Subsequently, the cells captured on the 100 × 100 μm^2 antibody-activated areas were counted and recorded as the captured cell density (cells/(100 $\mu m)^2$) on the y-axis shown in Figure 4.5. For comparison, a set of parallel experiments was carried out under identical conditions of silicon surface preparation, bacterial growth, incubation time, and temperature in which the antibody-activated substrates were incubated with bacterial cultures immediately after they were activated. The results of both sets of experiments are shown in Figure 4.5.

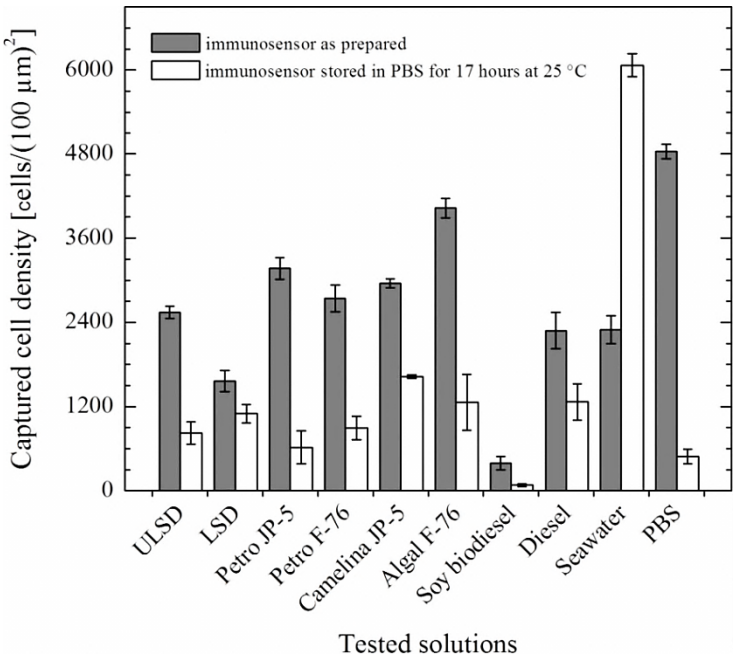

Figure 4.5. Stability of antibody-modified patterns on silicon substrates stored in PBS buffer for 17 hours at 25 °C. Antibodies preserve their binding affinities towards the fimbriae of bacteria. The dark-colored bars correspond to immunosensors used immediately, while the white bars correspond to immunosensors stored for 17 hours before use. The x-axis shows various fuels and aqueous media used to capture bacteria.

As is clear from the data, there was a reduction in the captured cell density in all media except seawater. This ranged from as low as ~30% for LSD to as high as ~80% for petro JP-5. These results suggest that antibodies, although reduced, preserve their binding affinities when incubated in PBS for a prolonged time (17 hours). The opposite was found in seawater, where the captured cell density increased by almost 60% after storage. It is conceivable that this increase in cell density is related to the physiological state of the bacteria. For instance, a high fimbriae expression on the surface of the bacteria will increase the immobilization efficiency, provided that a high density of antibodies per unit area on the substrate surface is available for bacterial capture [9]. This hypothesis was confirmed in the work presented in Chapter 3. Also, the apparent decrease in the binding

efficiency for bacteria suggested by Figure 4.5 might be a direct consequence of bacterial physiology. We try extremely hard to maintain identical conditions within sets of experiments. However, we are dealing with living organisms, not chemical compounds; one reproducible lesson we learned from these experiments is that a slight unforeseen variation in bacterial physiology can lead to larger than anticipated variations in bacterial response. This we leave to microbiologists to sort out; it is beyond the scope of this thesis.

Label-Free Detection and Sorting of Multiple Bacterial Strains in a Mixed Culture

A number of species of bacteria have already been identified and characterized in various hydrocarbon fuels, and some of them degrade fuels [105]. It would be desirable to detect and identify preselected organisms simultaneously in a single experiment. Antibody-based microarrays have the potential to address this need [123]. The concept of this technique is the preparation of antibody spots on prepared glass slides through the direct deposition of antibody solutions as the last step [9]. An advantage of this technique is that, in principle, it is possible to fabricate a test surface with as many antibody spots as are needed for the detection and sorting of mixed cultures of bacteria. These antibody spots need to be printed systematically such that each group of spots has a specific antibody targeting a specific surface antigen of a bacterial strain within the mixed culture [9]. Thus, once inoculated with a solution of a mixed bacterial culture, the antibody spots will immobilize bacteria through the specific antibody-antigen interactions. The unknown bacteria will be detected and identified according to the specific locations of the antibodies which captured bacteria. In our previous study, the rapid detection and

identification of multiple pathogens with which PBS buffer had been inoculated by coupling the immunoimmobilization method with microarray technology was demonstrated [9]. From here on we will refer to these surfaces as immunomicroarrays. It is important to emphasize here that no secondary labeling is needed to image these bacteria. This makes the method simple, accurate, and fast to use.

Figure 4.6 shows optical images of immobilized bacteria at two different incubation times on an immunomicroarray spot (~100-μm diameter) initially decorated with polyclonal anti-CFA/I antibodies using the microplotting system for the detection of *E. coli* H10407 cells under ambient conditions in a soy biodiesel/seawater mixture at a 9:1 ratio by volume. The top panel in the figure shows the cells captured after 30 minutes of incubation, and the bottom panel shows the same spot after 60 minutes of incubation. As expected, the bacteria on the spot are denser after 60 minutes of incubation (bottom panel). Because of the sharp separation between the antibody-modified spot and the nonmodified area of the silicon substrate, immunomicroarrays can be regarded as effective substrates for detecting, identifying, and quantifying targeted bacteria [15]. An additional advantage of using these surfaces for bacterial detection is that, compared to etched silicon substrates (e.g., Figure 4.4), immunomicroarrays offer a more practical approach to immobilizing live cells in a liquid environment [15]. Finally, based on the needs of specific applications [123], the spot diameter of an antibody pattern can be adjusted by changing the tip diameter and the spot separation. For example, in our previous work we reduced the spot diameter size to ~25 μm using glass tips with an inner diameter of ~5 μm [15].

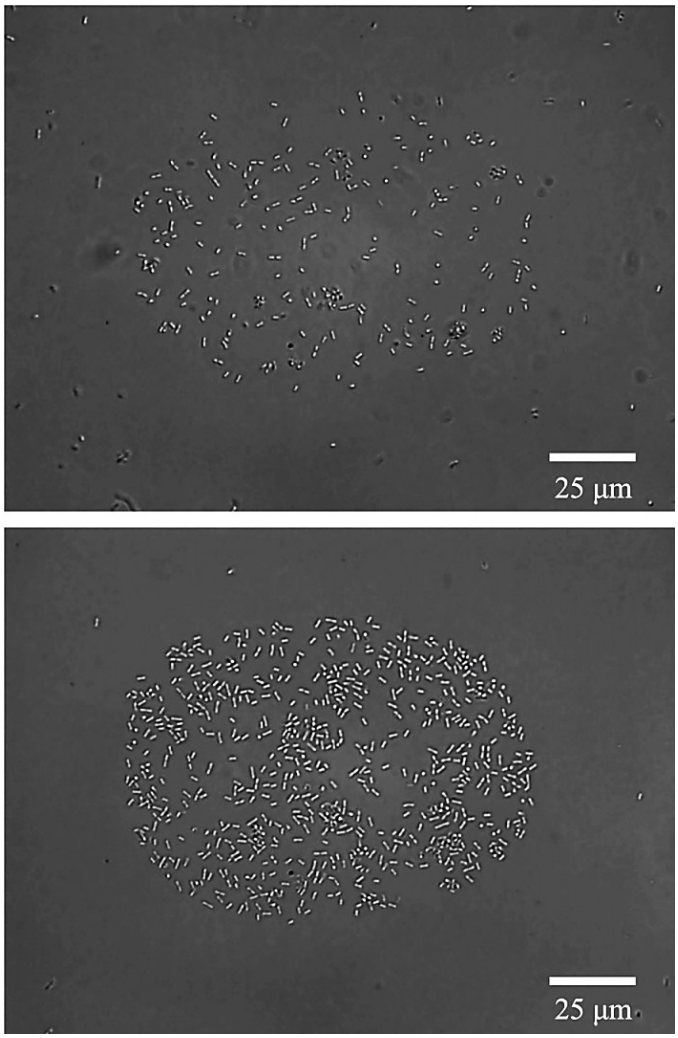

Figure 4.6. Immunomicroarray detection of *E. coli* H10407 (at a concentration of ~3.0×10^7 cells/mL) in a soy biodiesel/seawater mixture (9:1 ratio by volume) under ambient conditions. The image in the top panel was taken after 30 minutes of incubation; the image in the bottom panel, after 60 minutes of incubation.

Proof of concept experiments were carried out to demonstrate the use of the immunoimmobilization method for label-free detection and sorting of multiple bacterial strains present in a liquid environment. Two different fluorescent strains of *E. coli*, H10407 (red) and 3030-2 (green), mixed at equal concentrations (top panel in Figure 4.7), were used to inoculate (a) camelina JP-5 and (b) seawater.

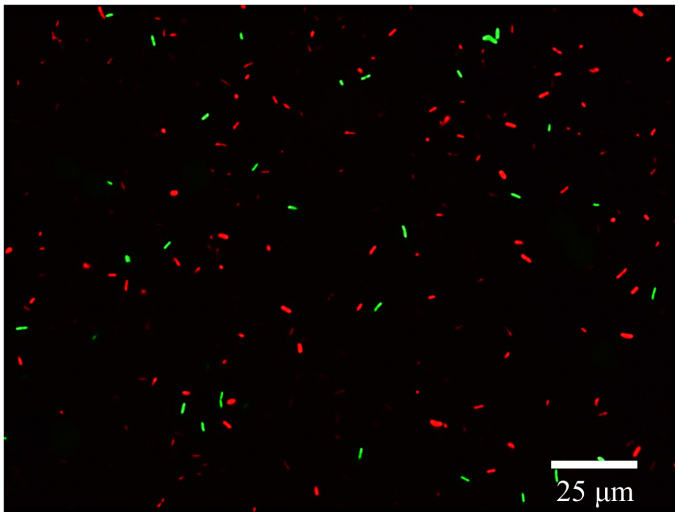

Figure 4.7. A seawater medium containing two *E. coli* strains at equal concentrations (~3.0 × 10^7 cells/mL). *E. coli* strain H10407 fluoresces red and strain 3030-2 fluoresces green (top panel).

The results demonstrate clearly that the proposed system is capable of sorting specific bacteria from a mixed culture (~3.0 × 10^7 cells/mL per strain) in either environment in one hour of incubation time (top panels of Figures 4.8 and 4.11). In these epifluorescence images each red (or green) spot corresponds to a single *E. coli* H10407 (or 3030-2) bacterium. Cross-reactivity was also examined using high-magnification images from selected spots to determine the degree to which the antibody to red-fluorescing cells interacted with green-fluorescing cells and vice versa. The magnified images of spots in Figure 4.8 shown in the right panels of Figures 4.9 and 4.10 clearly reveal the selective binding of the green and red cells to their corresponding antibodies because of the specificity of the antibody-antigen interactions. In both cases, we do observe a low level of cross-reactivity, in that a small fraction (5−10%) of bacteria react with the antibodies raised against the other bacteria. This is attributed to the limited specificity of the polyclonal antibodies used in these experiments [9].

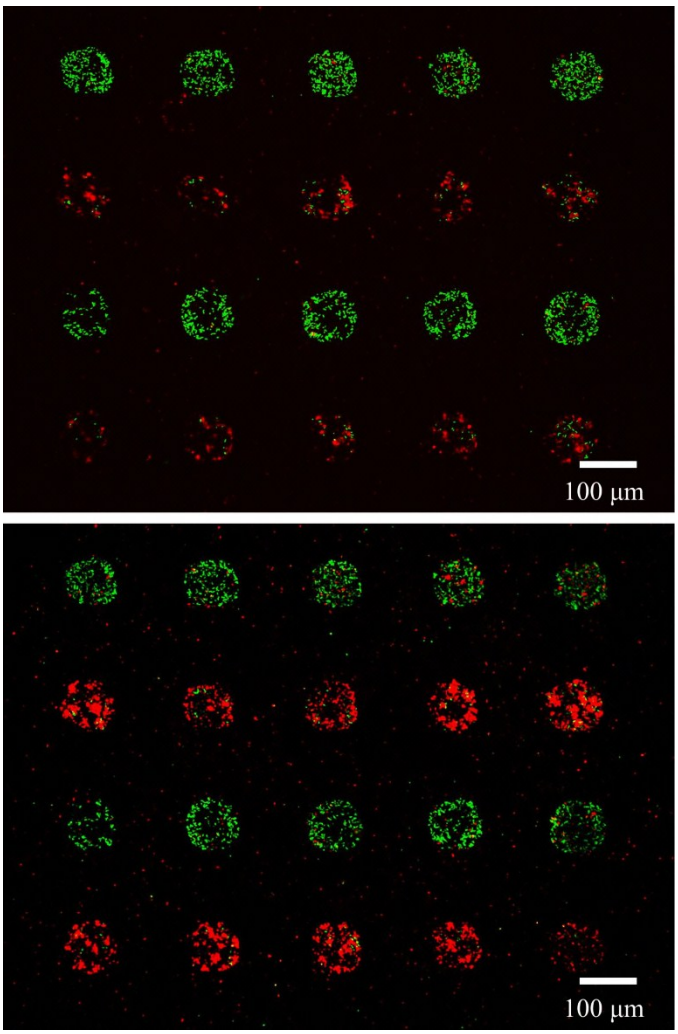

Figure 4.8. Sorting two *E. coli* strains, H10407 (red) and 3030-2 (green), mixed in equal concentrations (~3.0 × 10^7 cells/mL) in camelina JP-5 fuel. These are epifluorescence images of an area of immunoimmobilized living cells on an immunoarray (top) after one hour of incubation and (bottom) after 19 hours of waiting in a cell-free environment. All the excess cells in the lower panel are due to the division of cells that were captured previously (top panel). The division rate of the cells is slow because the PBS environment lacks nutrients.

After one hour of capture time in fuel (seawater), the incubated slides were washed gently with PBS buffer inside petri dishes to remove loosely bound cells from the substrate. Subsequently, these slides were kept inside a nearly cell-free PBS medium and allowed to incubate for 19 hours at 25 °C. The bottom panels of Figures 4.9 and 4.10 (as

well as the bottom panels of Figures 4.8 and 4.11) show the accumulation of cells through cell division (self-enrichment) on the spots where bacteria were initially immobilized. As explained above, this accumulation results mostly from the division of cells captured previously by the immunomicroarray.

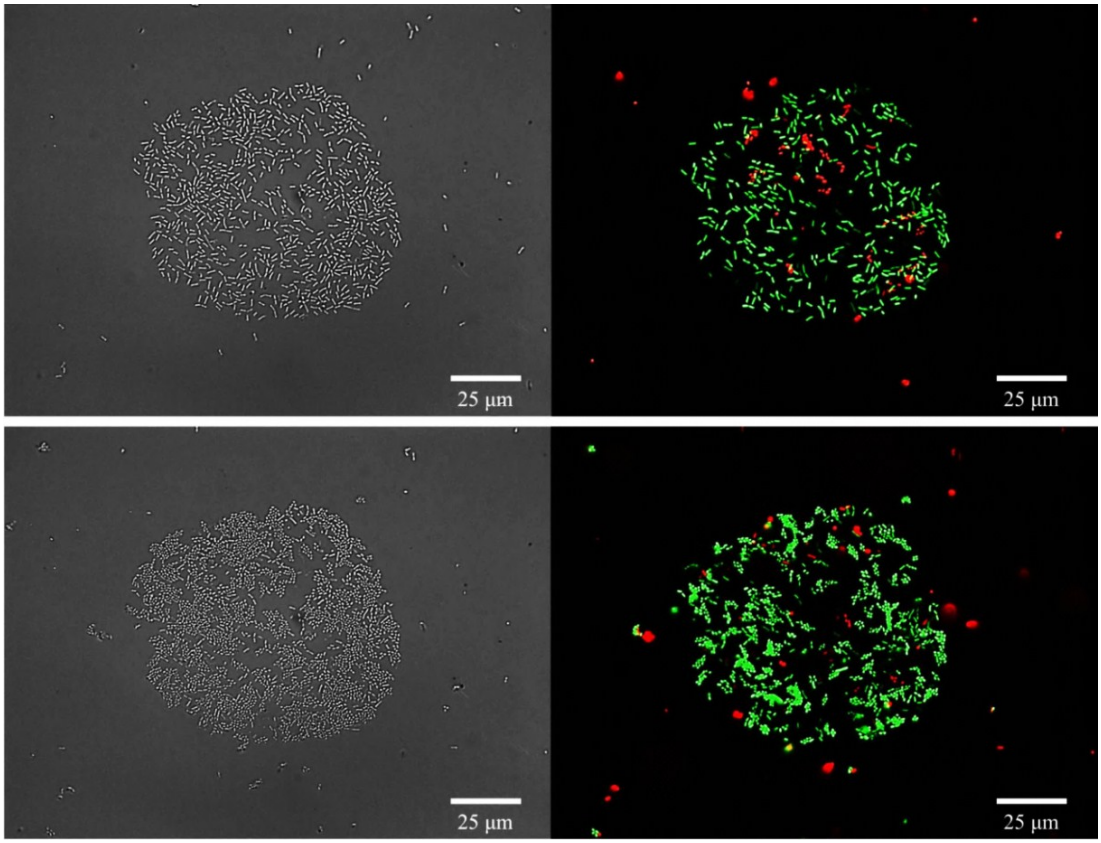

Figure 4.9. High-magnification images of one of the immunoarray spots shown in Figure 4.8, taken to examine the cross-reactivity of *E. coli* H10407 (red) cells with the antibodies raised against the 3030-2 (green) cells. The panels on the left show bright field images, and the panels on the right show epifluorescence images of the same area. The top panels show the spot after one hour of incubation, and the bottom panels show it after 19 hours of incubation. The selective binding of the green cells to their corresponding antibodies is clearly revealed, although a small fraction (~8%) of the red cells also bonded to and multiplied at these sites.

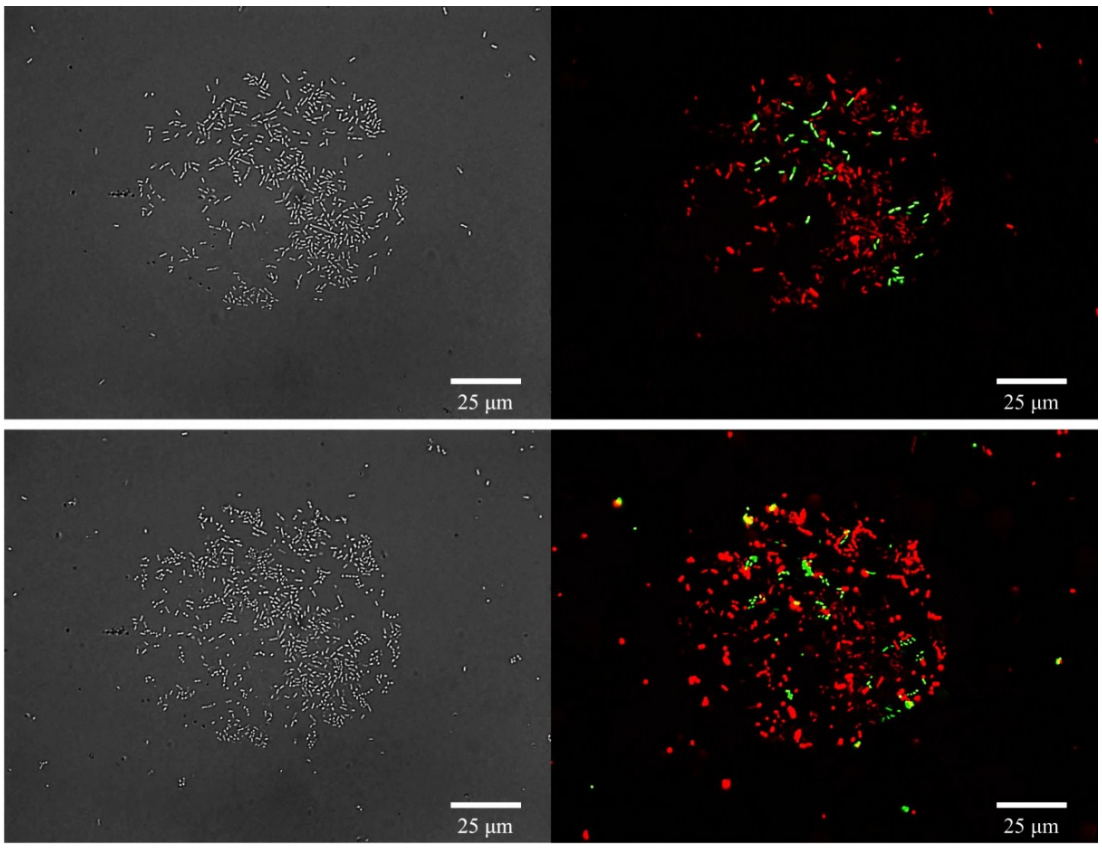

Figure 4.10. High-magnification images of one of the spots shown in Figure 4.8, taken to examine the cross-reactivity of *E. coli* 3030-2 (green) with the antibodies raised against *E. coli* H10407 (red) cells. The panels on the left show bright field images, and the panels on the right show epifluorescence images of the same area. The top panels show the spot after one hour of incubation, and the bottom panels show it after 19 hours of incubation. The selective binding of the red cells to their corresponding antibodies is clearly revealed, although a small fraction (~6%) of the green cells also bonded to these sites.

Finally, the reader should note here that not all attached cells fluoresce with equal intensity. Typically, we observe 30−40% more bacteria on the antibody-patterned spots in bright field images (Figures 4.9 and 4.10, left panels) than in corresponding epifluorescence images because of quenching or a failure of the cells to fluoresce. Therefore, it is expected for the epifluorescence images to show on the average fewer attached bacteria. These preliminary experiments do support the claim that only specific

bacteria (with minimum cross-reactivity) will bind with their complementary antibodies in both fuel and seawater environments [9]; i.e., the results show that the bacteria exhibit low specific binding to noncomplementary antibodies. The prolonged incubation times produce no degradation of the immunomicroarrays (even in cell-free media) and promote self-enrichment of the antibody-covered areas.

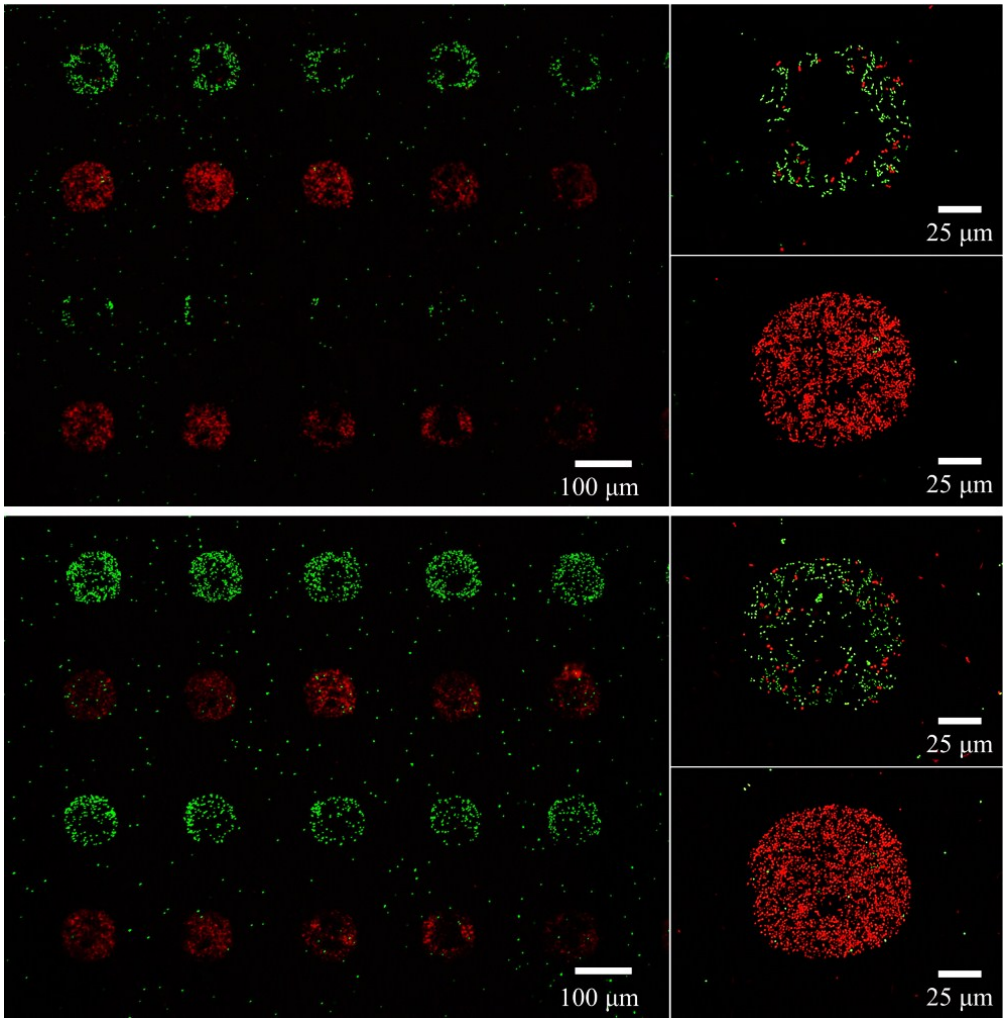

Figure 4.11. Sorting two *E. coli* strains, H10407 (red) and 3030-2 (green), mixed in equal concentrations (~3.0 × 10^7 cells/mL) in seawater using immunomicroarray technology. The top panel is the epifluorescence image of an area of immunoimmobilized live cells after one hour of incubation, and the bottom panel shows the same area after 19 hours of incubation. The magnified images clearly reveal the low cross-reactivity of each cell.

Discussion and Perspectives

Among the species of bacteria that have been identified in fuels, those that degrade fuels by utilizing hydrocarbons as their source of energy are a major concern for the defense and industrial sectors, including the Navy, and the shipping, aviation, oil and gas industries. For example, it has been shown that *Pseudomonas aeruginosa* (an aerobic bacterium) has a tremendous tendency to degrade 95% of diesel fuel within two weeks [121]. At the same time, it is well known that the metabolic activities of anaerobic bacteria near metal surfaces modify the local environment in ways that accelerate microbially influenced corrosion (MIC) on the metal surfaces [124]. The fuel-degrading, sulfate-reducing bacterium *Desulfoglaeba alkanexedens* (*D. alkanexedens*) ALDC^T isolated by Davidova *et al*. [125] is a good example of such anaerobic bacteria (*see* Figure 4.12). It is important to state that the corrosion caused by this type of bacteria is highly localized, leaving its mark on Fe surface as pits and corrosion deposits. Thus, it is necessary to monitor microbial growth and activity on metal surfaces and at fuel/seawater interfaces and to investigate the interactions of bacteria with each other and with their surroundings that lead to fuel and material deterioration.

The results discussed in this chapter reveal that the immunoimmobilization method described in this thesis can be utilized for the rapid and sensitive detection of bacteria in fuels. It has been demonstrated that if the correct antibody-antigen pairs are used immunomicroarrays can spatially separate specific bacterial strains from a mixture suspended in fuel, enabling simultaneous detection and identification. The immuno-immobilization method additionally offers a satisfactory platform for studying early

events in the biodeterioration processes mentioned above. For example, taking into account that immunoimmobilized cells grow into mature biofilms, immunomicroarrays can be employed to study biocorrosive model organisms involved in fuel and material deterioration. For instance, the possible synergetic interactions between SRB and sulfur-oxidizing bacteria (SOB) [124] can be studied on surfaces on which the individual SRB and SOB are separated from each other by a distance of ~250 μm. Unlike previous studies focusing on the macroscale investigation of biocorrosion [126, 127], this method offers a platform on which planktonic cells and colonization events can be controlled, a corrosion process can be instigated, and spatial correlations among metabolic activity, biotically produced minerals and localized corrosion attacks can be investigated. The knowledge gained from these investigations can be used to mitigate biocorrosion and biodeterioration in, say, ballast fuel tanks in the early stages of biocolonization.

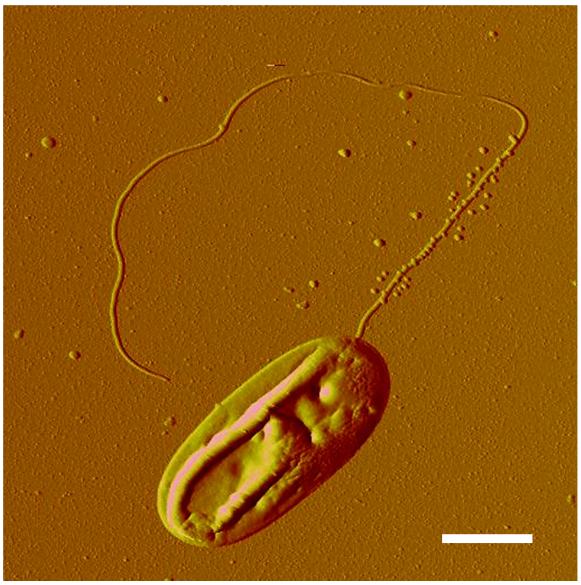

Figure 4.12. Atomic force microscope image of *D. alkanexedens* ALDC^{T}. The long appendage that extends from the surface of the bacterium is its flagellum. The scale bar is 1 μm.

To demonstrate the feasibility of using the immunoimmobilization method to detect *D. alkanexedens* ALDC^T bacteria in their physiological environment, series of experiments were conducted under anoxic conditions. Prior to bacterial incubation, 100 × 100 μm^2 patterned silicon substrates were first activated following the procedure described in Chapter 2, then decorated with polyclonal antibodies raised against the whole surface of ALDC^T (it is worth acknowledging here that the production of an antibody against ALDC^T was done for the first time at the Department of Immunology and Infectious Diseases of Montana State University at Bozeman as a collaborative effort between ICAL and Dr. Xinghong Yang and that the ALDC^T cells were grown and extracted at the Department of Botany and Microbiology of Oklahoma University at Norman.) The antibody-activated silicon substrates were incubated in Widdel solution [125] containing ALDC^T that had grown for 6 months (these organisms grow slowly), and bacterial capture was allowed for one hour at 25 °C under anoxic conditions. As described above, incubated silicon substrates were washed with PBS to remove loosely bound cells from the substrate surface and make the medium cell-free. Finally, the cells that remained on the patterned areas of the silicon substrates were observed in PBS in air with an optical microscope in reflection mode.

As shown in Figure 4.13, the immunosensor surfaces successfully immobilized *D. alkanexedens* cells on antibody-patterned areas of the silicon substrate. Knowing that the ALDC^T strain has a doubling time of ~53 days at 31−37 °C [125], the concentration of cells within the inoculum medium is expected to be in the range between 10^5 and 10^6 cells/mL. Consequently, based on our previous observations related to immobilizing *E.*

coli cells in this range, the low number of captured ALDC^T cells within the patterned area of the silicon substrate is well within the acceptable count. Also, from the optical image it seems that a portion of the antibody-binding sites are occupied by what appears to be biogenic sulfur/sulfide compounds (black spots within the bright area), which reduces the immunosensor capture efficiency. These compounds are known to be end products of bacterial metabolism [128]. Nonetheless, the preliminary results suggest that the immunoimmobilization method is a good platform for effectively capturing SRB in their physiological environment for future biocorrosion and biodeterioration experiments.

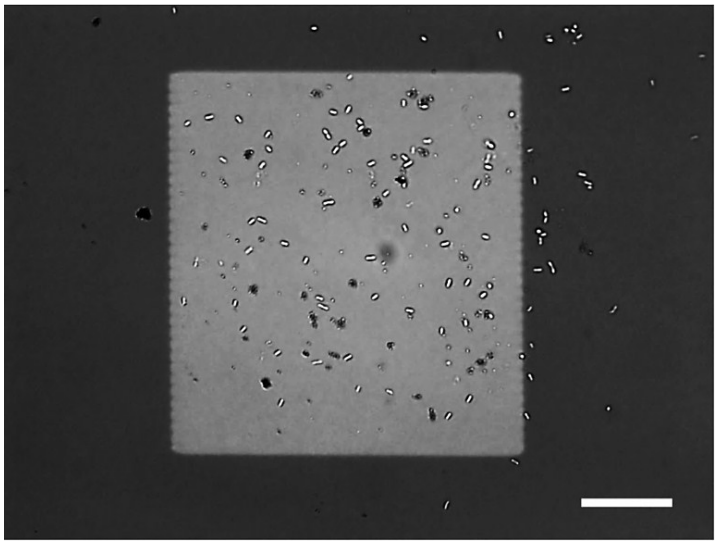

Figure 4.13. Immobilization of *D. alkanexedens* ALDC^T on silicon patterns modified with polyclonal anti-ALDC^T under anoxic conditions. The scale bar is 25 μm.

The slow growth of SRB may be problematic, especially when highly concentrated bacteria are desired on microarray patterns so that their interactions with both the substrate surface and the surroundings can be studied. Thus, it is necessary to find ways to trap and concentrate bacteria. As discussed in Chapter 3, one way of successfully concentrating them is to take advantage of the self-enrichment of immuno-

immobilized bacteria. However, as the doubling times for some SRB, such as ALDC^T, are rather long, an alternative method is necessary. Here, we developed one such approach. The design concept of the method is to pass, in a controlled fashion, low-concentration bacterial solutions through activated quartz (or glass) wool by some means, such as a syringe pump. The bacteria are (a) captured on the surfaces of antibody-activated fibers of glass wool (*see* Figure 4.14) and (b) entrapped within the 3 D network.

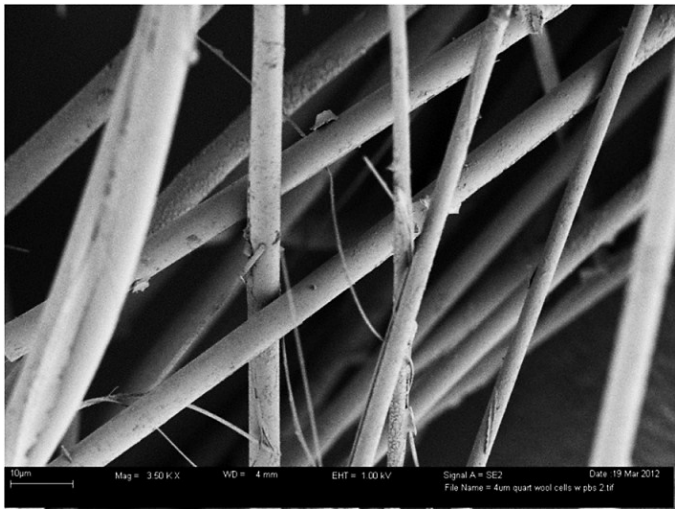

Figure 4.14. Scanning field emission electron microscope image of 3 D structured microfibers of quartz wool. The surface of each of these fibers was activated using linker chemistry to covalently bind antibodies for bacterial capture.

In what follows, we present the results of proof of concept experiments which we conducted in a PBS environment using our model *E. coli* H10407 red-fluorescing bacteria. The experimental setup is shown in Figure 4.15. The steps involved in the chemistry for activating the wool fibers to bind antibodies covalently were the same as those described in Chapter 3, and each step was monitored with XPS. As shown in Figure 4.16, the final accumulation of 9.7% N on the fiber surfaces demonstrates that antibodies can be successfully bound to the surfaces of these fibers.

Figure 4.15. An experimental setup for entrapment and concentration of bacteria present at low concentrations in liquid environments using antibody-modified quartz wool (1). The bacteria (2) were entrapped and concentrated by being passed, in a controlled fashion using a syringe and pump system (3 and 4), through activated quartz wools.

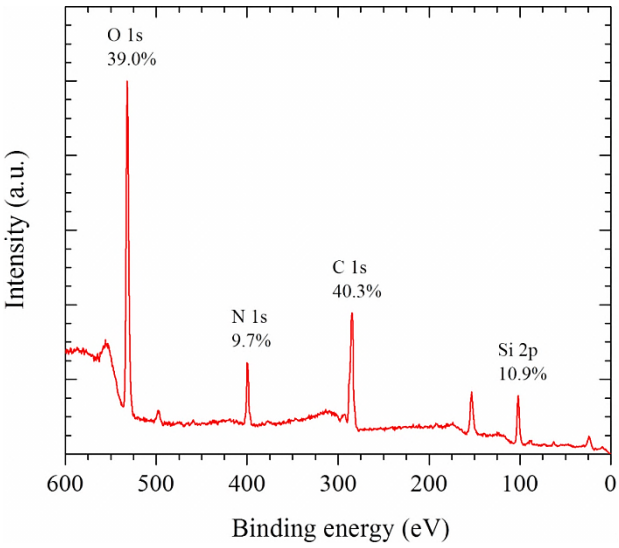

Figure 4.16. Survey XPS spectrum of anti-CFA/I-modified quartz wool. The 9.7% N clearly reveals the successful immobilization of antibodies using linker chemistry.

The results of these experiments are very promising, as we clearly observed entrapped bacteria on the surfaces of the fibers. We have filed for a provisional patent based on this idea. The top panel in Figure 4.17 shows an epifluorescence image of a small fraction of the quartz fibers, placed between two thin glass slides and imaged using a 100× oil-immersion objective lens.

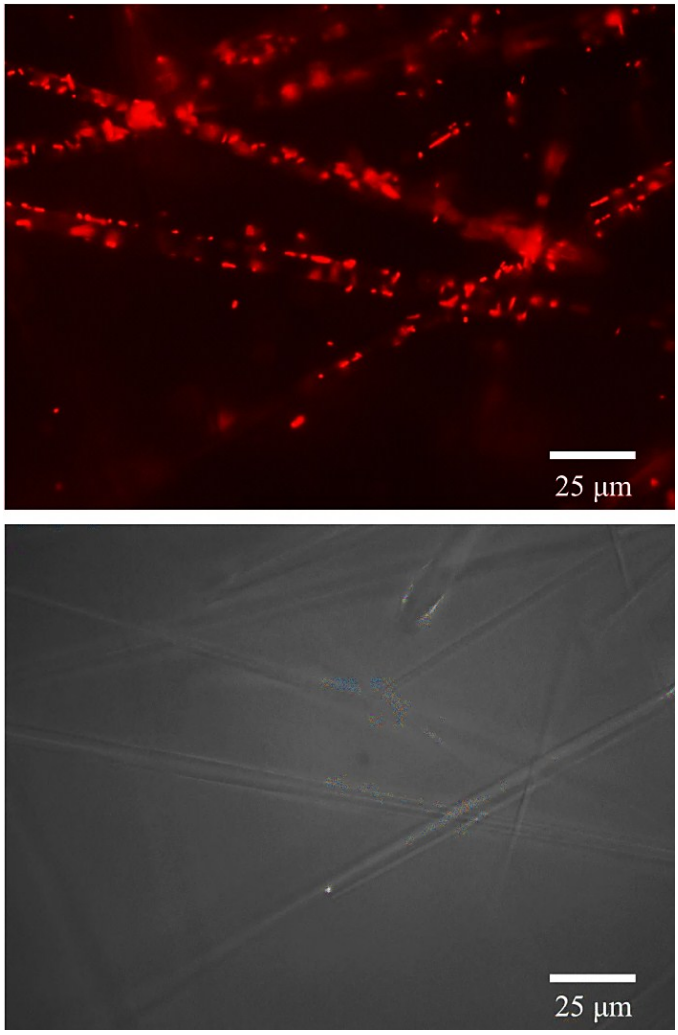

Figure 4.17. The top panel is an epifluorescence image of *E. coli* H10407 bacteria (red spots) captured on the anti-CFA/I activated surfaces of quartz wool fibers. The bottom panel is a bright field image of the same area.

Compared to the bright field image in the bottom panel, the epifluorescence image clearly

shows that the bacteria are successfully immobilized on individual fibers. As explained before, the reader should note that such epifluorescence images show only a small portion of the actually immobilized bacteria because of the quenching of bacterial fluorescing proteins. Nevertheless, the initial experiments show an efficient capture of *E. coli* at a concentration of ~10^7 cells/mL, suggesting this method is an effective way to capture and concentrate SRB for future applications. In fact, this technique is now routinely used in our corrosion experiments funded by the Office of Naval Research.

To conclude, we developed the immunoimmobilization method to answer the need for rapid, sensitive and simultaneous detection of trace bacteria present in fuels. Further, we developed an activated 3 D network of activated microfibers as an efficient way to entrap these bacteria. The initial experimentation shows great potential for using these systems to capture, sort, entrap and, hence, concentrate low concentrations of bacteria in contaminated systems such as fuels and water. Some of these techniques are now being used in our laboratory for federally funded research programs, and a patent application is pending.

5. SUMMARY

General Conclusions

In this thesis we have presented an efficient method of capturing living bacteria in liquid environments such as PBS, seawater and Navy fuels. This method is based on antibody-antigen interactions on activated, patterned silicon surfaces. To the best of our knowledge, ours is the first group to demonstrate a full monolayer of coverage within less than an hour using specific living bacteria on an activated area. The fundamental reason for our method producing such a successful, high-density bacterial immobilization is the use of antibodies raised against bacterial surface antigens such as fimbriae, lipopolysaccharides (LPS), and flagella to immobilize organisms in well-defined patterns on polished and highly characterized silicon surfaces. This type of immobilization, in this thesis referred to as immunoimmobilization, produces an efficient, reliable immobilization of living bacterial cells. Once captured, bacteria remain at their locations, maintain their viability and divide to populate their immediate surroundings. This is because the daughter cells also remain on the antibody-activated areas, contributing to the self-enrichment of the captured bacteria.

To achieve a high capture efficiency and reproducibility, it is essential to have an active antibody covalently tethered to a flat surface with sufficient freedom of motion to orient itself relative to the appropriate epitopes of a surface antigen of a bacterium that happens to be within close proximity of the tethered antibody. For this purpose, we used a simple linker chemistry optimized by us to increase the bacterial capture rate by taking advantage of covalent silane couplings on silicon surfaces. This coupling involved a

three-step reaction process: (1) deposition of a 3-aminopropyltriethoxysilane (APTES) layer, (2) reaction of the APTES amine groups with n-[ß-maleimidopropyloxy]-succinimide ester (BMPS) as a cross-linker and (3) coupling to the antibodies through the maleimide groups of the cross-linker and the sulfhydryl groups of the antibodies. The key to the success of this chemistry lies with characterization of the activated surface using surface-sensitive techniques. Using X-ray photoelectron spectroscopy (XPS) we characterized silicon surfaces prior to and following each step of the chemical modification process and verified the presence of chemical bonding of the nano-tether that links the antibody to the silicon surface. We optimized the density of the antibodies on the surface by correlating the atomic concentrations of N with the bacterial capture rate. The results suggest that a concentration of no more than 1 μg/mL of antibody solution is needed for the effective, reproducible immobilization of antibodies. Using scanning Auger microscopy and fluorescence optical microscopy, we verified the uniform surface coverage and orientation of the antibodies covalently bound to the silicon surface by flexible tethers. This resulted in an efficient, fairly reproducible immobilization of living bacteria on activated, patterned polished silicon surfaces. Our detection sensitivity was limited by the field of view of an optical microscope with a 60× water-immersion objective lens: a single bacterium within a 200 × 200 μm^2 field of view can be imaged. Although we did not conduct more systematic studies than are reported in the thesis with dead bacteria, preliminary studies indicate that activated surfaces are more effective at immobilizing live organisms than dead organisms.

To assess the rate of cell capture during the initial immunoimmobilization process

for a given antibody-antigen pair of a given strain of bacteria, we developed a *new* technique for determining the rate of capture for living *Salmonella enterica* (*S. enterica*) and *Escherichia coli* (*E. coli*) in an aqueous environment. The technique relies on activating 100 × 100 μm^2 patterns of silicon substrate for bacterial immobilization. We used a focused ion beam of our time-of-flight secondary ion mass spectrometry (ToF-SIMS) to create 100 × 100 μm^2 patterns and passivated the pattern-free regions of the silicon using 2-[methoxy-(polyethyleneoxy)propyl]trimethoxysilane (PEG-silane) to ensure that only the patterned areas on the silicon surface were available for bacterial immobilization. In this way, we created antibody-activated patterns on silicon substrate which could be imaged clearly with a high-end optical microscope as a function of time. High-resolution images of an activated square were taken at one-second intervals for a period of 90 minutes, which allowed us to plot the density of immunoimmobilized bacterial cells as a function of time. The initial rate of capture, in the first 10 minutes of incubation, allowed us to obtain the initial capture rate as a function of the cell concentration in the solution. The rate of attachment in terms of the number of cells immobilized per unit time per unit area per cell concentration in PBS solution was determined to be $(7.2 \pm 0.3) \times 10^{-6}$ cells/(min·$(100\ \mu m)^2$)/(cells/mL) for *S.* Typhimurium and $(1.1 \pm 0.1) \times 10^{-6}$ cells/(min·$(100\ \mu m)^2$)/(cells/mL) for *E. coli*, both expressing colonization factor antigen I (CFA/I) fimbriae. We attributed the difference (a factor of seven) between the rates to the fact that the antibodies were prepared against the fimbriae of *S.* Typhimurium and not those of *E. coli*, even though the CFA/I in the *S.* Typhimurium strain were activated by the genes obtained from the *E. coli* strain.

In some instances, however, we observed premature or early saturation of our sensor surfaces with a less than ideal density of captured bacteria. This puzzles us and threatens the reproducibility of the ultimate capture density on the activated surface. In principle, regardless of the type of antibody on the activated surface the saturation density on the activated area should be independent of the antibody-antigen interactions: it should only be limited by the steric hindrance of bacteria. This premature saturation of activated area has also been reported in the literature [85, 87], but no explanation has been offered. The saturation curve fits fairly well to the Langmuir isotherm curves [92], which suggests that besides bacteria there are other antigens, not attached to the bacteria, which interact with these antibodies in the activated areas, rendering them inactive. Our hypothesis is that these are surface antigens shed by the planktonic or dead bacteria. This will need substantial time and financial commitment to clarify; it is left for the next student to determine.

We demonstrated that the immunoimmobilization approach has a detection limit of ~3×10^4 cells/mL, which produces on the average a single immobilized bacterium in a 100×100 μm^2 antibody-activated area in 30 minutes. However, self-enrichment of the immobilized organisms improves the odds of detection as time passes. Furthermore, using the methodology of this thesis we have developed a bio-trap, in which solutions with a low concentration of bacteria can easily be concentrated by a factor of 10^3 in a reasonable time (about one hour), after which the immunoimmobilization technique can be used in a downstream application. This makes the method readily applicable to DNA analysis and to the sorting and culturing of bacteria from a mixed culture in a short period

of time (about one hour) for further identification and/or studies. In this thesis we demonstrated for the first time that antibodies maintain their structure, functionality and stability in a fuel environment. We demonstrated that immunoimmobilization can be used as a platform for a fairly fast (hours), sensitive (~10^4 cells/mL), specific, label-free detection system in fuel environments. Cell concentrations as low as ~10^2 cells/mL can be detected in Navy fuels using a model aerobic bacterium if we increase the time of incubation up to 24 hours. We also demonstrated that these antibody-activated areas can serve as prototype label-free sensors and that they can be used as a platform for detecting and sorting specific organisms in a mixed culture in a microarray setting. The unique feature of this approach is the immobilization of a very small amount of living bacteria over the area of a round spot with a diameter of ~100 μm using microplotting technology. The immunoimmobilization concept is also applied to immobilizing anaerobic species using a fuel-degrading, sulfate-reducing bacterium, *Desulfoglaeba alkanexedens* ALDC^T. The advantages of the immunoimmobilization approach developed in this thesis can be summarized as follows:

1) Selectivity: The specific interaction between the bacterial surface antigen and the corresponding antibody enables the capture of the targeted bacteria.

2) Speed: The simultaneous detection and identification of multiple pathogens is possible with a single test within an hour.

3) Fundamental science: Studies on individual or small groups of bacteria provide information on their interaction with the local environment.

4) Single-cell manipulation: Nano- or micro-scale manipulation of an individual cell is possible under physiological conditions, as was demonstrated in our earlier publication [8].

5) Self-enrichment: The cell population increases by cell division at the locations where the organisms are immunoimmobilized.

6) One-step detection: The cells can easily be detected without extra steps, such as tagging with fluorescent agents, by using an optical microscope with high sensitivity.

7) Testing drugs: Antimicrobial drugs can be tested for efficacy on living pathogens with single-cell resolution.

8) Bio-trapping and concentration: Trace amounts of bacteria (~10 cells/mL) in contaminated liquids can be concentrated by a factor of 10^3 in ~1 hour for use in downstream applications for quantification and identification.

Closing Remarks

A complete understanding of every aspect of the immunoimmobilization method described in this thesis would require further studies. One of the most important unsolved issues relates to reproducibility issues. This work laid down the foundations for work on this topic and set forth a working hypothesis. These and other issues in the field are left for the next student. The results presented in this thesis demonstrate that the immuno-immobilization method will have a broad impact in the Navy; in the biomedical,

environmental, and biosafety-related fields; and in the food, aviation, shipping, and oil and gas industries, as a rapid method for detecting, identifying, quantifying, and monitoring pathogens in a wide variety of physical environments. As a result of the work in this thesis, a provisional patent application has been filed by us on trapping and concentrating living microorganisms to pave the way for downstream biosensor applications such as the immunoimmobilization approach described in this thesis. Biotech companies such as EMD Millipore and Promega have shown high interest in the bio-trap idea, and we are currently discussing a possible collaboration with one of these companies. However, the most important aspect of our success in this thesis can be traced to bringing two seemingly unrelated fields, namely, surface science and biology, together. This work is an example of a truly multidisciplinary approach to solving challenging problems in the 21st century.

REFERENCES CITED

1. B. Byrne, E. Stack, N. Gilmartin, R. O'Kennedy, "Antibody-based sensors: principles, problems and potential for detection of pathogens and associated toxins", *Sensors*, **9**, 4407-4445 (2009).

2. V. Velusamy, K. Arshak, O. Korostynska, K. Oliwa, C. Adley, "An overview of foodborne pathogen detection: in the perspective of biosensors", *Biotechnol. Adv.*, **28**, 232-254 (2010).

3. Y.W. Tang, C.W. Stratton (Eds.), *Advanced techniques in diagnostic microbiology*, Springer: New York, 2006.

4. X.Y. Han, "Bacterial identification based on 16S ribosomal RNA gene sequence analysis", in: *Advanced techniques in diagnostic microbiology*, Y.W. Tang, C.W. Stratton (Eds.), Springer: New York, 2006, pp. 323-333.

5. J.E. Clarridge, "Impact of 16S rRNA gene sequence analysis for identification of bacteria on clinical microbiology and infectious diseases", *Clin. Microbiol. Rev.*, **17**, 840-862 (2004).

6. J.T. Keer, L. Birch, "Molecular methods for the assessment of bacterial viability", *J. Microbiol. Methods*, **53**, 175-183 (2003).

7. Y.C. Yeh, L.R. Comolli, K.H. Downing, L. Shapiro, H.H. McAdams, "The *Caulobacter* Tol-Pal complex is essential for outer membrane integrity and the positioning of a polar localization factor", *J. Bacteriol.*, **192**, 4847-4858 (2010).

8. Z. Suo, R. Avci, M. Deliorman, X. Yang, D.W. Pascual, "Bacteria survive multiple puncturings of their cell walls", *Langmuir*, **25**, 4588-4594 (2009).

9. Z. Suo, X. Yang, M. Deliorman, L. Cao, R. Avci, "Capture efficiency of *Escherichia coli* in fimbriae-mediated immunoimmobilization", *Langmuir*, **28**, 1351-1359 (2012).

10. P. Polyakov, C. Soussen, J.B. Duan, J.F.L. Duval, D. Brie, G. Francius, "Automated force volume image processing for biological samples", *Plos One*, **6**, (2011).

11. S. Campbell, M.L. Landry, "Rapid antigen tests", in: *Advanced techniques in diagnostic microbiology*, Y.W. Tang, C.W. Stratton (Eds.), Springer: New York, 2006, pp. 23-41.

12. K. Hechemy, R.W. Stevens, H.A. Gaafar, "Detection of *Escherichia coli* antigens by a latex agglutination test", *Appl. Microbiol.*, **28**, 306-311 (1974).

13. P.D. Skottrup, M. Nicolaisen, A.F. Justesen, "Towards on-site pathogen detection using antibody-based sensors", *Biosens. Bioelectron.*, **24**, 339-348 (2008).

14. Z. Suo, R. Avci, X. Yang, D.W. Pascual, "Efficient immobilization and patterning of live bacterial cells", *Langmuir*, **24**, 4161-4167 (2008).

15. Z. Suo, X. Yang, R. Avci, M. Deliorman, P. Rugheimer, D.W. Pascual, Y. Idzerda, "Antibody selection for immobilizing living bacteria", *Anal. Chem.*, **81**, 7571-7578 (2009).

16. P. Arenkov, A. Kukhtin, A. Gemmell, S. Voloshchuk, V. Chupeeva, A. Mirzabekov, "Protein microchips: use for immunoassay and enzymatic reactions", *Anal. Biochem.*, **278**, 123-131 (2000).

17. S.W. Howell, H.D. Inerowicz, F.E. Regnier, R. Reifenberger, "Patterned protein microarrays for bacterial detection", *Langmuir*, **19**, 436-439 (2003).

18. T. Cha, A. Guo, X.Y. Zhu, "Enzymatic activity on a chip: the critical role of protein orientation", *Proteomics*, **5**, 416-419 (2005).

19. T. Kawaguchi, D.R. Shankaran, S.J. Kim, K.V. Gobi, K. Matsumoto, K. Toko, N. Miura, "Fabrication of a novel immunosensor using functionalized self-assembled monolayer for trace level detection of TNT by surface plasmon resonance", *Talanta*, **72**, 554-560 (2007).

20. T. Wink, S.J. van Zuilen, A. Bult, W.P. van Bennekom, "Self-assembled monolayers for biosensors", *Analyst*, **122**, R43-R50 (1997).

21. S.K. Bhatia, L.C. Shriver-Lake, K.J. Prior, J.H. Georger, J.M. Calvert, R. Bredehorst, F.S. Ligler, "Use of thiol-terminal silanes and heterobifunctional crosslinkers for immobilization of antibodies on silica surfaces", *Anal. Biochem.*, **178**, 408-413 (1989).

22. L.C. Shriver-Lake, B. Donner, R. Edelstein, K. Breslin, S.K. Bhatia, F.S. Ligler, "Antibody immobilization using heterobifunctional crosslinkers", *Biosens. Bioelectron.*, **12**, 1101-1106 (1997).

23. A. Rezania, R. Johnson, A.R. Lefkow, K.E. Healy, "Bioactivation of metal oxide surfaces. 1. Surface characterization and cell response", *Langmuir*, **15**, 6931-6939 (1999).

24. F. Darain, K.L. Gan, S.C. Tjin, "Antibody immobilization on to polystyrene substrate: on-chip immunoassay for horse IgG based on fluorescence", *Biomed. Microdevices*, **11**, 653-661 (2009).

25. A. Kausaite-Minkstimiene, A. Ramanaviciene, J. Kirlyte, A. Ramanavicius, "Comparative study of random and oriented antibody immobilization techniques on the binding capacity of immunosensor", *Anal. Chem.*, **82**, 6401-6408 (2010).

26. S. Cohen, C. Milstein, "Structure of antibody molecules", *Nature*, **214**, 449-452 (1967).

27. D. Briggs, J.T. Grant (Eds.), *Surface analysis by Auger and x-ray photoelectron spectroscopy*, IM and SurfaceSpectra: Trowbridge, UK, 2003.

28. D. Pleul, F. Simion, "X-ray photoelectron spectroscopy", in: *Polymer surfaces and interfaces: characterization, modification and applications*, M. Stamm (Ed.), Springer: Berlin, 2008, pp. 71-89.

29. J.M. Hollander, W.L. Jolly, "X-ray photoelectron spectroscopy", *Acc. Chem. Res.*, **3**, 193-200 (1970).

30. J.C. Riviere, "Auger electron spectroscopy", *Contemp. Phys.*, **14**, 513-539 (1973).

31. R. Shimizu, "Quantitative analysis by Auger electron spectroscopy", *Jpn. J. Appl. Phys.*, **22**, 1631-1642 (1983).

32. D. Briggs, M.P. Seah (Eds.), *Practical surface analysis by Auger and X-ray photoelectron spectroscopy*, Wiley: New York, 1983.

33. D.A. Shirley, "High-resolution X-ray photoemission spectrum of valence bands of gold", *Phys. Rev. B*, **5**, 4709-4714 (1972).

34. J.F. Moulder, W.F. Stickle, P.E. Sobol, K.D. Bomben, *Handbook of X-ray photoelectron spectroscopy*, Perkin-Elmer, Phisical Electronics Division: Eden Prairie, MN, 1993.

35. J.C. Vickerman, D. Briggs (Eds.), *ToF-SIMS: surface analysis by mass spectrometry*, IM and SurfaceSpectra: Huddersfield, UK, 2001.

36. D. Pleul, F. Simion, "Time-of-flight secondary ion mass spectrometry", in: *Polymer surfaces and interfaces: characterization, modification and applications*, M. Stamm (Ed.), Springer: Berlin, 2008, pp. 91-102.

37. B.W. Schueler, "Microscope imaging by time-of-flight secondary ion mass spectrometry", *Microsc. Microanal. Microstruct.*, **3**, 119-139 (1992).

38. R. Avci, A.M. Hagenston, N.L. Equall, G.S. Groenewold, G.L. Gresham, D.A. Dahl, "Ion extraction from insulating fibers in ToF-SIMS", *Surf. Interface Anal.*, **27**, 789-796 (1999).

39. Z. Suo, R. Avci, M.H. Schweitzer, M. Deliorman, "Porphyrin as an ideal biomarker in the search for extraterrestrial life", *Astrobiology*, **7**, 605-615 (2007).

40. G.S. Groenewold, M.M. Cortez, A.K. Gianotto, G.L. Gresham, J.E. Olson, R.V. Fox, B.M. White, W.F. Bauer, R. Avci, M. Deliorman, E. Williams, "Surface analysis of particulates from laboratory hood exhaust manifold", *Surf. Interface Anal.*, **39**, 547-553 (2007).

41. G.S. Groenewold, G.L. Gresham, R. Avci, M. Deliorman, "Characterization of bidentate phosphoryl compounds on soil particulates using SIMS", *Surf. Interface Anal.*, **41**, 244-250 (2009).

42. G.S. Groenewold, R. Avci, R.V. Fox, M. Deliorman, Z. Suo, L. Kellerman, "Characterization of arsenic contamination on rust from ton containers", *Ind. Eng. Chem. Res.*, Submitted (2012).

43. A. Benninghoven, B. Hagenhoff, E. Niehuis, "Surface MS: probing real-world samples", *Anal. Chem.*, **65**, 630A-640A (1993).

44. M.F. Hochella, D.W. Harris, A.M. Turner, "Scanning Auger microscopy as a high-resolution microprobe for geologic materials", *Am. Mineral.*, **71**, 1247-1257 (1986).

45. G. Binnig, C.F. Quate, C. Gerber, "Atomic force microscope", *Phys. Rev. Lett.*, **56**, 930-933 (1986).

46. J.A. Howarter, J.P. Youngblood, "Optimization of silica silanization by 3-aminopropyltriethoxysilane", *Langmuir*, **22**, 11142-11147 (2006).

47. W. Kern, "The evolution of silicon wafer cleaning technology", *J. Electrochem. Soc.*, **137**, 1887-1892 (1990).

48. H. Baumgartner, V. Fuenzalida, I. Eisele, "Ozone cleaning of the Si-SiO_2 system", *Appl. Phys. A*, **43**, 223-226 (1987).

49. J. Ramm, E. Beck, A. Zueger, A. Dommann, R.E. Pixley, "Hydrogen cleaning of silicon wafers. Investigation of the wafer surface after plasma treatment", *Thin Solid Films*, **228**, 23-26 (1993).

50. Y. Han, D. Mayer, A. Offenhausser, S. Ingebrandt, "Surface activation of thin silicon oxides by wet cleaning and silanization", *Thin Solid Films*, **510**, 175-180 (2006).

51. J.J. Cras, C.A. Rowe-Taitt, D.A. Nivens, F.S. Ligler, "Comparison of chemical cleaning methods of glass in preparation for silanization", *Biosens. Bioelectron.*, **14**, 683-688 (1999).

52. M. Grundner, H. Jacob, “Investigations on hydrophilic and hydrophobic silicon (100) wafer surfaces by X-ray photoelectron and high-resolution electron energy loss-spectroscopy”, *Appl. Phys. A*, **39**, 73-82 (1986).

53. A. Papra, N. Gadegaard, N.B. Larsen, “Characterization of ultrathin poly(ethylene glycol) monolayers on silicon substrates”, *Langmuir*, **17**, 1457-1460 (2001).

54. M. Cerruti, S. Fissolo, C. Carraro, C. Ricciardi, A. Majumdar, R. Maboudian, “Poly(ethylene glycol) monolayer formation and stability on gold and silicon nitride substrates”, *Langmuir*, **24**, 10646-10653 (2008).

55. S. Sharma, R.W. Johnson, T.A. Desai, “Evaluation of the stability of nonfouling ultrathin poly(ethylene glycol) films for silicon-based microdevices”, *Langmuir*, **20**, 348-356 (2004).

56. J. Kim, G.J. Holinga, G.A. Somorjai, “Curing induced structural reorganization and enhanced reactivity of amino-terminated organic thin films on solid substrates: observations of two types of chemically and structurally unique amino groups on the surface”, *Langmuir*, **27**, 5171-5175 (2011).

57. E.A. Smith, W. Chen, “How to prevent the loss of surface functionality derived from aminosilanes”, *Langmuir*, **24**, 12405-12409 (2008).

58. A.K. Chauhan, D.K. Aswal, S.P. Koiry, S.K. Gupta, J.V. Yakhmi, C. Surgers, D. Guerin, S. Lenfant, D. Vuillaume, “Self-assembly of the 3-aminopropyltrimethoxysilane multilayers on Si and hysteretic current-voltage characteristics”, *Appl. Phys. A*, **90**, 581-589 (2008).

59. E.T. Vandenberg, L. Bertilsson, B. Liedberg, K. Uvdal, R. Erlandsson, H. Elwing, I. Lundstrom, “Structure of 3-aminopropyl triethoxy silane on silicon oxide”, *J. Colloid Interface Sci.*, **147**, 103-118 (1991).

60. S.J. Xiao, M. Textor, N.D. Spencer, H. Sigrist, “Covalent attachment of cell-adhesive, (Arg-Gly-Asp)-containing peptides to titanium surfaces”, *Langmuir*, **14**, 5507-5516 (1998).

61. K.C. Popat, E.E.L. Swan, T.A. Desai, “Modeling of RGDC film parameters using X-ray photoelectron spectroscopy”, *Langmuir*, **21**, 7061-7065 (2005).

62. M.J. Zhu, M.Z. Lerum, W. Chen, “How to prepare reproducible, homogeneous, and hydrolytically stable aminosilane-derived layers on silica”, *Langmuir*, **28**, 416-423 (2012).

63. R.G. Acres, A.V. Ellis, J. Alvino, C.E. Lenahan, D.A. Khodakov, G.F. Metha, G.G. Andersson, “Molecular structure of 3-aminopropyltriethoxysilane layers

formed on silanol-terminated silicon surfaces", *J. Phys. Chem. C*, **116**, 6289-6297 (2012).

64. F.X. Zhang, M.P. Srinivasan, "Self-assembled molecular films of aminosilanes and their immobilization capacities", *Langmuir*, **20**, 2309-2314 (2004).

65. T. Ramanathan, F.T. Fisher, R.S. Ruoff, L.C. Brinson, "Amino-functionalized carbon nanotubes for binding to polymers and biological systems", *Chem. Mater.*, **17**, 1290-1295 (2005).

66. K.M.R. Kallury, U.J. Krull, M. Thompson, "X-ray photoelectron spectroscopy of silica surfaces treated with polyfunctional silanes", *Anal. Chem.*, **60**, 169-172 (1988).

67. L.D. White, C.P. Tripp, "Reaction of (3-aminopropyl)dimethylethoxysilane with amine catalysts on silica surfaces", *J. Colloid Interface Sci.*, **232**, 400-407 (2000).

68. E. Asenath-Smith, W. Chen, "How to prevent the loss of surface functionality derived from aminosilanes", *Langmuir*, **24**, 12405-12409 (2008).

69. M.A. Firestone, M.L. Shank, S.G. Sligar, P.W. Bohn, "Film architecture in biomolecular assemblies. Effect of linker on the orientation of genetically engineered surface-bound proteins", *J. Am. Chem. Soc.*, **118**, 9033-9041 (1996).

70. L.A. Chrisey, G.U. Lee, C.E. O'Ferrall, "Covalent attachment of synthetic DNA to self-assembled monolayer films", *Nucleic Acids Res.*, **24**, 3031-3039 (1996).

71. G. Mattson, E. Conklin, S. Desai, G. Nielander, M.D. Savage, S. Morgensen, "A practical approach to crosslinking", *Mol. Biol. Rep.*, **17**, 167-183 (1993).

72. M.D. Partis, D.G. Griffiths, G.C. Roberts, R.B. Beechey, "Cross-linking of protein by ω-maleimido alkanoyl N-Hydroxysuccinimido esters", *J. Protein Chem.*, **2**, 263-277 (1983).

73. J.D. Gregory, "The stability of N-Ethylmaleimide and its reaction with sulfhydryl groups", *J. Am. Chem. Soc.*, **77**, 3922-3923 (1955).

74. G. Acharya, C.L. Chang, C. Savran, "An optical biosensor for rapid and label-free detection of cells", *J. Am. Chem. Soc.*, **128**, 3862-3863 (2006).

75. J.A. Camarero, "New developments for the site-specific attachment of proptein to surface", *Biophys. Rev. Lett.*, **1**, 1-28 (2006).

76. R. Charlermroj, O. Gajanandana, C. Barnett, K. Kirtikara, N. Karoonuthaisiri, "A chemiluminescent antibody array system for detection of foodborne pathogens in milk", *Anal. Lett.*, **44**, 1085-1099 (2011).

77. C.R. Taitt, Y.S. Shubin, R. Angel, F.S. Ligler, "Detection of *Salmonella enterica* serovar Typhimurium by using a rapid, array-based immunosensor", *Appl. Environ. Microbiol.*, **70**, 152-158 (2004).

78. A.G. Gehring, D.M. Albin, A.K. Bhunia, S.A. Reed, S.I. Tu, J. Uknalis, "Antibody microarray detection of *Escherichia coli* O157:H7: quantification, assay limitations, and capture efficiency", *Anal. Chem.*, **78**, 6601-6607 (2006).

79. A. Wolter, R. Niessner, M. Seidel, "Detection of *Escherichia coli* O157:H7, *Salmonella typhimurium*, and *Legionella pneumophila* in water using a flow-through chemiluminescence microarray readout system", *Anal. Chem.*, **80**, 5854-5863 (2008).

80. M. Magliulo, P. Simoni, M. Guardigli, E. Michelini, M. Luciani, R. Lelli, A. Roda, "A rapid multiplexed chemiluminescent immunoassay for the detection of *Escherichia coli* O157:H7, *Yersinia enterocolitica*, *Salmonella typhimurium*, and *Listeria monocytogenes* pathogen bacteria", *J. Agric. Food Chem.*, **55**, 4933-4939 (2007).

81. F. Liu, M. Dubey, H. Takahashi, D.G. Castner, D.W. Grainger, "Immobilized antibody orientation analysis using secondary ion mass spectrometry and fluorescence imaging of affinity-generated patterns", *Anal. Chem.*, **82**, 2947-2958 (2010).

82. V. Langer, R. Niessner, M. Seidel, "Stopped-flow microarray immunoassay for detection of viable *E. coli* by use of chemiluminescence flow-through microarrays", *Anal. Bioanal. Chem.*, **399**, 1041-1050 (2011).

83. S.T. Pathirana, J. Barbaree, B.A. Chin, M.G. Hartell, W.C. Neely, V. Vodyanoy, "Rapid and sensitive biosensor for *Salmonella*", *Biosens. Bioelectron.*, **15**, 135-141 (2000).

84. D.A. Boehm, P.A. Gottlieb, S.Z. Hua, "On-chip microfluidic biosensor for bacterial detection and identification", *Sens. Actuators B*, **126**, 508-514 (2007).

85. J.R. Premkumar, O. Lev, R.S. Marks, B. Polyak, R. Rosen, S. Belkin, "Antibody-based immobilization of bioluminescent bacterial sensor cells", *Talanta*, **55**, 1029-1038 (2001).

86. V. Duplan, E. Frost, J.J. Dubowski, "A photoluminescence-based quantum semiconductor biosensor for rapid *in situ* detection of *Escherichia coli*", *Sens. Actuators B*, **160**, 46-51 (2011).

87. J.M. Simpson-Stroot, E.A. Kearns, P.G. Stroot, S. Magana, D.V. Lim, "Monitoring biosensor capture efficiencies: development of a model using GFP-expressing *Escherichia coli* O157:H7", *J. Microbiol. Methods*, **72**, 29-37 (2008).

88. J.T. Connelly, A.J. Baeumner, "Biosensors for the detection of waterborne pathogens", *Anal. Bioanal. Chem.*, **402**, 117-127 (2012).

89. C.A. Rowe-Taitt, J.W. Hazzard, K.E. Hoffman, J.J. Cras, J.P. Golden, F.S. Ligler, "Simultaneous detection of six biohazardous agents using a planar waveguide array biosensor", *Biosens. Bioelectron.*, **15**, 579-589 (2000).

90. K. Rijal, A. Leung, P.M. Shankar, R. Mutharasan, "Detection of pathogen *Escherichia coli* O157:H7 AT 70 cells/mL using antibody-immobilized biconical tapered fiber sensors", *Biosens. Bioelectron.*, **21**, 871-880 (2005).

91. J.M. Simpson, D.V. Lim, "Rapid PCR confirmation of *E. coli* O157:H7 after evanescent wave fiber optic biosensor detection", *Biosens. Bioelectron.*, **21**, 881-887 (2005).

92. L.S. Jung, C.T. Campbell, "Sticking probabilities in adsorption of alkanethiols from liquid ethanol solution onto gold", *J. Phys. Chem. B*, **104**, 11168-11178 (2000).

93. C.S. Chen, R.A. Durst, "Simultaneous detection of *Escherichia coli* O157:H7, *Salmonella* spp. and *Listeria monocytogenes* with an array-based immunosorbent assay using universal protein G-liposomal nanovesicles", *Talanta*, **69**, 232-238 (2006).

94. T.B. Tims, D.V. Lim, "Confirmation of viable *E. coli* O157:H7 by enrichment and PCR after rapid biosensor detection", *J. Microbiol. Methods*, **55**, 141-147 (2003).

95. P. Zhu, D.R. Shelton, J.S. Karns, A. Sundaram, S. Li, P. Amstutz, C.M. Tang, "Detection of water-borne *E. coli* O157 using the integrating waveguide biosensor", *Biosens. Bioelectron.*, **21**, 678-683 (2005).

96. B. Johnson-White, B.C. Lin, F.S. Ligler, "Combination of immunosensor detection with viability testing and confirmation using the polymerase chain reaction and culture", *Anal. Chem.*, **79**, 140-146 (2007).

97. P.P. Banada, A.K. Bhunia, "Antibodies and immunoassays for detection of bacterial pathogens", in: *Principles of bacterial detection: biosensors, recognition receptors, and microsystems*, M. Zourob, S. Elwary, A.P.F. Turner (Eds.), Springer: New York, 2008,

98. B.K. Hahm, A.K. Bhunia, "Effect of environmental stresses on antibody-based detection of *Escherichia coli* O157 : H7, *Salmonella enterica* serotype Enteritidis and *Listeria monocytogenes*", *J. Appl. Microbiol.*, **100**, 1017-1027 (2006).

99. L. Cao, Z. Suo, T. Lim, S. Jun, M. Deliorman, C. Riccardi, L. Kellerman, R. Avci, X. Yang, "Role of overexpressed CFA/I fimbriae in bacterial swimming", *Phys. Biol.*, **9**, 036005 (2012).

100. S.H. Lee, E. Ruckenstein, "Adsorption of proteins onto polymeric surfaces of different hydrophilicities: a case study with bovine serum albumin", *J. Colloid Interface Sci.*, **125**, 365-379 (1988).

101. V. Raikos, S.S. Vamvakas, D. Sevastos, J. Kapolos, G. Karaiskakis, A. Koliadima, "Water content, temperature and biocide effects on the growth kinetics of bacteria isolated from JP-8 aviation fuel storage tanks", *Fuel*, **93**, 559-566 (2012).

102. N.A. Yemashova, V.P. Murygina, D.V. Zhukov, A.A. Zakharyantz, M.A. Gladchenko, V. Appanna, S.V. Kalyuzhnyi, "Biodeterioration of crude oil and oil derived products: a review", *Rev. Environ. Sci. Biotechnol.*, **6**, 315-337 (2007).

103. G. Hill, "Sampling methods for detecting microbial contamination in fuel tanks and systems", in: *Fuel and fuel system microbiology - fundamentals, diagnosis, and contamination control*, F.J. Passman (Ed.), ASTM International: West Conshohocken, PA, 2003, pp. 14-23.

104. R.A. Neihof, M.E. May, "Microbial contamination of naval fuels", *Dev. Ind. Microbiol.*, **23**, 167-176 (1982).

105. C.C. Gaylarde, F.M. Bento, J. Kelley, "Microbial contamination of stored hydrocarbon fuels and its control", *Rev. Microbiol.*, **30**, 1-10 (1999).

106. R.M. Atlas, "Microbial degradation of petroleum hydrocarbons: an environmental perspective", *Microbiol. Rev.*, **45**, 180-209 (1981).

107. H.R. Beller, A.M. Spormann, P.K. Sharma, J.R. Cole, M. Reinhard, "Isolation and characterization of a novel toluene-degrading, sulfate-reducing bacterium", *Appl. Environ. Microbiol.*, **62**, 1188-1196 (1996).

108. Z. Lewandowski, H. Beyenal, "Mechanisms of microbially influenced corrosion", in: *Marine and industrial biofouling*, H.C. Flemming, P.S. Murthy, R. Venkatesan, K.E. Cooksey (Eds.), Springer: Berlin, 2009, pp. 35-65.

109. ASTM Standard D6469, "Standard guide for microbial contamination in fuels and fuel systems", ASTM International: West Conshohocken, PA, 2011.

110. S.L. Ross Environmental Research, "Determine if Ohmsett is suitable for researching, testing and training in biofuel spill response", Project #M07PC13061 Report to MMS, U.S. Department of the Interior: Herndon, VA, 2010.

111. I.A. Davidova, L.M. Gieg, M. Nanny, K.G. Kropp, J.M. Suflita, “Stable isotopic studies of n-alkane metabolism by a sulfate-reducing bacterial enrichment culture”, *Appl. Environ. Microbiol.*, **71**, 8174-8182 (2005).

112. K. Daly, R.J. Sharp, A.J. McCarthy, “Development of oligonucleotide probes and PCR primers for detecting phylogenetic subgroups of sulfate-reducing bacteria”, *Microbiology*, **146**, 1693-1705 (2000).

113. M.E. Rauch, H.W. Graef, S.M. Rozenzhak, S.E. Jones, C.A. Bleckmann, R.L. Kruger, R.R. Naik, M.O. Stone, “Characterization of microbial contamination in United States Air Force aviation fuel tanks”, *J. Ind. Microbiol. Biotechnol.*, **33**, 29-36 (2006).

114. V. Raikos, S.S. Vamvakas, J. Kapolos, A. Koliadima, G. Karaiskakis, “Identification and characterization of microbial contaminants isolated from stored aviation fuels by DNA sequencing and restriction fragment length analysis of a PCR-amplified region of the 16S rRNA gene”, *Fuel*, **90**, 695-700 (2011).

115. American Society for Microbiology, “Manual of microbiological methods”, McGraw-Hill: New York, 1957.

116. G.C. Blanchard, "Mechanism of microbiological contamination of jet fuel and development of techniques for detection of microbial contamination", Technical Documentary Report APL-TDR-64-70 Part III, Air Force Aero Propulsion Laboratory: Wright-Patterson Air Force Base, OH, 1966.

117. P. Edmonds, J.J. Cooney, “Identification of microorganisms isolated from jet fuel systems”, *Appl. Microbiol.*, **15**, 411-416 (1967).

118. E.N. Efremenko, R.E. Azizov, A.A. Raeva, V.M. Abbasov, S.D. Varfolomeyev, “An approach to the rapid control of oil spill bioremediation by bioluminescent method of intracellular ATP determination”, *Int. Biodeterior. Biodegrad.*, **56**, 94-100 (2005).

119. P.T.C. Lopes, C. Gaylarde, “Use of immunofluorescence to detect the fungus *Hormoconis resinae* in aviation kerosine”, *Int. Biodeterior. Biodegrad.*, **37**, 37-40 (1996).

120. C.A. Bailey, M.E. May, “Evaluation of microbiological test kits for hydrocarbon fuel systems”, *Appl. Environ. Microbiol.*, **37**, 871-877 (1979).

121. J.T. Bartis, L. Van Bibber, *Alternative fuels for military applications*, RAND: Santa Monica, CA, 2011.

122. L.Q. Maurice, H. Lander, T. Edwards, W.E. Harrison, “Advanced aviation fuels: a look ahead via a historical perspective”, *Fuel*, **80**, 747-756 (2001).

123. C. Wingren, C.A.K. Borrebaeck, "Protein microarray technologies for detection and identification of bacterial and protein analytes", in: *Principles of bacterial detection: biosensors, recognition receptors, and microsystems*, M. Zourob, S. Elwary, A.P.F. Turner (Eds.), Springer: New York, 2008, pp. 715-729.

124. I.B. Beech, S.A. Campbell, "Accelerated low water corrosion of carbon steel in the presence of a biofilm harbouring sulphate-reducing and sulphur-oxidising bacteria recovered from a marine sediment", *Electrochim. Acta*, **54**, 14-21 (2008).

125. I.A. Davidova, K.E. Duncan, O.K. Choi, J.M. Suflita, "*Desulfoglaeba alkanexedens* gen. nov., sp nov., an n-alkane-degrading, sulfate-reducing bacterium", *Int. J. Syst. Evol. Microbiol.*, **56**, 2737-2742 (2006).

126. Y. Tanji, Y. Morono, A. Soejima, K. Hori, H. Unno, "Structural analysis of a biofilm which enhances carbon steel corrosion in nutritionally poor aquatic environments", *J. Biosci. Bioeng.*, **88**, 551-556 (1999).

127. J.S. Lee, R.I. Ray, E.J. Lemieux, A.U. Falster, B.J. Little, "An evaluation of carbon steel corrosion under stagnant seawater conditions", *Biofouling*, **20**, 237-247 (2004).

128. T. Wind, R. Conrad, "Sulfur compounds, potential turnover of sulfate and thiosulfate, and numbers of sulfate-reducing bacteria in planted and unplanted paddy soil", *FEMS Microbiol. Ecol.*, **18**, 257-266 (1995).